

Effect of Cutting Tool Coating on the Machinability of Inconel 718

By

Abhay Bhatt

Department of Mechanical Engineering

McGill University, Montreal

October 2006

A Thesis Submitted to the Faculty of Graduate Studies and Research in Partial
Fulfillment of the Requirement for the Degree of
Master of Engineering

© Abhay Bhatt, 2006



Library and
Archives Canada

Bibliothèque et
Archives Canada

Published Heritage
Branch

Direction du
Patrimoine de l'édition

395 Wellington Street
Ottawa ON K1A 0N4
Canada

395, rue Wellington
Ottawa ON K1A 0N4
Canada

Your file *Votre référence*
ISBN: 978-0-494-28589-3
Our file *Notre référence*
ISBN: 978-0-494-28589-3

NOTICE:

The author has granted a non-exclusive license allowing Library and Archives Canada to reproduce, publish, archive, preserve, conserve, communicate to the public by telecommunication or on the Internet, loan, distribute and sell theses worldwide, for commercial or non-commercial purposes, in microform, paper, electronic and/or any other formats.

The author retains copyright ownership and moral rights in this thesis. Neither the thesis nor substantial extracts from it may be printed or otherwise reproduced without the author's permission.

AVIS:

L'auteur a accordé une licence non exclusive permettant à la Bibliothèque et Archives Canada de reproduire, publier, archiver, sauvegarder, conserver, transmettre au public par télécommunication ou par l'Internet, prêter, distribuer et vendre des thèses partout dans le monde, à des fins commerciales ou autres, sur support microforme, papier, électronique et/ou autres formats.

L'auteur conserve la propriété du droit d'auteur et des droits moraux qui protègent cette thèse. Ni la thèse ni des extraits substantiels de celle-ci ne doivent être imprimés ou autrement reproduits sans son autorisation.

In compliance with the Canadian Privacy Act some supporting forms may have been removed from this thesis.

Conformément à la loi canadienne sur la protection de la vie privée, quelques formulaires secondaires ont été enlevés de cette thèse.

While these forms may be included in the document page count, their removal does not represent any loss of content from the thesis.

Bien que ces formulaires aient inclus dans la pagination, il n'y aura aucun contenu manquant.


Canada

Abstract

This research is an assessment of the machinability of a nickel-based alloy Inconel 718 using a finish turning operation with carbide coated and uncoated tools having fine and medium grain size substrates, and the same tool geometry (a round tool shape geometry with a 0° rake angle and 7° clearance angle). In addition, orthogonal machining tests were carried out to generate experimental data for future identification of the constitutive laws of Inconel 718 (its behavior under high stress, strains, strain rates, and temperatures). The finish turning of this alloy was evaluated in terms of tool life, tool wear mechanisms, cutting forces, surface roughness, and chip formation process. The cutting speed range evaluated was from 50 to 100 m/min, and the feed range was from 0.075 to 0.125 mm/rev. Throughout the machining tests, the depth of cut was kept constant and equal to 0.25 mm. Tungsten carbide uncoated tool having fine grain size ($<1\mu\text{m}$), strong and sharp cutting edges were found to be the most suitable tool material and tool geometry for the finish turning of Inconel 718 at a cutting speed of 50 m/min, and, moreover, yielded the best tool life of 53 minutes. When finish turning at a cutting speed of 75 m/min, a single layer PVD (TiAlN= $3\mu\text{m}$) carbide tool yielded the best tool life of 12 minutes. At a cutting speed of 100 m/min, triple layer CVD coated tools (TiCN/Al₂O₃/TiN = $15\mu\text{m}$) produced the best performance, yielding an 8 minutes of tool life. During the machining tests, the common wear mechanisms of the three different tools were adhesion, abrasion, and diffusion. Flank wear was the dominant tool failure mode of all three tools. The analysis of chip morphology showed that no phase transformation existed even though the material was deformed. The increase of micro-hardness was confirmed by micro-hardness measurements on chips, as compared to the initial micro-hardness of the material (Inconel 718). Cutting forces for all the different tools were relatively low ($< 300\text{ N}$) when the cutting edge was new. For the finish turning operation, surface roughness of ($<1\mu\text{m}$) was achieved in all the cutting tests.

Résumé

Ce travail de recherche présente une évaluation de l'usinabilité de l'alliage à base de nickel Inconel 718 en tournage de finition. Les outils utilisés sont en carbure de tungstène à grain moyen ou fin, revêtus et non revêtus. Les outils ont une géométrie unique: des pastilles circulaires avec un angle d'attaque de 0° et un angle de dépouille de 7° . En outre, des essais de coupe orthogonale ont été effectués pour produire les données expérimentales nécessaires à l'identification du comportement de l'Inconel 718 sous des contraintes, des déformations, des vitesses de déformation et des températures très élevées. Le tournage de finition de l'Inconel 718 a été évaluée en termes de la durée de vie de l'outil, des mécanismes d'usure de l'outil, des efforts de coupe, de la rugosité des surfaces usinées et de la morphologie des copeaux. Les vitesses de coupe utilisées ont été dans la plage de 50 à 100 m/min. Les vitesses d'avance ont été dans la plage de 0,075 à 0,125 mm/tour. La profondeur de coupe a été maintenue constante et égale à 0.25 mm dans tous les essais d'usinage. Les pastilles de carbure de tungstène à grains fins ($< 1\mu\text{m}$), non revêtues et ayant des arêtes de coupe vives se sont avérées les plus appropriées pour le tournage de l'Inconel 718 à vitesse réduite jusqu'à 50 m/min. En outre, ces pastilles ont eu la plus longue durée de vie, une durée de 53 minutes. Les pastilles de carbure revêtues par une couche de 3 microns de TiAlN (PVD) ont été mieux adaptées pour des vitesses de coupe légèrement plus élevées de l'ordre de 75 m/min. Sous ces conditions, ces pastilles ont eu une durée de vie de 12 minutes. Pour des vitesses de coupe atteignant les 100 m/min, les pastilles de carbures revêtues par triple-couches de 15 microns de TiCN/Al₂O₃/TiN (CVD) ont eu une meilleure durée de vie de l'ordre de 8 minutes. Durant les différents tests de tournage, les mécanismes d'usure les plus communs sont: l'usure par adhésion, l'usure par abrasion et l'usure par diffusion. L'usure de la face de dépouille était le mode de défaillance le plus dominant de ces pastilles. L'analyse microstructurale des copeaux a montré qu'il n'y a pas de changement de phase lors de la formation du copeau. Des mesures de micro-dureté ont montré une augmentation de la dureté au cours du processus de formation du copeau (Inconel 718), comme en

comparaison de la micro-dureté d'initiale du matériel. Dans les différents essais de coupe, les efforts de coupe ont été relativement faibles (< 300 N) quand les arêtes de coupe sont vives. La rugosité moyenne des surfaces usinées a été au-dessous d'un micron.

Acknowledgements

I would like to express my gratitude to my principal supervisor Prof. Helmi Attia and co-supervisor Prof. Vincent Thomson for their invaluable guidance in the accomplishment of this research work. An additional gratefulness is extended to Mr. Raul Vargas for his contributions in the development of this thesis, and to Dr. Nejah Tounsi for his constructive comments. I also would like to thank Prof. Helmi Attia for the financial support, and for the opportunity to access the equipment used for the machining tests performed during the course of this research at the Aerospace Manufacturing Technology Centre (AMTC), National Research Council Canada (NRC). I also am grateful to Mr. Danen Challen for his technical help and support on the performance of the machining tests. As well, my deep appreciation is extended to all the members at AMTC, NRC who helped during the experimental phase, and to Mrs. Helen Campbell at McGill University for her help with SEM images.

Lastly, I would like to express my sincere thanks to my parents, my family members, and my friends for their many contributions in helping me to complete my Masters degree.

Table of Contents

Abstract	ii
Résumé	iii
Acknowledgements	v
Table of Contents	vi
List of Figures	ix
List of Tables	xvi
Chapter 1 Introduction	1
1.1 General.....	1
1.2 Thesis Objective.....	4
1.3 Thesis Scope	4
1.4 Thesis Organization	5
Chapter 2 Literature Review	6
2.1 Metal Cutting Principles	6
2.2 Metallurgy of Inconel 718	8
2.3 Machining Research on Inconel 718.....	12
2.3.1 Cutting Forces.....	12
2.3.2 Tool Life and Tool Wear	17
2.3.3 Cutting Temperature	21
2.3.4 Surface Finish	22
2.3.5 Chip Formation.....	25
2.4 Conclusions.....	26
Chapter 3 Experimental Work	28
3.1 Machine Tool.....	28
3.2 Cutting Tool.....	28
3.2.1 Tool Holders	29
3.2.2 Tool Material and Geometries	30
3.3 Workpiece Material	31
3.4 Tool Wear Measurement.....	32

3.5	Force Measurement.....	33
3.6	Chip Analysis.....	34
3.7	Workpiece Surface Roughness Measurement	35
3.8	Cutting Fluid	35
3.9	Experimental Matrix	35
3.10	Contact Length Measurement.....	38
Chapter 4 Results and Discussions.....		39
4.1	Introduction.....	39
4.2	Experimental Results Obtained in Orthogonal Machining.....	39
4.2.1	Experimental Results Obtained When Performing Orthogonal Machining With a 2 mm Width of Cut	40
4.2.1.1	Cutting Forces.....	40
4.2.1.2	Chip Analysis.....	41
4.2.1.3	Evaluation of Shear Stress, Shear Strain, and Strain Rate.....	45
4.2.1.4	Contact Length.....	47
4.2.2	Experimental Results Obtained When Performing Orthogonal Machining With a 3 mm Width of Cut	48
4.2.2.1	Cutting Forces.....	48
4.2.2.2	Chip Analysis.....	52
4.2.2.3	Evaluation of Shear Stress, Strain and Strain Rate.....	54
4.2.2.4	Contact Length.....	55
4.3	Finish Turning Operation.....	60
4.3.1	Tool Wear Mechanisms and Tool Failure Modes.....	60
4.3.1.1	Tool Wear Mechanism at a Low Cutting Speed (50 m/min).....	61
4.3.1.1.1	Chip Morphology and Metallurgical Analysis at a Low Cutting Speed (50 m/min).....	65
4.3.1.1.2	Forces at Low Cutting speed (50 m/min).....	69
4.3.1.1.3	Tool Life at Low Cutting Speed (50 m/min)	71
4.3.1.2	Tool Wear Mechanism at a Medium Cutting Speed (75 m/min).....	75
4.3.1.2.1	Chip Morphology and Metallurgical Analysis at a Medium Cutting Speed (75 m/min).....	77

4.3.1.2.2	Forces at Medium Cutting Speed (75 m/min).....	78
4.3.1.2.3	Tool Life at Medium Cutting Speed (75 m/min).....	86
4.3.1.3	Tool Wear Mechanism at a High Cutting Speed (100 m/min)	89
4.3.1.3.1	Chip Morphology and Metallurgical Analysis at a High Cutting Speed (100 m/min).....	91
4.3.1.3.2	Forces at a High Cutting Speed (100 m/min)	93
4.3.1.3.3	Tool Life at a High Cutting Speed (100/min).....	97
4.3.2	Surface Finish	99
Chapter 5 Conclusions and Future Recommendations.....		103
5.1	Conclusions.....	103
5.2	Recommendations for Future Work.....	105
References.....		107

List of Figures

Figure 1.1: Classification of super alloys [5].....	2
Figure 2.1: Orthogonal cutting mechanism: (a) basic turning operation, (b) two dimensional orthogonal turning.	6
Figure 2.2: Crystallography of the γ'' phase, after Nevitt (a) unit cell, (b) close-packed plane [15, 16]	9
Figure 2.3: Pseudo-equilibrium diagram for Inconel 718 showing stability of various phases at different temperatures [6, 12].....	11
Figure 2.4: Time-Temperature-Precipitation (T-T-P) diagram for Inconel 718 showing the typical heat treatment cycle [6, 12].....	11
Figure 2.5: Rhomboid shape geometry.....	13
Figure 2.6: Local tool temperatures v/s cutting speed [34]	22
Figure 2.7: Optical micrographs of the Inconel 718 chip at 61 m/min showing the transition (i.e. from a continuous chip to shear localized chip) where shear localization is beginning to take place [12]	26
Figure 3.1: Experimental setup: (a) orthogonal machining, (b) oblique finish turning operation, (1) workpiece, (2 & 3) tool, (4) chuck/spindle, (5) force transducer, (6) surface roughness measurement instrument, and (7) chip collector.....	29
Figure 3.2: Sandvik triangular turning tool holder employed in the orthogonal machining tests	30
Figure 3.3: Kennametal round turning tool holder employed in the oblique finish machining tests.....	30
Figure 3.4: Tool wear measurement setup (1) tool (2) tool holder (3) x-y stage.....	32
Figure 3.5: Tool wear criteria [52].....	32
Figure 3.6: Forces direction during machining process (a) orthogonal cutting (b) oblique finish turning.....	33
Figure 3.7: Image of chips placement in the bakelite mounting.....	34
Figure 3.8: Contact length measurement	38

Figure 4.1: Effect of cutting speed and feed on cutting forces and mean tool-face temperature	43
Figure 4.2: Effect of cutting speed and feed on chip thickness	44
Figure 4.3: Effect of cutting speed and feed on torque.....	44
Figure 4.4: Effect of cutting speed and feed on width of chip.....	45
Figure 4.5: Effect of cutting speed and feed on shear stress, strain, and strain rate	46
Figure 4.6: Effect of cutting speed and feed on chip-tool contact length with 2 mm width of cut	47
Figure 4.7: Effect of shear angle and chip-tool contact length with 2 mm width of cut ..	48
Figure 4.8: Effect of speed and feed on cutting forces and mean tool-face temperature for 3 mm width of cut.....	50
Figure 4.9: Effect of cutting speed and feed on torque for a 3 mm width of cut.....	50
Figure 4.10: Effect of width of cut on forces, mean tool-face temperature, and torque with a feed of 0.2 mm/rev	52
Figure 4.11: Effect of cutting speed and feed on (a) chip thickness and (b) width of chip for a 3 mm width of cut.....	53
Figure 4.12: Effect of width of cut on chip thickness and width of chip with a feed of 0.2 mm/rev	54
Figure 4.13: Effect of cutting speed and feed on shear stress, strain, and strain rate for a 3 mm width of cut	56
Figure 4.14: Effect of width of cut on shear stress, shear strain, and strain rate with a feed of 0.2 mm/rev.....	57
Figure 4.15: Effect of cutting speed and feed on contact length for a 3 mm width of cut	58
Figure 4.16: Effect of shear angle and chip-tool contact length with 2 mm width of cut	58
Figure 4.17: Effect of width of cut on contact length with feed 0.2 mm/rev.....	59
Figure 4.18: Effect of width of cut on the curling of chip with feed 0.2 mm/rev.....	59
Figure 4.19: Effect of width of cut on the curling of chip with feed 0.3 mm/rev.....	60
Figure 4.20: Different tool wear modes [60]	61
Figure 4.21: SEM images for a speed of 50 m/min and a feed of 0.075 mm/rev: (a) rake and flank face for an uncoated tool at 33.55 mins, (b) rake and flank face for a single layer PVD coated tool at 24.34 mins, and (c) rake and flank face for	

a triple layer CVD coated tool at 2.5 mins.....	62
Figure 4.22: Chemical analysis of the tool rake face for an uncoated tool (a) Before Cutting and (b) After Cutting; Chemical analysis of the tool rake face for a single layer PVD TiAlN coated tool (c) Before Cutting and (d) After Cutting, and Chemical analysis of the tool rake face for a triple layer CVD TiCN/Al ₂ O ₃ /TiN coated tool (e) Before Cutting and (f) After Cutting.....	63
Figure 4.23: Triple layer CVD (TiCN/Al ₂ O ₃ /TiN) coated tool (a) rake face (b) flank face	64
Figure 4.24: SEM images for a speed of 50 m/min and a feed of 0.1 mm/rev: (a) rake and flank face for an uncoated tool at 38.85 mins, (b) rake and flank face for a single layer PVD coated tool at 19.75 mins, and (c) rake and flank face for a triple layer CVD coated tool at 11.60 mins	64
Figure 4.25: SEM images for a speed of 50 m/min and a feed of 0.125 mm/rev: (a) rake and flank face for an uncoated tool at 27.42 mins, (b) rake and flank face for a single layer PVD coated tool at 20.32, and (c) rake and flank face for a triple layer CVD coated tool at 8.19 mins	65
Figure 4.26: SEM Image for Inconel 718 with the spot marked (a) where the chemical analysis is done (b, c, d) using SEM.....	66
Figure 4.27: Chip image for the uncoated tool at a cutting speed of 50 m/min and a feed	67
Figure 4.28: Chip image with the spot marked where the chemical analysis is done (a); chemical analysis using SEM (b, c, d) for a speed of 50 m/min and a feed of 0.075 mm/rev with an uncoated tool showing no phase transformation	67
Figure 4.29: Chip image at a cutting speed of 50 m/min and a feed of 0.1 mm/rev for a single layer PVD coated tool	68
Figure 4.30: Chip image with the spot marked where the chemical analysis is done (a); chemical analysis using SEM (b, c, d) for a speed of 50 m/min and a feed of 0.1 mm/rev with a single layer PVD TiAlN coated tool showing no phase transformation	68
Figure 4.31: Micro-hardness measurement done at three areas (A, B, C).....	69
Figure 4.32: Forces with three different tools when the tool edge is sharp at speed 50	

m/min and three different feeds (a) thrust force, (b) feed force, and (c) cutting force	70
Figure 4.33: Variation of flank wear rate with cutting time, showing the initial wear, steady wear, and severe wear periods	72
Figure 4.34: Tool wear progression for three different tools at cutting speed of 50 m/min and feeds of (a) 0.075 mm/rev (b) 0.1 mm/rev (c) 0.125 mm/rev	74
Figure 4.35: SEM images for a speed of 75 m/min and a feed of 0.075 mm/rev: (a) rake and flank face for an uncoated tool at 8.56 mins, (b) rake and flank face for a single layer PVD coated tool at 13.91 mins, and (c) rake and flank face for a triple layer CVD coated tool at 10.39 mins	76
Figure 4.36: SEM images for a speed of 75 m/min and a feed of 0.1 mm/rev: (a) rake and flank face for an uncoated tool at 6.67 mins, (b) rake and flank face for a single layer PVD coated tool at 13.63 mins, and (c) rake and flank face for a triple layer CVD coated tool at 6.34 mins	76
Figure 4.37: SEM images for a speed of 75 m/min and a feed of 0.125 mm/rev: (a) rake and flank face for an uncoated tool at 5.94 mins, (b) rake and flank face for a single layer PVD coated tool at 8.31 mins, and (c) rake and flank face for a triple layer CVD coated tool at 8.61 mins	77
Figure 4.38: Chip image for an uncoated tool at a cutting speed of 75 m/min and a feed of 0.075 mm/rev	79
Figure 4.39: Chip image with the spot marked where the chemical analysis is done (a) chemical analysis using SEM (b, c, d) for a speed of 75 m/min and a feed of 0.075 mm/rev with an uncoated tool showing no phase transformation	79
Figure 4.40: Chip image for uncoated tool at a cutting speed of 75 m/min and a feed of 0.1 mm/rev	80
Figure 4.41: Chip image with the spot marked where the chemical analysis is done (a); chemical analysis using SEM (b, c, d) for a speed of 75 m/min and a feed of 0.1 mm/rev with an uncoated tool showing no phase transformation	80
Figure 4.42: Chip image for uncoated tool at a cutting speed of 75 m/min and a feed of 0.1 mm/rev	81
Figure 4.43: Chip image with the spot marked where the chemical analysis is done (a);	

chemical analysis using SEM (b, c, d) for a speed of 75 m/min and a feed of 0.125 mm/rev with an uncoated tool showing no phase transformation	81
Figure 4.44: Chip image for single layer PVD coated tool at a cutting speed of 75 m/min and a feed of 0.1 mm/rev	82
Figure 4.45: Chip image with the spot marked where the chemical analysis is done (a); chemical analysis using SEM (b, c, d) for a speed of 75 m/min and a feed of 0.1 mm/rev with a single layer PVD TiAlN coated tool showing no phase transformation	82
Figure 4.46: Chip image for a triple layer CVD coated tool at a cutting speed of 75 m/min and a feed of 0.075 mm/rev	83
Figure 4.47: Chip image with the spot marked where the chemical analysis is done (a); chemical analysis using SEM (b, c, d) for a speed of 75 m/min and a feed of 0.075 mm/rev with a triple layer CVD (TiCN/Al ₂ O ₃ /TiN) coated tool showing no phase transformation	83
Figure 4.48: Chip image for a triple layer CVD coated tool at a cutting speed of 75 m/min and a feed of 0.1 mm/rev	84
Figure 4.49: Chip image with the spot marked where the chemical analysis is done (a); chemical analysis using SEM (b, c, d) for a speed of 75 m/min and a feed of 0.1 mm/rev with a three layer CVD (TiCN/Al ₂ O ₃ /TiN) coated tool showing no phase transformation	84
Figure 4.50: Chip image for a triple layer CVD coated tool at a cutting speed of 75 m/min and a feed of 0.125 mm/rev	85
Figure 4.51: Chip image with the spot marked where the chemical analysis is done (a); chemical analysis using SEM using (b, c, d) for a speed of 75 m/min and a feed of 0.125 mm/rev with a three layer CVD (TiCN/Al ₂ O ₃ /TiN) coated tool showing no phase transformation	85
Figure 4.52: Forces with three different tools when the tool edge is sharp at speed 75 m/min and three different feeds (a) thrust force, (b) feed force, and (c) cutting force	87
Figure 4.53: Tool wear progression for three different tools at a speed of 75 m/min and feeds of (a) 0.075 mm/rev, (b) 0.1 mm/rev, and (c) 0.125 mm/rev	89

Figure 4.54: SEM images for a speed of 100 m/min and a feed of 0.075 mm/rev: (a) rake and flank face for an uncoated tool at 2.18 mins, (b) rake and flank face for a single layer PVD coated tool at 7.57 mins, and (c) rake and flank face for a triple layer CVD coated tool at 8.83 mins	90
Figure 4.55: SEM images for a speed of 100 m/min and a feed of 0.1 mm/rev: (a) rake and flank face for an uncoated tool at 1.98 mins, (b) rake and flank face for a single layer PVD coated tool at 6.51 mins, and (c) rake and flank face for a triple layer CVD coated tool at 8.41 mins	90
Figure 4.56: SEM images for a speed of 100 m/min and a feed of 0.1 mm/rev: (a) rake and flank face for an uncoated tool at 1.56 mins, (b) rake and flank face for a single layer PVD coated tool at 3.80 mins, and (c) rake and flank face for a triple layer CVD coated tool at 7.64 mins	91
Figure 4.57: Chip images for the uncoated tool at a speed of 100 m/min and a feed of 0.075 mm/rev	92
Figure 4.58: Chip image with the spot marked where the chemical analysis is done (a); chemical analysis using SEM (b, c, d) for a speed of 100 m/min and a feed of 0.075 mm/rev with an uncoated tool showing no phase transformation	92
Figure 4.59: Chip images for a single layer PVD tool at a speed of 100 m/min and a feed of 0.1 mm/rev.....	93
Figure 4.60: Chip image with the spot marked where the chemical analysis is done (a); chemical analysis using SEM (b, c, d) for a speed of 100 m/min and a feed of 0.1 mm/rev with a single layer PVD TiAlN coated tool showing no phase transformation.....	93
Figure 4.61: Forces with three different tools when the tool edge is sharp at speed 100 m/min and three different feeds (a) thrust force, (b) feed force, and (c) cutting force	95
Figure 4.62: Tool wear progression for three different tools at a 100 m/min speed and feeds of (a) 0.075 mm/rev, (b) 0.1 mm/rev, and (c) 0.125 mm/rev	99
Figure 4.63: Effect of cutting speed and feed on surface roughness when the tool edge is sharp.....	100
Figure 4.64: Effect of cutting speed and feed on surface roughness when the tool edge	

reaches tool failure criteria.....	101
Figure 4.65: Showing nose wear for CVD coated triple layer (TiCN/Al ₂ O ₃ /TiN) at a speed of 50 m/min and a feed of 0.1 mm/rev.....	102
Figure 5.1: Tool wear mechanisms for all three tools	103
Figure 5.2: Optimum cutting conditions in terms of tool life for all three tools.....	105
Figure 5.3: Optimum cutting conditions in terms of surface roughness Ra (μm) for all three tools.....	105

List of Tables

Table 1.1: Different nickel alloys with their applications [4].....	3
Table 2.1: Chemical composition of nickel-based super alloy Inconel 718 [11]	8
Table 2.2: Summary of structure-controlling phases in typical nickel-base super alloys	10
Table 2.3: Properties of Inconel 718 [11]	12
Table 3.1 Properties of uncoated and coated tools used during the orthogonal and oblique finish turning operations	31
Table 3.2: Machining conditions tested in Phase I of the experimental work (orthogonal cutting) with 2 mm width of cut	36
Table 3.3: Machining conditions tested in Phase I of the experimental work (orthogonal cutting) with 3 mm width of cut	37
Table 3.4: Machining conditions tested in Phase II of the experimental work (oblique finish turning) with a constant depth of cut of 0.25 mm.....	37
Table 4.1: Comparative Analysis of the percentage increase of $\tan \phi$ with the percentage increase of feed	44
Table 4.2: Effect of shear angle with an increase in the cutting speed.....	47
Table 4.3: Effect of width of cut on forces, cutting temperature, and torque at a cutting speed of 10 m/min and feed of 0.3 mm/rev	52
Table 4.4: Effect of width of cut on chip thickness and width of chip at a cutting speed of 10 m/min and feed of 0.3 mm/rev.....	54
Table 4.5: Effect of width of cut on shear stress, shear strain, and strain rate at a cutting speed of 10 m/min and feed of 0.3 mm/rev	58
Table 4.6: Effect of shear angle with an increase in the cutting speed	58
Table 4.7: Effect of width of cut on contact length with feed 0.3 mm/rev	59
Table 4.8: Micro-hardness measurement for a cutting speed of 50 m/min	69
Table 4.9: Time duration at which three regions formed at cutting speed of 50 m/min...	73
Table 4.10: Micro-hardness measurement for a cutting speed of 75 m/min	78
Table 4.11: Time duration at which three regions formed at cutting speed of 75 m/min.	86
Table 4.12: Micro-hardness measurement for a cutting speed of 100 m/min	92

Table 4.13: Comparison of the micro-hardness values of the chip at three different cutting speeds and feeds for uncoated tool	94
Table 4.14: Comparison of the micro-hardness values of the chip at three different cutting speeds and feeds for single layer PVD coated tool.....	96
Table 4.15: Comparison of the micro-hardness values of the chip at three different cutting speeds and feeds for triple layer CVD coated tool	96
Table 4.16: Time duration at which three regions formed at cutting speed of 100 m/min	97
Table 4.17: Ideal Surface Roughness values for three different feeds	100

1.1 General

Nickel based alloys especially Inconel 718, are extremely important in the aerospace industry. Owing to its high-temperature mechanical properties, such as resistance to oxidation and corrosion, high tensile stress, and rupture stress, etc., it has been widely applied in the manufacture of finished components in the aerospace industry and nuclear reactors. In addition, they also are used in marine, industrial, and vehicular gas turbines, space vehicles, rocket engines, submarines, steam power plants, petrochemical equipment, and other high-temperature applications. However, the combined effects of poor thermal properties, high-temperature strength, a tendency to severe work hardening, and high tool workpiece affinity make the machining of Inconel 718 very difficult because these properties result in high temperature, stress, and a thick adhering layer at the tool-work interface during machining [1, 2, 3]. Therefore, it is highly important to investigate the machinability of Inconel 718 for rough and finish turning operations. Figure 1.1 shows the classification of super alloys used in various industries.

Different nickel based alloys available in a wide variety of composition are illustrated in Table 1.1.

The term *machinability* describes the ease of machining. It is the property of a material that governs the ease or difficulty with which a material can be machined using a cutting tool [33]. Machinability of a material is usually defined in terms of three factors [3]:

- (1) Tool life and tool wear.
- (2) Power and force requirements, which include cutting forces with temperature.
- (3) Surface finish and integrity of the machined part.

A material with good machinability will produce small chips, need low cutting forces and energy expenditure, be capable of being machined quickly, and give a long tool life. Ductile and soft materials have poor machinability. A relative measure of machinability is given by the machinability index. It is based on tool life, surface finish, cutting force and power consumption. For e.g., machinability index based on cutting speed needed to give a prescribed tool life: $M_T = V_{T,1}/V_{T,2}$, where T is the time (60 min), V is the cutting speed and suffix 1 refers to the tool material and suffix 2 refers to the reference tool material (steel) [4]. The higher the machinability index, the better the machinability.

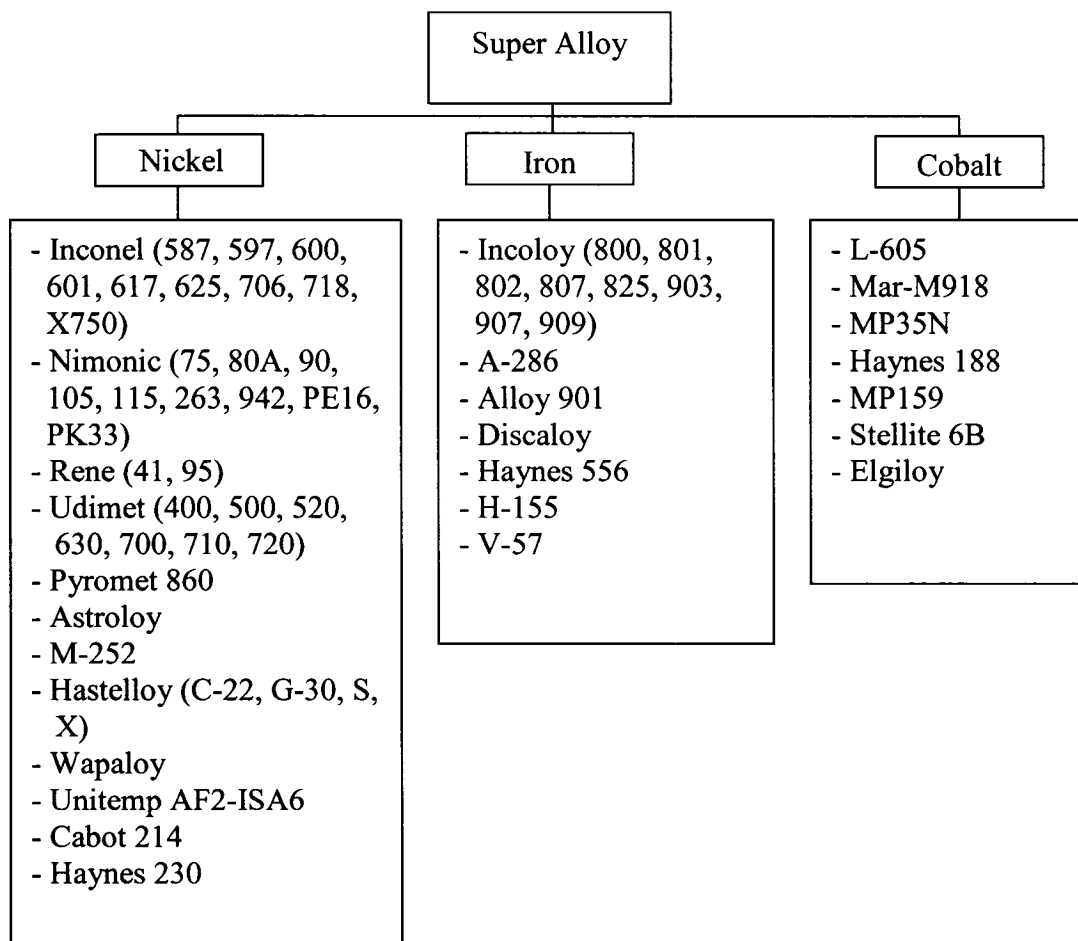


Figure 1.1: Classification of super alloys [5]

Nickel based super alloys have some characteristics that are responsible for poor machinability, which are summarized as follows [6-9]:

- (i) A major part of their strength is maintained during machining due to their high temperature properties.

Table 1.1: Different nickel alloys with their applications [4]

Alloy	Condition	Ultimate Tensile Strength (MPa)	Yield Strength (MPa)	Elongation in 50 mm (%)	Typical Applications
Astroloy	Wrought	770	690	25	Forgings for high temperature
Hastelloy X	Wrought	255	180	50	Jet engine sheet parts
IN-100	Cast	885	695	6	Jet engine blades and wheels
IN-102	Wrought	215	200	10	Super heater and jet engine parts
Inconel 625	Wrought	285	275	125	Aircraft engines and structures, chemical processing equipment
Inconel 718	Wrought	340	330	88	Jet engine and rocket parts
MAR-M-200	Cast	840	760	4	Jet engine blades
MAR-M-432	Cast	730	605	8	Integrally cast turbine wheels
Rene 41	Wrought	620	550	19	Jet engine parts
Udimet 700	Wrought	690	635	27	Jet engine parts
Waspaloy	Wrought	525	515	35	Jet engine parts

- (ii) Work hardening occurs rapidly during machining, which is a major factor contributing to notch wear at the tool nose and/or depth of cut.
- (iii) Cutting tools suffer high abrasive wear owing to the presence of hard abrasive carbides in the superalloy.
- (iv) Chemical reaction occurs at high cutting temperatures when machining with commercially available cutting tool materials, leading to a high diffusion wear rate.
- (v) Welding or adhesion of nickel alloys onto the cutting tool frequently occur during machining, causing severe notching as well as spalling on the tool rake face due to the consequent pull-out of the tool materials.

- (vi) A tough and continuous chip is produced, which is difficult to control during machining, thereby contributing to the degradation of the cutting tool by seizure and cratering.
- (vii) The poor thermal diffusivity of nickel-based alloys often generates high temperature at the tool tip as well as high thermal gradients in the cutting tool.

1.2 Thesis Objective

The objective of this research is twofold. The first objective is to generate experimental data for the future identification of the constitutive laws of materials. The constitutive law determines the flow stress of metals, which depends on strain, strain rate, and temperature [10]. The second objective is to assess the machinability of Inconel 718 under a finish turning operation, which includes the evaluation of the following:

- (i) Tool wear mechanisms.
- (ii) Cutting force measurements.
- (iii) Chip formation and chip morphology.
- (iv) Tool wear progression with time.
- (v) Surface Roughness of the machined surface.

This research was affiliated with the Aerospace Manufacturing Technology Centre-National Research Council (AMTC-NRC). The experimental work was done at the AMTC-NRC research facility on the Boehringer NG 200 (2 spindles and 6 axes) CNC machine. Also, for the chip analysis, the specimens were prepared at AMTC-NRC. Scanning Electron Microscopy was done at the Materials and Mining Department at McGill University.

1.3 Thesis Scope

The following describe the scope of the thesis work:

- (i) To evaluate the cutting parameters that can yield best tool life and surface roughness
- (ii) To measure the cutting forces during the online finish turning operation and tool wear and surface roughness during in situ operation

- (iii) To understand the tool wear progression as a function of time, cutting forces and surface roughness as a function of cutting speed and feed variation
- (iv) To evaluate the performance of uncoated tools, single layer pressure vapor deposition (PVD) (TiAlN = 3 μm) coated tools, and triple layer chemical vapor deposition (CVD) (TiCN/Al₂O₃/TiN = 15 μm) coated tools
- (v) To study the chip formation process during the finish turning operation

1.4 Thesis Organization

The thesis comprises of five chapters. Chapter 2 is an in-depth critical literature review of the previous research published in the area of the machinability of Inconel 718 and Nickel-based alloys.

Chapter 3 describes the experimental setup used to evaluate the machinability of Inconel 718. It describes in detail the procedures adapted to measure cutting forces, tool wear and to study chip morphology. A test procedure according to International Organization for Standardization (ISO) was developed and implemented during the course of this research.

Chapter 4 presents the results obtained in the course of the present study. Various aspects such as tool life, cutting forces, chip morphology, and surface finish were investigated with respect to varying cutting conditions, namely cutting speeds and feeds.

Chapter 5 lays out the conclusion of the present research and proposes recommendations for future work.

This chapter reviews the literature on the machining of Inconel 718, mostly the studies done on the finish turning operation. The review begins with studies on the principles of metal cutting and continues with the research done on the machining of Inconel 718, including cutting forces, tool life and tool wear, cutting temperature, surface roughness, and chip formation.

2.1 Metal Cutting Principles

The principle of metal cutting will be introduced to explain the analytical approach used to understand the process. The “cutting process” is basically a removal of material from the surface of the workpiece in the form of chips as illustrated in Figure 2.1(a). The formation of chips is represented by a two dimensional model illustrated in Figure 2.1(b).

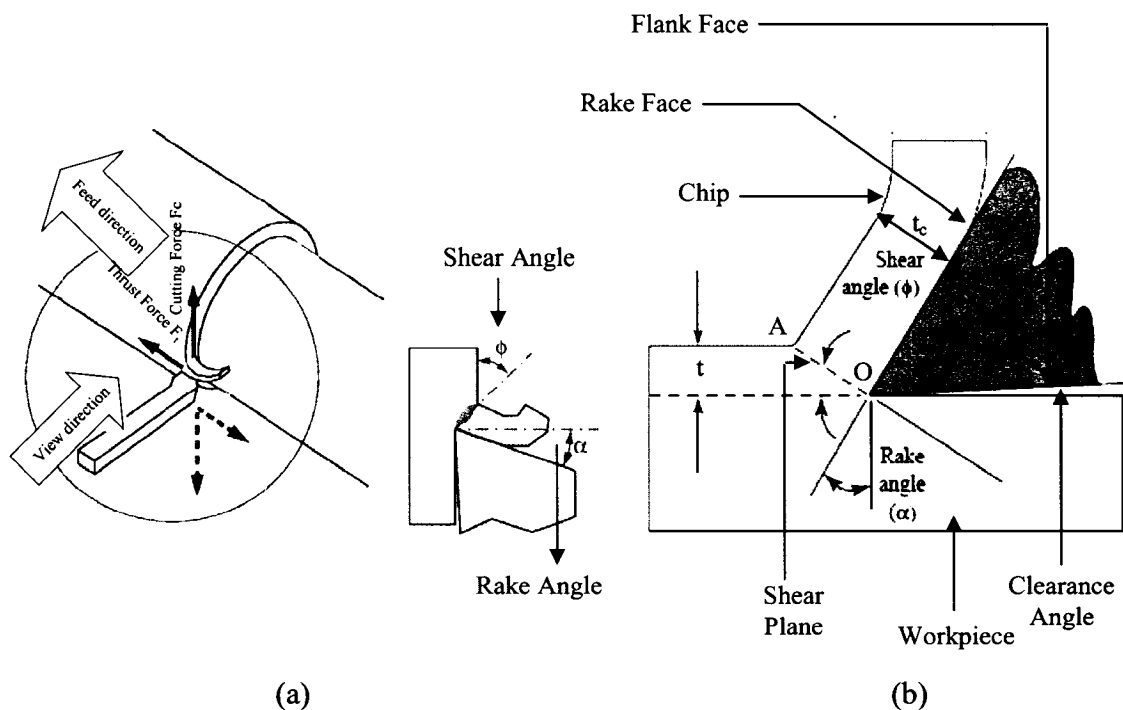


Figure 2.1: Orthogonal cutting mechanism: (a) basic turning operation, (b) two dimensional orthogonal turning.

In this model, a tool moves along the workpiece at a certain velocity (V). The depth of cut is identified as t . A chip is produced just ahead of the tool by the shearing of the material continuously along the shear plane (OA). The shear angle (ϕ), which is the angle formed between the cutting speed direction and the shear plane (1) [3], can be determined using equation 2.1:

$$\tan \phi = \frac{r \cos \alpha}{1 - r \sin \alpha} \quad (2.1)$$

where r represents the cutting ratio, and α is the rake angle shown in Figure 2.1(b). The “cutting ratio,” which is the ratio of feed (t) to the chip thickness (t_c), is determined using equation (2.2) [3]:

$$r = \frac{t}{t_c} \quad (2.2)$$

By knowing the shear angle (ϕ), it is possible to evaluate the shear stress (τ), the strain (γ), and the strain rate ($\dot{\gamma}$) of the material. Equations 2.3 to 2.5 can be used to calculate these parameters [3]:

$$\tau = \frac{(F_c \cos \phi - F_t \sin \phi) \sin \phi}{bt} \quad (2.3)$$

$$\gamma = \frac{\cos \alpha}{\sin \phi \cos(\phi - \alpha)} \quad (2.4)$$

$$\dot{\gamma} = \frac{\cos \alpha V_c}{\cos(\phi - \alpha) \Delta y} \quad (2.5)$$

In these equations, b represents the width of cut, and t is the depth of cut. F_c is the cutting force acting in the direction of the cutting speed (V_c) and F_t is the thrust force acting in the direction normal to the cutting velocity, i.e., perpendicular to the workpiece, which are experimentally measured using a dynamometer. V_c represents the cutting speed (m/min), and Δy is the spacing of successive shear planes [3].

2.2 Metallurgy of Inconel 718

The weight percentage chemical composition of Inconel 718 used during the experiment is given in the Table 2.1. Inconel 718 is a precipitation-strengthened (Ni_3Nb or γ'') nickel-iron base super alloy that contains 5.1-5.3 wt % Nb [6].

Table 2.1: Chemical composition of nickel-based super alloy Inconel 718 [11]

Element	Ni	Fe	Cr	Al	B	C	Co	Cu	Mn	Mo	Nb	P	S	Si	Ti
%Wt	52.5	18	19	0.5	0.006	0.08	1	0.3	0.35	3	5.1	0.015	0.015	0.35	0.9

The FCC austenite matrix, γ , is a solid solution of Fe, Cr, and Mo in nickel. However, solid solution strengthening is not considered to be a major factor for strengthening at elevated temperatures [6, 12]. The presence of carbides is expected to provide very little strengthening. The small amount of carbon present is used as a deoxidant and forms the primary MC-type carbides (basically with Ti, Mo, and Nb) that help to refine grain size during hot working and heat treating, and that also help to form a small amount of grain boundary carbides (predominantly M_{23}C_6 type with Cr) [12, 13].

The various precipitates that form in Inconel 718 under appropriate heat treating conditions are [6]:

- i) A body centered tetragonal ordered structure, Ni_3Nb meta-stable precipitate (A_3B -type compound) or γ'' phase is coherent with and uniformly distributed in the γ matrix. About 20 vol % of this phase is present in the alloy under fully

treated and aged conditions [14]. Figure 2.2 shows the crystallography of the γ'' phase [15,16].

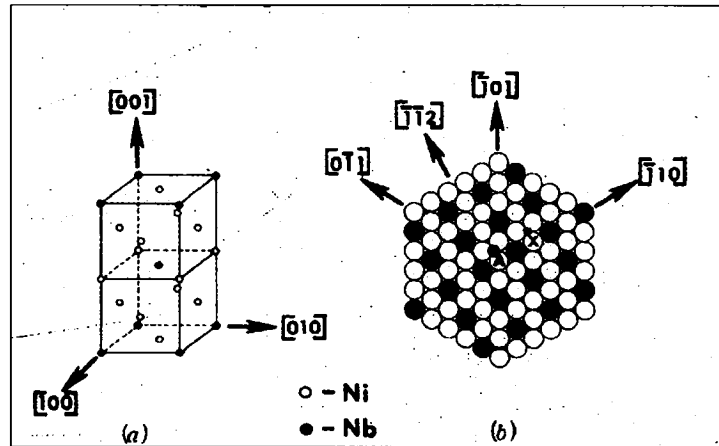


Figure 2.2: Crystallography of the γ'' phase, after Nevitt (a) unit cell, (b) close-packed plane [15, 16]

- ii) A face-centered cubic Ni_3 (Al, Ti) meta-stable precipitate or γ' phase is present in a small amount of fine ordered. The γ' phase is spherical in shape, rich in Al and Ti, and coherent with the γ matrix.
- iii) An orthorhombic Ni_3Nb phase or δ phase decorates the grain boundaries. The δ phase is used to pin the grain boundaries and inhibit grain growth during solution heat treatment.

From [3], it has been found that mostly two phases are dominant: γ'' phase and δ phase, along with some M_{23}C_6 type with Cr, which are shown in Table 2.2 [6].

Also, in addition to the above mentioned precipitates, Inconel 718 also is capable of performing an intragranular platelet or Widmanstatten array of η phase, HCP structured Ni_3Ti [13].

In view of the uniform distribution of the fine size γ'' and γ' in the matrix, an optical examination of wrought Inconel 718 generally reveals austenite matrix with δ platelets decorating the grain boundaries and the presence of isolated MC carbides [17].

Figure 2.3 shows the pseudo-equilibrium diagram for Inconel 718, depicting the stability of various phases at different temperatures. Figure 2.4 shows the Time-Temperature-Precipitation (T-T-P) diagram, showing the typical heat treatment cycles for solution treatment and aging for Inconel 718 after Muzyka [13].

Table 2.2: Summary of structure-controlling phases in typical nickel-base super alloys

Alloy	Phase	Solvus Temperature (Limit of Stability)
A-286	γ'	1525 °F (855 °C)
	η (Ni ₃ Ti)	1625 °F (915 °C)
718	γ''	1625 °F (915 °C)
	δ (Ni ₃ Cb)	1825 °F (995 °C)
706	γ'' or γ'	1625 °F (885 °C)
	η (Ni ₃ Ti) and/or (Ni ₃ Cb)	1750 °F (955 °C)
901	γ'	1725 °F (940 °C)
	η (Ni ₃ Ti)	1825 °F (995 °C)
Pyromet 860	γ'	1750 °F (955 °C)
	η (Ni ₃ Ti)	1825 °F (955 °C)

The primary strengthening mechanism for Inconel 718 is age hardening due to the presence of a fine uniform metastable γ'' precipitate distributed throughout the matrix [56]. At room temperature, slip in Inconel 718 is heterogeneous in nature and confined to planar bands of varying widths, with dislocation pairs in the matrix and no dislocation structure observable in γ'' particles, which are sheared extensively [18]. At higher temperatures, the deformation is homogeneously distributed and is comprised of a uniform tangle of dislocations [18]. Also, thermo-mechanical properties play an important role in shear localization [19]. Table 2.3 gives some physical and mechanical properties of Inconel 718 [11].

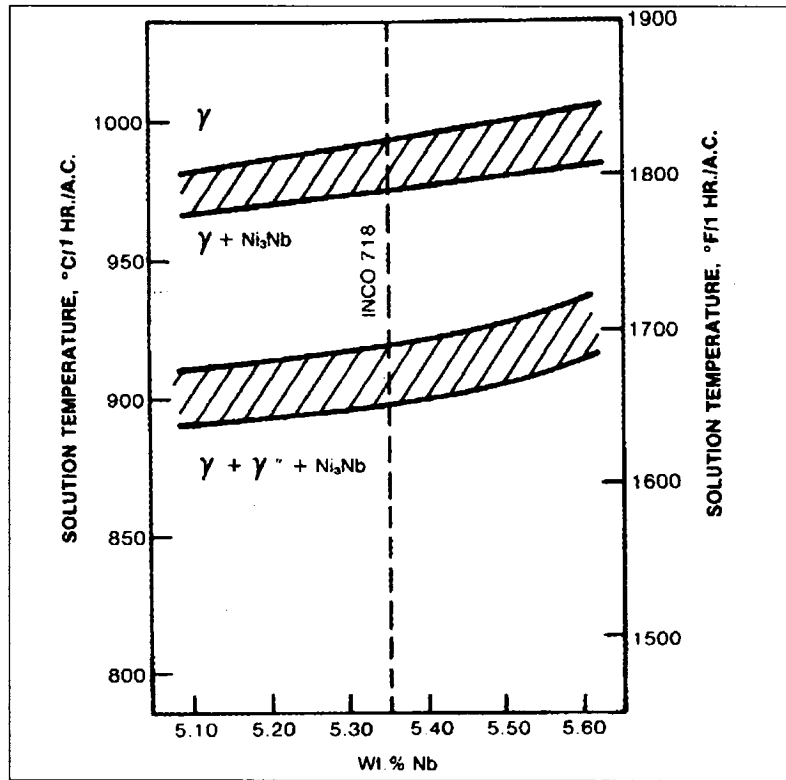


Figure 2.3: Pseudo-equilibrium diagram for Inconel 718 showing stability of various phases at different temperatures [6, 12]

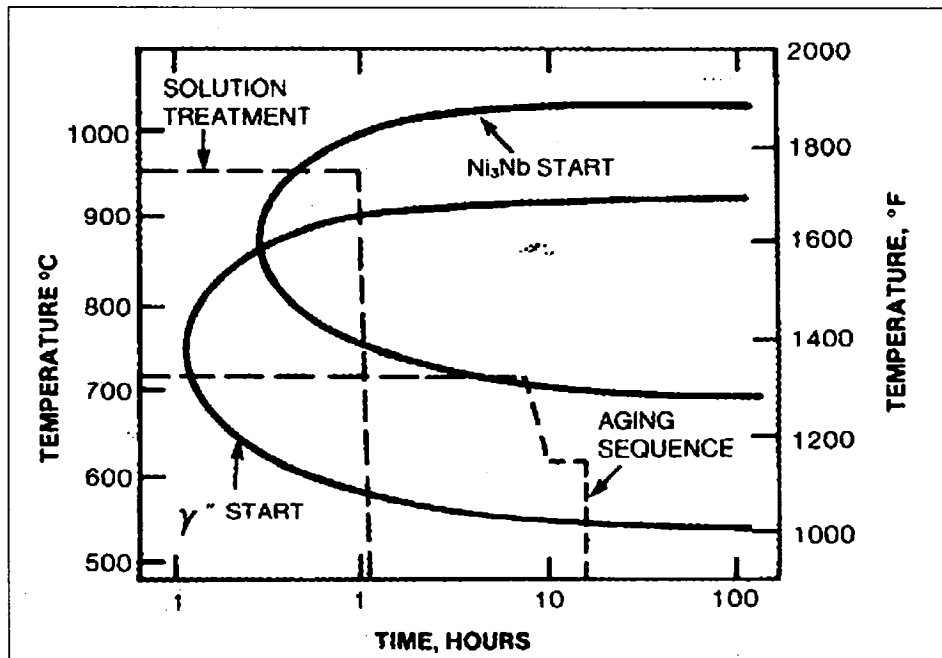


Figure 2.4: Time-Temperature-Precipitation (T-T-P) diagram for Inconel 718 showing the typical heat treatment cycle [6, 12]

Table 2.3: Properties of Inconel 718 [11]

Density (g/cm ³)	8.19
Melting Range (°C)	1260-1338
Ultimate Tensile Strength (MPa)	1375
Yield Tensile Strength (MPa)	1100
Elongation at break (%)	25
Coefficient of thermal expansion (µm/m°C)	13
Heat Capacity (J/g°C)	0.435
Thermal Conductivity (W/mK)	11.4

2.3 Machining Research on Inconel 718

The information presented in this section mainly deals with the experimental results obtained from the turning tests on Inconel 718. A large amount of information exists pertaining to the machining of Inconel 718. Most of the experimental results in the literature are based on the roughing operation, where a high depth of cut is involved, for example, between 1 to 3 mm. This information serves as a reference point for the possible difficulties that can be encountered when machining Inconel 718—pertains to the *machinability assessment* of cutting forces, tool wear and tool life, cutting temperatures, surface finish, and chip formation process.

2.3.1 Cutting Forces

Research has been done on many cutting conditions, and the forces involved have been measured. Most researchers measure the cutting forces, and explain their significance, but not for the finishing operation where the depth of cut is much less.

Rahman et al. [20] measured the cutting forces for Inconel 718 under wet cutting conditions. The two tools used for the cutting operation had a rhomboid shaped geometry: (i) K type substrate, TiN PVD coated cemented carbide grade EH20Z-UP and (ii) Multi Al₂O₃ CVD coated cemented carbide grade AC25. Figure 2.5 shows the image

for the rhomboid shaped geometry tool. The cutting parameters tested were: (i) cutting speed ranges from 30 m/min to 50 m/min, (ii) feed ranges from 0.2 mm/rev to 0.4 mm/rev, and (iii) a constant depth of cut of 2 mm. These researchers found that the cutting forces and axial forces increase as feed rate and cutting time increase. The cutting force increases, on an average by 600 N, as feed rate increases from 0.2 mm/rev to 0.4 mm/rev. No significant change was found in cutting force as cutting speed increased from 30 m/min to 40 m/min. Also, a CVD coated tool generates higher cutting forces compared to a PVD coated tool. The results obtained agree with the conclusion drawn by Yeo [21] for machining Inconel 718 using cemented carbide tools.

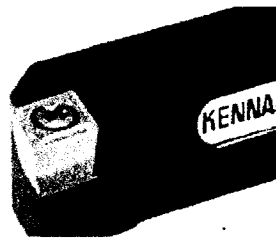


Figure 2.5: Rhomboid shape geometry

Ezugwu et al. [23] also measured the component forces (cutting force, F_c , feed force, F_f , and radial force, F_r) under wet cutting conditions for Inconel 718. A single layer (TiN) PVD coated carbide tool and a multilayer (TiN/TiCN/TiN) PVD coated carbide tool were used, having a rhomboid shape geometry for the machining trials. The cutting parameters tested were: (i) cutting speed ranges from 29 m/min and 42 m/min, (ii) feed ranges from 0.13 mm/rev and 0.25 mm/rev, and (iii) a constant depth of cut of 2 mm. The researchers observed a significant reduction in component forces when machining at a higher cutting speed and a lower feed. This is due to the reduction on the tool-chip and tool-workpiece contact lengths/areas caused by the thinner chips produced and the softening of the work material in the shear zone by the heat generated at higher speed conditions.

As well, Ezugwu et al. [32] measured the component forces (cutting force, F_c , feed force, F_f , and radial force, F_r) under wet cutting conditions for the nickel-based C-

263 alloy. The two types of tools used had a rhomboid shaped geometry: (i) a single layer (TiAlN) PVD coated carbide tool and (ii) a multilayer (TiN/TiCN/TiN) PVD coated carbide tool. The cutting parameters tested were: (i) cutting speed ranges from 54 m/min and 68 m/min, (ii) a constant feed of 0.076 mm/rev, and (iii) a depth of cut ranging from 0.635 mm and 1.25 mm. Contrary to expectation, the researchers observed the feed forces to be higher than the cutting forces, particularly towards the end of the machining. The component forces also were higher when machining at a higher cutting speed. The TiAlN coated tool gave higher component forces than the TiN/TiCN/TiN coated tool during machining. This result is probably due to the adverse effect of the burr formation and work hardening of the workpiece material during prolonged machining.

Chodhury et al. [33] measured the cutting forces when machining Inconel 718 under dry cutting conditions. The two types of tools used had a rhomboid shaped geometry: (i) an uncoated carbide tool, grade H13A and (ii) a coated carbide tool ($\text{Al}_2\text{O}_3/\text{TiC}$), grade GC3015. The cutting parameters tested were: (i) cutting speed ranges from 7 m/min to 45 m/min, (ii) feed ranges from 0.12 mm/rev to 0.3 mm/rev, and (iii) depth of cut ranges from 0.8 mm to 2 mm. The researchers observed that the cutting force decreases when the cutting speed increases, but increases when the feed or depth of cut increases.

Alauddin et al. [22] measured the cutting forces in the end milling of Inconel 718 under dry cutting conditions. An uncoated tungsten carbide tool was used. The cutting parameters tested were: (i) cutting speed ranges from 11 m/min to 25 m/min, (ii) feed ranges from 10 mm/min to 65 mm/min, and (iii) axial depth of cut ranging from 0.4 mm to 2 mm. The researchers observed that cutting forces decrease as the cutting speed increases, which can be attributed to the following: (i) as cutting speed decreases, the shear angle also decreases giving rise to a long shear plane for a fixed shear strength (an increase in shear-plane area increases the shear forces required to produce the stress required for deformation) and (ii) at a low cutting speed, the friction coefficient increases, hence increasing the cutting forces. The researchers also observed that the cutting force

increases as the feed rate and the axial depth of cut increase for up and down end milling. This result is due to the size of cut per tooth increasing as the axial depth of cut increases.

Liu et al. [30] measured the cutting forces in the milling of Inconel 718 under dry and wet cutting conditions. A triple layer (TiCN/Al₂O₃/TiN) coated carbide tool was used. The cutting parameters tested were: (i) cutting speed ranges from 30 m/min to 120 m/min, (ii) feed ranges from 0.03 mm/tooth to 0.25 mm/tooth, and (iii) axial depth of cut ranging from 2 mm to 6 mm, and radial depth of cut ranging from 1 mm to 6 mm. The researchers observed that under a dry cutting condition, the cutting forces decrease appreciably as the cutting speed increases from 30 m/min to 60 m/min. However, the cutting forces increase as the cutting speed exceeds 60 m/min to 120 m/min. The phenomenon may be attributed to the following two effects that take place with an increase in the cutting speed from 30 m/min to 60 m/min: (1) increase in the shear angle will decrease the shear-plane area, which in turn, decreases the shear force to produce the stress for deformation, and (2) increase in the cutting temperature results in decrease of friction coefficient. Due to these two effects, the cutting forces are decreasing. However, when the cutting speed increases from 60 m/min to 120 m/min, the cutting force increases, which may be owing to the high-frequency impact force. This high frequency impact force could be dominant than the above two effects at higher cutting speeds beyond 60 m/min. The researchers also observed that the cutting forces increase as the feed rate and the axial and radial depth of cut increase. The cutting forces observed under wet cutting conditions were lower than those found during dry cutting conditions.

Uhlmann et al. [24] measured the cutting forces created when a polycrystalline cubic boron nitride (PCBN) tool, with chamfered and round cutting edge geometry, was used for cutting Inconel 718 under wet cutting conditions. The cutting parameters tested were: (i) cutting speed ranges from 300 m/min to 1250 m/min, (ii) a constant feed of 0.1 mm/rev, and (iii) a constant depth of cut of 0.5 mm. The researchers observed lower cutting force components (cutting force F_c , feed force F_f , and radial force F_r) in the range of 50 to 150 N with the rounded cutting edge geometry.

Ezugwu et al. [25] measured the cutting forces created when a Nano-Ceramic cutting tool was used to cut Inconel 718 under wet cutting conditions. In their experiments, three different types of ceramic tools were used, all having square shaped cutting edge geometry. The tools used were: (i) $\text{Al}_2\text{O}_3+\text{SiC}$ (ii) $\text{Al}_2\text{O}_3+\text{TiCN}+\text{ZrO}_2$, and (iii) $\text{Si}_3\text{N}_4+\text{SiC}$. The cutting parameters tested were: (i) cutting speed ranges from 230 m/min to 270 m/min, (ii) feed ranges from 0.125 mm/rev to 0.15 mm/rev, and (iii) depth of cut ranges from 1.5 to 3 mm. The researchers observed that the cutting forces decreased when the cutting speed of an alumina based micron grain tool or nano-grain ceramic tool increased. On the other hand, the cutting forces generated while machining with the Si_3N_4 based nano-grain tool increased with speed. This result is due to the effect of temperature on the softening and/or super plasticity of the ceramic tools used for machining. A further increase in the cutting speed from 250 m/min to 270 m/min generates higher temperatures that are beyond the critical value, promoting a super plastic flow that causes deformation of the cutting edge, and the consequent alteration of the cutting edge geometry.

Schlauer et al. [26] measured the cutting forces in face grooving—which gives quasi-orthogonal cutting—for Inconel 718 under wet cutting conditions using an alumina ceramic tool with a wide chamfer cutting edge. The cutting parameters tested were: (i) cutting speed ranges from 10 m/min to 810 m/min and (ii) feed ranges from 0.01 mm/rev to 0.11 mm/rev. The researchers show that an increase in feed or a decrease in speed causes the cutting forces to increase—a similar observation to the data published in [27]. The result for feed force also was similar to the result for cutting force, and at a lower feed of 0.01 mm, the feed force exceeds the cutting force at all cutting speeds by a factor of 1.2 to 1.6.

S. M. Darwish [28] also measured the cutting forces for Inconel 718 using cubic boron nitride (CBN) and ceramic tools under dry cutting conditions. The cutting parameters tested were: (i) cutting speed ranges from 32 m/min to 125 m/min, (ii) feed ranges from 0.075 mm/rev to 0.6 mm/rev, and (iii) depth of cut ranges from 0.5 mm to 2 mm. He observed that the cutting forces associated with ceramic tools were always lower

than those associated with CBN tools. He also observed that the cutting forces increase when the cutting speed increases, which may be related to the chipping of the cutting tool associated with a higher cutting speed. Contradictory results were reported by Arunachalam et al. [29, 34], who measured the cutting forces with CBN and ceramic tools, having a square and round shaped geometry, under wet cutting conditions. The cutting parameters tested were: (i) cutting speed ranges from 150 m/min to 375 m/min, (ii) constant feed of 0.15 mm/rev, and (iii) a constant depth of cut of 0.5 mm to 1.0 mm. The researchers observed that as the cutting speed increases, the cutting forces decrease. The reason for this result is related to temperature generation, for example, as cutting speed increases, machining becomes more adiabatic. The heat generated in the shear zone cannot be conducted away during the very short time in which the metal passes through this zone, so the temperature rise softens the metal aiding grain boundary dislocation and thus reduces the cutting forces.

Ezugwu et al. [31] measured the cutting forces for Inconel 718 by using a whisker reinforced alumina ceramic tool, with round shaped cutting edge geometry, under wet cutting conditions. The cutting parameters tested were: (i) cutting speed ranges from 200 m/min to 300 m/min, (ii) feed ranges from 0.1 mm/rev to 0.2 mm/rev, (iii) coolant supply pressure ranges from 11 MPa to 20.3 MPa, and (iv) a constant depth of cut of 0.5 mm. The researchers observed that at higher coolant supply pressures for finishing conditions, lower cutting forces (lower frictional forces) are generated due to the improved cooling and lubrication at the cutting interface, and also due to the chip segmentation caused by the high-pressure coolant jet.

2.3.2 Tool Life and Tool Wear

Research has been done on a variety of tools and geometry to cut Inconel 718 during various cutting conditions. Different types of tools such as carbides, ceramic, and cubic boron nitride have been tested to cut this material. Nickel-based alloys have poor machinability, and they work-harden during machining, resulting in the poorest tool life. Of the WC carbide-based tools, those having fine grain size ($< 1 \mu\text{m}$) and straight WC-Co composition work best. Acceptable tool life is achievable when using this type of tool

provided that the average flank wear is less than a predefined value when the cutting speed is kept approximately around 50 m/min.

Rahman et al. [20] reported a 42 min tool life when an EH20-UP (PVD coated) carbide tool was employed at a cutting speed of 30 m/min, a 0.2 mm/rev feed, and a side cutting edge angle of 45°. The tool life of the EH20-UP tool was mainly dependent on average flank wear ($> 300 \mu\text{m}$), whereas for the AC25 (CVD coated) carbide tool, the tool life criterion was depth of cut (DOC) notch wear ($> 800 \mu\text{m}$).

Ezugwu et al. [23] reported a 48 min tool life for Inconel 718 when a multilayer (TiN/TiCN/TiN) PVD coated carbide tool was employed at a cutting speed of 29 mm/min and a 0.25 mm/rev feed. The tool failure criterion was average flank wear ($\geq 400 \mu\text{m}$). The researchers observed that a multilayer PVD coated tool performed better than a single layer PVD coated tool. Flank wear was the dominant tool failure mode at cutting speeds up to 42 mm/min. The multilayer (TiN/TiCN/TiN) PVD coated carbide tool gives a tool life of 30 min at a cutting speed of 42 mm/min, a feed of 0.13 mm/rev, and a 1.0 mm depth of cut. When machining Inconel 718A, a lower flank wear rate also was reported for the multilayer coated carbide tool. Also, Ezugwu et al. [44] reported a 68 min when a multilayer (TiN/TiCN/TiN) PVD coated carbide tool was employed at a cutting speed of 32 m/min, a 0.13 mm/rev feed, and a 1.00 mm depth of cut. Again the tool failure criterion was average flank wear.

Ezugwu et al. [32] reported a 50 min tool life—for cutting nickel alloy C-263—when single layer PVD TiAlN and multilayer PVD TiN/TiCN/TiN coated carbide tools were employed at a cutting speed of 54 m/min and a 0.635 mm depth cut. The tool rejection criterion was average flank wear ($400 \mu\text{m}$). However, at a higher depth cut of 2.54 mm, the triple layer TiN/TiCN/TiN coated tools outperformed the single layer TiAlN coated tools by about four times in terms of the length of tool life. Even at higher speeds, the triple layer tool performed better than the single layer tools.

Chodhury et al. [33] reported on the tool life of both coated and uncoated carbide tools (having a rhomboid shaped geometry) used to cut Inconel 718 at different dry cutting conditions. Their results showed that in most of the cutting conditions, the tool life of the uncoated carbide tool was better than the coated carbide tool.

Jindal et al. [36] reported on the tool life of coated carbide tools (having a rhomboid shaped geometry) that were used to cut Inconel 718 under wet cutting conditions. The coated carbide tools used were: (i) PVD TiN, (ii) PVD TiCN, and (iii) PVD TiAlN. The cutting parameters tested were: (i) cutting speeds: 46 m/min and 76 m/min, (ii) a constant feed of 0.15 mm/rev, and (iii) a constant depth of cut of 1.5 mm. At both speeds, TiAlN and TiCN coated tools performed significantly better than tools with TiN coatings. The researchers also found that the TiAlN coated tool showed excellent resistance to maximum flank wear. In regards to the coated TiAlN tool, they reported a tool life of 18 min at a cutting speed of 46 m/min, and a tool life of 6 min at a cutting speed of 76 m/min. The end of tool life for all three coated carbide tools was dictated by maximum flank wear/nose wear (400 μm)

Ducros et al. [39] studied the TiN/AlTiN and CrN/TiN nano-layer coatings deposited on a cemented carbide tool (having a rhomboid shaped geometry) that used lubrication while cutting Inconel 718. The performance of the nano-layer coated tools was compared to multilayer coated and uncoated tools. The researchers reported a 7.5 min tool life when a nano-layer coated carbide tool was employed at a cutting speed of 40 m/min, a 0.2 mm/rev feed, and a 1.5 mm depth of cut. Again, the tool rejection criterion was uniform flank wear below a predefined value.

Prengel et al. [41] reported on the tool life of coated carbide tools used to cut Inconel 718 under wet cutting conditions. Three different types of coated tools were used having rhomboid shape geometry: (i) TiAlN-monolayer PVD coated carbide tool, (ii) TiAlN-multilayer PVD coated carbide tool, and (iii) TiN/TiCN/TiAlN-multilayer PVD coated carbide tool. The cutting parameters tested were: (i) cutting speed: 61 m/min and 76.2 m/min, (ii) feed: 0.125 mm/rev and 0.15 mm/rev, and (iii) depth of cut: 1.27 mm and

1.52 mm. The tool life was 7 min for TiAlN-multilayer tools, and 6 min for TiAlN-monolayer tools. The TiAlN-multilayer coating performed better than the TiAlN-monolayer and TiN/TiCN/TiAlN-multilayer coating at a high cutting speed. The main tool failure criterion was abrasive nose wear (400 μm) accompanied by plastic deformation.

Several wear mechanisms have been identified as responsible for the deterioration of carbide tools when machining Inconel 718: abrasive wear, adhesion of the workpiece material on the rake and flank faces, plastic deformation, BUE formation, chipping and breakage, flaking of tool materials close to the cutting edge or on the rake face, and crater wear on or very close to the cutting edge [35, 38, 39, 40, 41, 43, 44, 45].

Uhlmann et al. [24] measured tool wear when the PCNB tool is used. The main tool failure criterion was notch wear on the main cutting edge. Also, at a higher cutting speed of over 1000 m/min, chipping occurred on the cutting edge and on the braze joint between the tungsten carbide substrate and the PCBN layer.

Richards et al. [7] conducted a detailed overview of the use of ceramic tools for machining Nickel-based alloys. Excessive depth of cut (DOC) notching was reported as the predominant failure mode, irrespective of the tool material composition. Also, due to superior hot hardness, sialon shows greater flank wear than alumina when machining nickel-based alloys [37].

Ezugwu et al. [25] reported a 7 min tool life for a micron grain ceramic tool ($\text{Al}_2\text{O}_3+\text{SiC}$) used to machine Inconel 718 at a cutting speed of 230 m/min and a 0.125 mm/rev feed. The tool failure criterion was uniform flank wear ($\geq 400 \mu\text{m}$).

Ezugwu et al. [31] reported on the tool life for whisker reinforced ceramic tools at different coolant pressures, and found that with increasing coolant pressure of up to 15 MPa, the tool life was gradually improved upon having round shaped geometry. A tool life increase of up to 71 % was observed when machining Inconel 718 at a cutting speed

of 250 m/min and a feed rate of 0.2 mm/rev. The researchers also observed that doubling the feed rate from 0.1 to 0.2 mm/rev had no adverse effect on tool performance.

Arunachalam et al. [34] reported a 6.6 min tool life for a CBN cutting tool (having a round shaped geometry) used to machine Inconel 718 at a cutting speed of 150 m/min and a 0.15 mm/rev feed. The tool failure criterion was uniform flank wear (300 μm). The major cause of tool rejection in most of the tests was a crater on the rake face, which breaks through the cutting edge in the flank face, especially at the depth of cut notch wear region.

Several wear mechanisms have been identified as responsible for the deterioration of ceramic tools when machining Inconel 718. The main tool wear for ceramic tools was notch wear, characterized by the plastic flow towards the side of the chip, and a burr on the workpiece formed by the major cutting edge at a specific cutting speed [40, 42, 46].

2.3.3 Cutting Temperature

To the knowledge of the author of the present study, not much information on temperature conditions while turning nickel-based super alloy Inconel 718 has been published. However, Kitagawa et al. [42] did carry out an experimental study on tool temperature in relation to increasing cutting speeds when machining Inconel 718, by embedding a thermocouple in a ceramic tool. The experimental results shown in Figure 2.6 suggest that the temperature rises monotonically with increasing cutting speeds, where θ_R is the rake face temperature and θ_C and θ_N are flank face temperatures at two points, respectively.

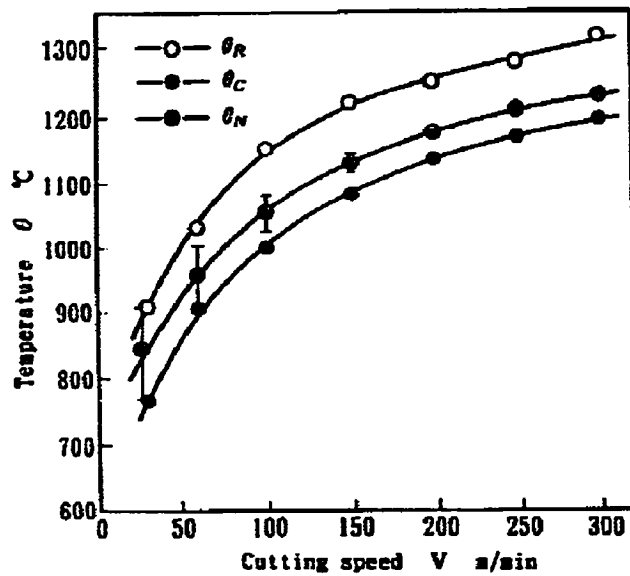


Figure 2.6: Local tool temperatures v/s cutting speed [34]

Narutaki et al. [46] measured the cutting temperature of the flank face and depth of cut line for ceramic tools used to machine Inconel 718. The natural thermocouple method, in which the thermocouple was composed of work material and tungsten wire buried in a ceramic tool, was used. The cutting temperature at the depth of cut line was reported to be over 1200°C at a cutting speed of 300 m/min, and it was higher than that of the flank face.

2.3.4 Surface Finish

Surface topography is of great importance in specifying the function of a surface. A significant proportion of component failure starts at the surface due to either an isolated manufacturing discontinuity or a gradual deterioration of the surface quality. An important parameter describing surface integrity is surface roughness. In the manufacturing industry, a surface must be within certain limits of roughness. Therefore, measuring surface roughness is vital to the quality control of machining the workpiece.

Uhlmann et al. [24] investigated the effect of cutting speed and cutting edge geometry on surface formation when machining Inconel 718 using a PCBN cutting tool.

The researchers found that the value of surface roughness was between 2.4 to 4.3 μm for the cutting speed ranges from 300 m/min to 1250 m/min and a constant feed of 0.1 mm/rev at a constant depth of cut of 0.5 mm.

Choudhury et al. [33] measured the surface roughness for Inconel 718 in turning operations that used coated and uncoated carbide tools under dry conditions. The researchers found that the surface roughness generated by the uncoated and coated tools is mostly influenced by the change in feed. Increase in depth of cut improves the surface finish produced by the coated carbide tools, while the opposite result occurs when uncoated tools are used.

Ezugwu et al. [44] measured the surface finish for Inconel 718 using coated carbide tools under wet conditions. From all the different coated tools that were used, the tool with the TiN coating produced a better surface finish due to the polishing action of the honed cutting edge, and the uniform flank wear generated during machining.

Arunachalam et al. [47] reported the results of their investigation into the surface integrity of the machined surface of age hardened Inconel 718 parts, in terms of surface finish and residual stresses while facing Inconel 718. A PVD TiAlN coated cemented carbide tool with rhomboid and square shaped geometries was used in both dry and wet conditions. The cutting parameters tested were: (i) cutting speed ranges from 40 m/min to 60 m/min, (ii) feed ranges from 0.1 mm/rev to 0.15 mm/rev, and (iii) a constant depth of cut of 0.5 mm. Lower values of surface roughness ($< 1 \mu\text{m}$) and tensile residual stresses (300 MPa) were obtained while facing with a coolant as compared to those values obtained when facing with identical cutting data, but without a coolant (surface roughness: approximately 1 μm and residual stress: 600 MPa).

Arunachalam et al. [49] studied the surface finish and residual stress components when machining (facing) age hardened Inconel 718. Two types of tools were used having square and round shaped geometries. The tools used were: (i) PVD TiAlN coated carbide and (ii) CVD-TiCN/Al₂O₃/TiN coated carbide. The results show that the round tools and

positive rake angles give lower values for surface roughness as compared to the square type with coolant giving better surface finish; whereas, the effects of cutting edge preparation and nose radius give higher values of surface roughness resulting in worse surface finish as compared to those tools with the square shaped geometry.

Ezugwu et al. [25] also investigated the effect of cutting speed on the surface of Inconel 718 when using Nano-ceramic cutting tools for the roughing operation. They found that surface finish deteriorates with prolonged machining, and an increase in the feed rate does not produce any significant change in the surface finish. The Si_3N_4 based tool produced the worst surface roughness value of $8 \mu\text{m}$ when machining at a feed rate of 0.125 mm/rev and a speed of 270 m/min .

Darwish [28] measured the surface roughness of Inconel 718 when carrying out the roughing operation with ceramic and CBN cutting tools under dry cutting conditions. From the experiments performed, Darwish found that the cutting speed has little effect on surface roughness, at both low and high feed rates; whereas, feed rate and depth of cut have a major effect on surface roughness. As for the effect of tool material, ceramic tools produce a 7% improvement of surface quality at high feed rate, and an average improvement of 10% at low feeds (as compared to the CBN cutting tool).

Ezugwu et al. [31] investigated surface roughness for Inconel 718 when using whisker reinforced ceramic tools under conventional and high-pressure coolant supplies. The researchers found that the surface roughness was very low when a round tool was used. With a round tool, a large contact radius is produced with the workpiece material, thus their ability to produce a high quality surface finish.

Arunachalam et al. [29, 34] measured surface roughness (after the first pass and at the end of tool life) when facing age hardened Inconel 718 with CBN and ceramic cutting tools with square and round geometries. Low surface roughness values were obtained when using a round tool, and a surface roughness as low as $0.20 \mu\text{m}$ was obtained with

the cutting parameters tested during the course of the experiments at the cutting speed of 150 m/min, feed of 0.15 mm/rev and a 0.5 mm depth of cut.

Ezugwu et al. [48] carried out experiments on a G-17 and Inconel 718 alloy using round and rhomboid shaped pure oxide ($\text{Al}_2\text{O}_3 + \text{ZrO}_2$) and mixed oxide ($\text{Al}_2\text{O}_3 + \text{TiC}$) ceramic tools. These experiments studied the extent of damage on the machined surfaces under optimum cutting conditions. Prolonged machining with the two grades of ceramic tools resulted in an increase in the hardness of the surface layer to well above the average hardness values of the work materials.

Darwish et al. [50] presented surface roughness models for turning Inconel 718 using different tool materials under dry cutting conditions, and a constant nose radius. Contours of surface roughness were developed to select the proper combination of the cutting speed and feed so to increase the metal removal rate without sacrificing the quality of surface roughness produced.

2.3.5 Chip Formation

Chip morphology and chip formation are issues of great importance in metal cutting in relation to the understanding the mechanism of material removal. When cutting difficult-to-cut material, improvements in productivity and part quality can be achieved by controlling chip formation.

A metallographic analysis of chips can reveal information about what happened during the cutting process. Also, chip analysis provides information on tool wear mechanism and tool life. Moreover, chip analysis helps to build an understanding of the effects that chip formation induces on the cutting forces and on the newly machined surface.

Not much work has been done regarding the detailed mechanism of chip formation when machining Inconel 718. In the literature, most studies have focused on Ti-alloys chips. Only Komanduri et al. [12] have investigated the deformation characteristics of chips when machining Inconel 718 at various speeds with hot-pressed

ceramic (alumina plus titanium carbide) and cubic boron nitride cutting tools. According to their research, the shear localized chips between the segments begin to form at about 61 m/min to 100 m/min. Figure 2.7 shows an example of a chip at a cutting speed of 61 m/min.

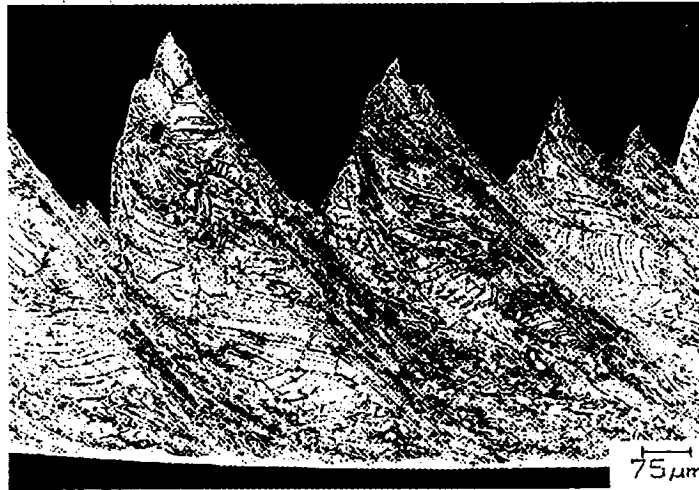


Figure 2.7: Optical micrographs of the Inconel 718 chip at 61 m/min showing the transition (i.e. from a continuous chip to shear localized chip) where shear localization is beginning to take place [12]

2.4 Conclusions

The following are the conclusions drawn from the literature for Inconel 718:

- 1) Most of the experiments have been conducted on the roughing operation for turning Inconel 718.
- 2) Coolant improves the performance of coated carbide tools (as compared to uncoated tools) with respect to tool life and surface roughness at higher speeds.
- 3) Most of the studies have focused on tools with square or rhomboid shaped geometries. No significant work, in regards to the finish operation, has been done with round coated carbide tools.
- 4) Neither has much work been done on measuring the tool-chip interface temperature for Inconel 718.
- 5) Different tool geometries have not been compared with respect to their effects on cutting parameters such as cutting forces, surface roughness, and tool wear with different grades for finishing operation of coated carbide grades.

- 6) No studies have been done on the effect of cutting speed on chip morphology when using carbide tools for machining Inconel 718, especially for the finish turning operation.
- 7) It has been proved that the surface roughness obtained with a round tool was lower than that obtained with square or rhomboid shaped tools.
- 8) The multilayer coated tools performed better than that of uncoated tools at higher cutting speed (> 50 m/min)

This thesis is aimed at filling in some of the gaps in the understanding of the behavior of Inconel 718 during machining. It also is concerned with testing the effects of cutting tool coatings on the machinability of Inconel 718, which includes tool wear mechanisms, cutting forces measurement, tool wear progression over time, surface roughness of the material, and chip morphology for the finish turning operation.

This chapter discusses the experimental setup for two operations: (1) Oblique finish turning and (2) Orthogonal machining. During the experiments, the cutting speed, feed, and depth of cut were controlled for both operations.

For the oblique finish turning operation, cutting forces, tool wear, and surface roughness were measured. These experiments were carried out to evaluate the machinability of Inconel 718 as described in the objectives in Chapter 1. For the analysis of the chip morphology, a special technique that was developed is discussed in Section 3.6. For orthogonal machining, the parameters measured were cutting forces, torque, contact length, chip thickness, and width of the chip. These experiments were conducted to understand the behavior of Inconel 718, and in the future for identification of the constitutive laws of this material under high strain, strain rate, and cutting temperature.

3.1 Machine Tool

All cutting tests were performed on a turning machine—the Boehringer NG 200 (2 spindles and 6 axes) CNC machine—with the following characteristics: a 36 kW spindle, a maximum spindle speed of 4000 rpm, and a maximum feed rate of 25 m/min. The experimental setup is shown in Figure 3.1.

3.2 Cutting Tool

Two different turning operations were investigated. The first dealt with orthogonal machining tests, while the second dealt with the finish turning operations. Both were used on Inconel 718. The tool used with the tool holder during these two operations will be described in this section.

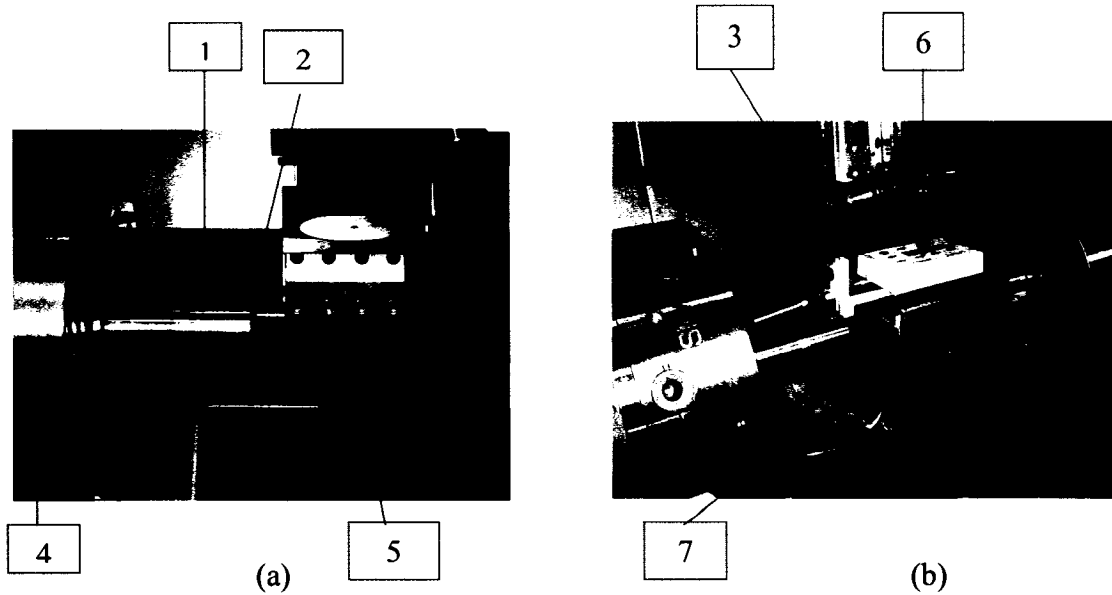


Figure 3.1: Experimental setup: (a) orthogonal machining, (b) oblique finish turning operation, (1) workpiece, (2 & 3) tool, (4) chuck/spindle, (5) force transducer, (6) surface roughness measurement instrument, and (7) chip collector

3.2.1 Tool Holders

Two types of tool holders were used in the experiments. In the first phase (orthogonal machining) the cutting forces and contact length were measured and the chip analysis was carried out. In the second phase (oblique finish turning) the influence of cutting conditions on tool wear, cutting forces, and the workpiece surface finish were investigated in detail

For the first phase of the experiment, a Sandvik STFCL 2020K11-A tool holder was used, as illustrated in the Figure 3.2. It has rake angle of 0° and an approach angle of 90° . In the second phase of the experiment, a Kennametal SRGCL 2525 M12 tool holder was used, as illustrated in the Figure 3.3. It has rake angle of 0° and an approach angle of 45° .

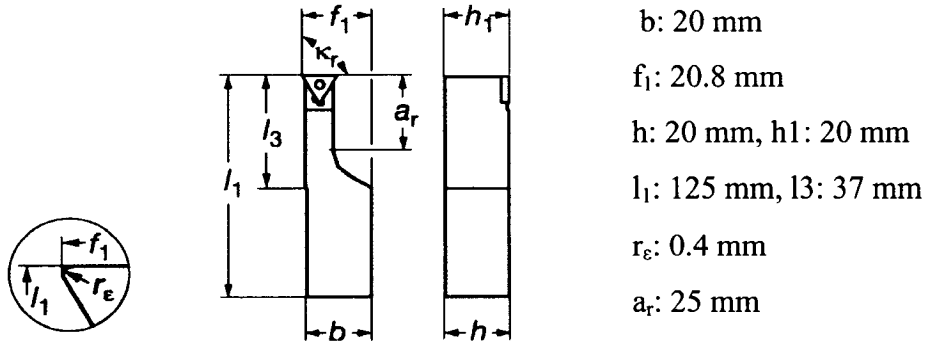


Figure 3.2: Sandvik triangular turning tool holder employed in the orthogonal machining tests

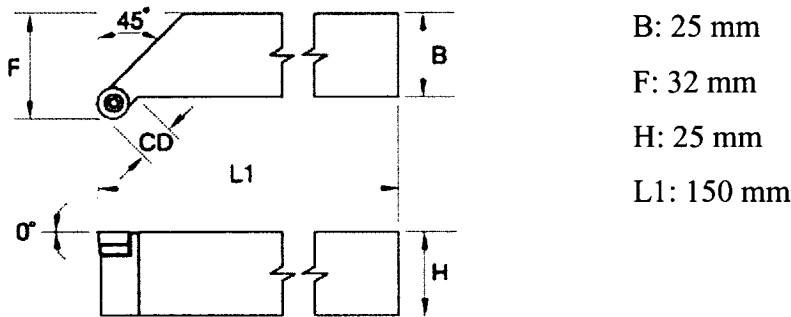
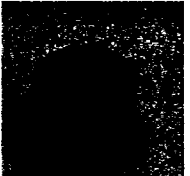


Figure 3.3: Kennametal round turning tool holder employed in the oblique finish machining tests

3.2.2 Tool Material and Geometries

In the orthogonal experiments, H13A Sandvik tool was used. This tool is manufactured using coarse tungsten carbide material and is uncoated. The cutting edge preparation includes a 0° rake angle, a 7° clearance angle, $75 \mu\text{m}$ edge roundness, and a 90° approach angle for H13A. Table 3.1 depicts the insert and the relevant details regarding the geometry. For the oblique finish turning operation, three different types of insert materials were used with the Kennametal tool. The geometry used had a 0° rake angle, a 5° top face rake angle, and a 7° clearance angle. A round insert was selected for the second phase considering the need for stronger cutting edges and the capability to withstand high thermal and mechanical loads which occur while machining Inconel 718. Table 3.1 depicts the different types of tools used during the experimental work, along with their geometries.

Table 3.1 Properties of uncoated and coated tools used during the orthogonal and oblique finish turning operations

Properties of the Tungsten Carbide Tools				
Properties	Type of Tool			
	H13A (Uncoated) TCMW 11 02 04	K313 (Uncoated) RCMT 12 04 M0	KC5010 (PVD TiAlN) Coated RCMT 12 04 M0	KC8050 (CVD TiCN/Al ₂ O ₃ /TiN) Coated RCMT 12 04 M0
				
Hardness HRA	93	93	93	90.6
Density g/cm ³	14.96	14.9	14.9	13.9
Tensile Rupture Strength TRS (MPa)	2200	3100	3100	-
Avg. Grain Size (μm)	Fine (Approx. 1 μm)	Fine (Approx. 1 μm)	Fine (Approx. 1 μm)	Medium (> 1 μm)
Binder	10.2% Co & WC 89.8%	6 % Co	6 % Co	7 % Co
Thickness of Coating (μm)	-	-	2/0.5/0.5 = 3	5/8/1.5 = 14.5
Edge Preparation (μm)	75	Honed Shaped	Honed Shaped	Honed Shaped
Rake Angle (°)	0	0	0	0
Clearance Angle (°)	7	7	7	7

3.3 Workpiece Material

Inconel 718, whose surface hardness is around 32 HRC, was used as the workpiece material during the experiments. The material was solution heat-treated and aged according to the AMS standard 5662 [51]. The workpiece was made 63 mm in diameter and about 150 mm long. Six specimens were prepared for the oblique finish turning

operation. For orthogonal machining, one specimen was made with a 2 mm width of cut, and another specimen was made with a 3 mm width of cut.

3.4 Tool Wear Measurement

The flank wear measurements for the oblique finish turning operation were recorded using a standard stereoscopic microscope (Nixon Model SMZ-2), which has an incorporated reticule eyepiece. The measurement was done using the x-y stage attached to the base of the microscope. The tool holder was kept vertical under the microscope without removing the insert from the tool holder and was mounted at the same position after measuring the wear. Figure 3.4 depicts the setup for wear measurement.

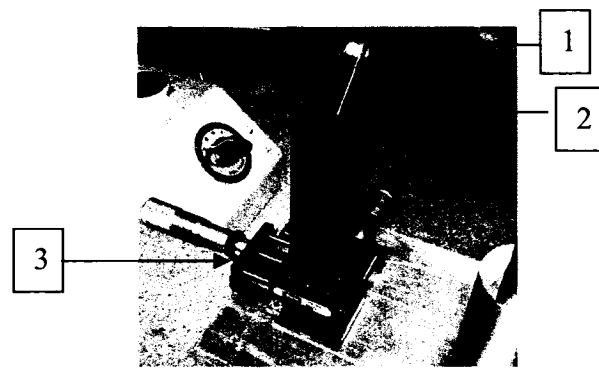


Figure 3.4: Tool wear measurement setup (1) tool (2) tool holder (3) x-y stage

Cutting tests were discontinued if any of the following failure criteria, as illustrated in the Figure 3.5 were reached in accordance with the International Standard ISO 3685 [52]:

- Average flank wear VB_{a} of 300 μm
- Maximum flank wear VB_{max} of 600 μm
- Notch wear VB_{N} of 800 μm

The worn inserts were further analyzed using a stereoscopic microscope (Olympus Model SZX 12), and the SEM analysis was done to study the wear mechanism.

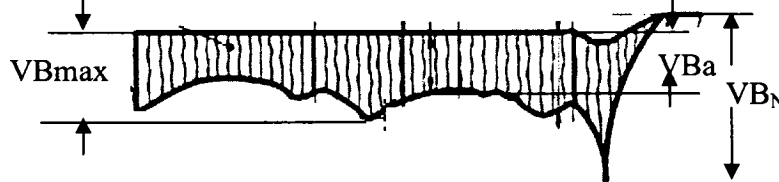


Figure 3.5: Tool wear criteria [52]

3.5 Force Measurement

The cutting forces were recorded for every test when the cutting edge was new, and during the first 25 seconds of cutting for both operations. A three component 9121 type Kistler dynamometer connected to a data acquisition system was used to record the forces for all the machining tests. Also, for orthogonal cutting, a four component 9272 Kistler dynamometer was used to measure the torque for some machining tests. Figure 3.6 (a) and (b) illustrates the direction of forces measured during machining process in the orthogonal and finish turning operations respectively.

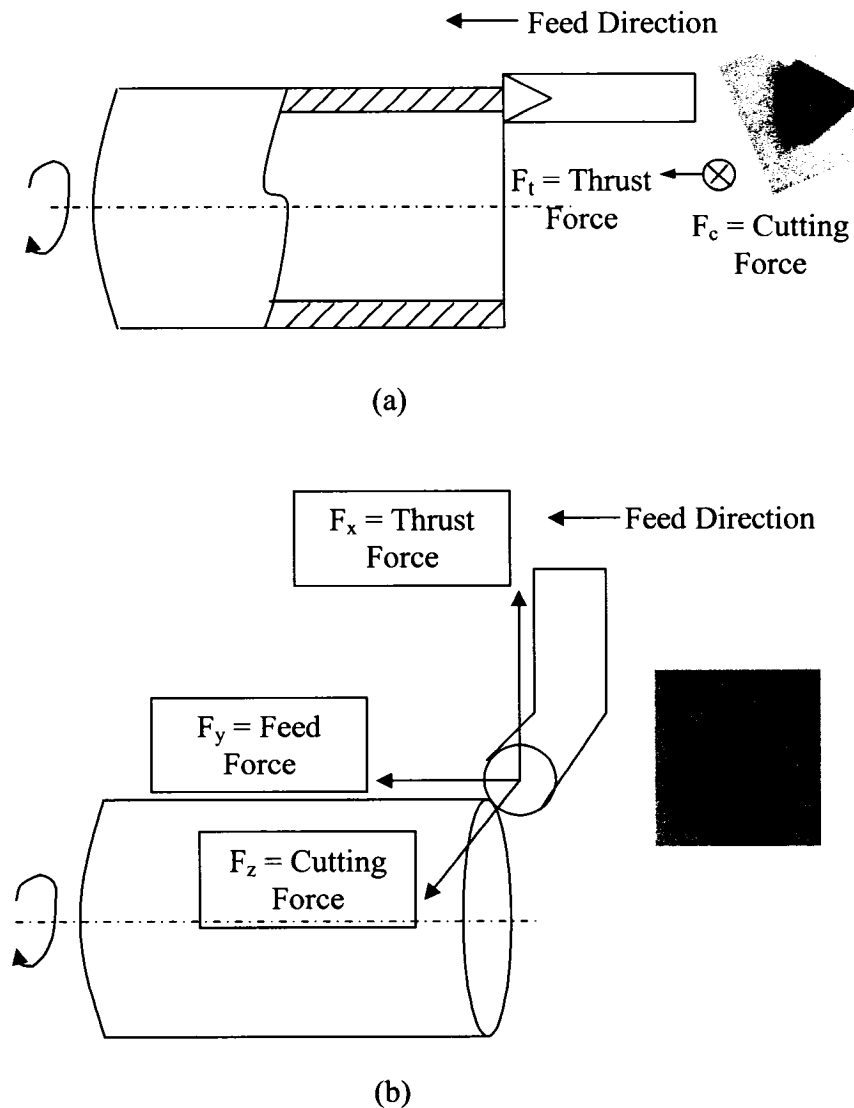


Figure 3.6: Forces direction during machining process (a) orthogonal cutting (b) oblique finish turning

3.6 Chip Analysis

The chips were collected for all oblique finish tests during the first cut when the insert cutting edges were new. They were then placed between small plastic holds in a sandwich-like fashion. The position of the chip within this sandwich was such that its cross section could be seen when the sandwich was held up to the eye (see Figure 3.7). Subsequently, this sandwich was kept vertical and upside down in a hot mounting press—the Struers LaboPress-3—and was hot mounted with bakelite powder at 180°C. This was followed by grinding and polishing.

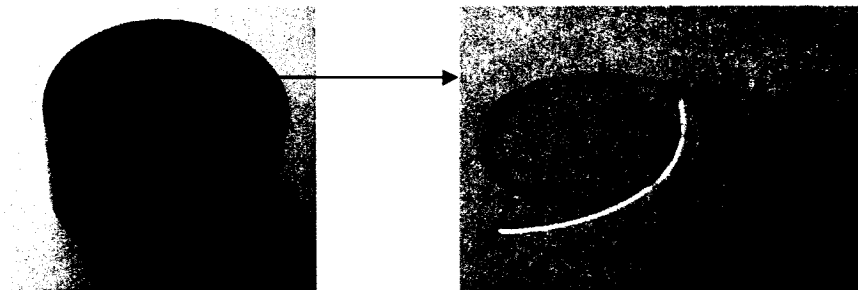


Figure 3.7: Image of chips placement in the bakelite mounting

The grinding was done using a silicon carbide paper (1200 grit size). After that, the polishing was achieved using two steps. In the first step, 9 and 3 μm diamond solutions were used for 4 minutes, while in the second step of polishing, a colloidal silica solution was used. Both the grinding and polishing operations were conducted on a Struers TegraPol-35 grinding and polishing machine.

After the final polishing, the chips were electro-etched using 4 volts for 2-8 seconds. The etchant used for electro-etching was a solution of 10 gms of Chromium Trioxide (CrO_3) and 100 ml of distilled water [53]. The electro-etching was done by a Struers LectroPol-5 electro-etch system. Before etching, the specimens were cleaned using an ultrasonic machine for 5 minutes. The etched chips were analyzed under an optical microscope (Olympus Model GX71) with a digital camera attached to it, and with a Scanning Electron Microscope (SEM). The microhardness measurements of the chips also were recorded using a 300 g load on a Struers Duramin A300 hardness testing

machine. In the orthogonal machining, the chip thickness and the width of chip were measured with the help of a vernier caliper.

3.7 Workpiece Surface Roughness Measurement

Surface roughness measurements (R_a) were taken after each pass. The measurement was conducted online with a portable Talysurf Surtronic 3+ instrument, without removing the workpiece from the spindle—using a cut-off (λ_c) of 0.8 mm and an evaluation length of 4 mm ($5 \times \lambda_c$). The failure criterion for the tool was kept at 3 μm surface roughness. The setup for the inline surface measurement is shown in Figure 3.1(b).

3.8 Cutting Fluid

All the machining tests used a coolant: a TRIM VHP^R water miscible cutting fluid supplied by Master Chemical Corporation with a 7.5% oil concentration producing a high lubricity and excellent heat extraction. The coolant concentration was monitored throughout the machining trials using a refractometer.

3.9 Experimental Matrix

The cutting conditions for the first phase, which are listed in Tables 3.2 and 3.3, were defined for the orthogonal experiments. The widths of the cut for this test were 2 mm and 3 mm, respectively.

For first phase, the conditions that were selected (see Table 3.2 and Table 3.3) are used to generate the experimental data under two dimensional, plane strain orthogonal machining for the future identification of material behavior under high stress, strain, strain rate, and temperature. For each cutting test, a new cutting edge was used.

The cutting conditions listed in Table 3.4 were defined for the oblique finish turning operation of Inconel 718 as suggested in [54]. Since no data is available in the existing literature for tool performance for machining Inconel 718 with carbide tools for the oblique finish turning operation, these cutting parameters (shown in Table 3.4) were

chosen. All the tests shown in Table 3.4 were performed with three different cutting tools, which are described in Section 3.2.

The tests performed were in accordance with the ISO procedure developed during the course of the research. A special tagging procedure was implemented for each test.

Table 3.2: Machining conditions tested in Phase I of the experimental work (orthogonal cutting) with 2 mm width of cut

Test No.	Cutting Conditions		Length of Cut (mm)	Tool
	Cutting Speed m/min	Feed mm/rev		
1	10	0.2	0.65	Uncoated Tungsten Carbide (H13A)
2	20	0.2	0.65	
3	30	0.2	0.65	
4	40	0.2	0.7	
5	60	0.2	0.75	
6	80	0.2	0.8	
7	10	0.3	0.7	
8	20	0.3	0.7	
9	30	0.3	0.8	
10	40	0.3	0.9	
11	60	0.3	1.15	
12	80	0.3	1.25	

Table 3.3: Machining conditions tested in Phase I of the experimental work (orthogonal cutting) with 3 mm width of cut

Test No.	Cutting Conditions		Length of Cut (mm)	Tool
	Cutting Speed m/min	Feed mm/rev		
13	10	0.15	0.9	Uncoated Tungsten Carbide (H13A)
14	15	0.15	0.9	
15	20	0.15	0.9	
16	10	0.2	1.2	
17	20	0.2	1.2	
18	10	0.3	1	

Table 3.4: Machining conditions tested in Phase II of the experimental work (oblique finish turning) with a constant depth of cut of 0.25 mm

Test No.	Cutting Speed (m/min)	Feed (mm/rev)	Tool
1	50	0.075	Uncoated (K313), Single Layer PVD coated (KC5010) and Triple Layer CVD coated (KC8050) Tungsten carbide
2		0.1	
3		0.125	
4	75	0.075	
5		0.1	
6		0.125	
7	100	0.075	
8		0.1	
9		0.125	

3.10 Contact Length Measurement

In the orthogonal test, the contact length was measured as illustrated in Figure 3.8. The purpose of measuring the contact length was to determine the friction law at the tool-chip interface [55]. The average value was taken for the contact length, which is given by $L = (L1+L2)/2$ as shown in Figure 3.8. L1 and L2 are defined as the maximum and minimum lengths of contact, respectively, where a material adhesion exists on the rake face.

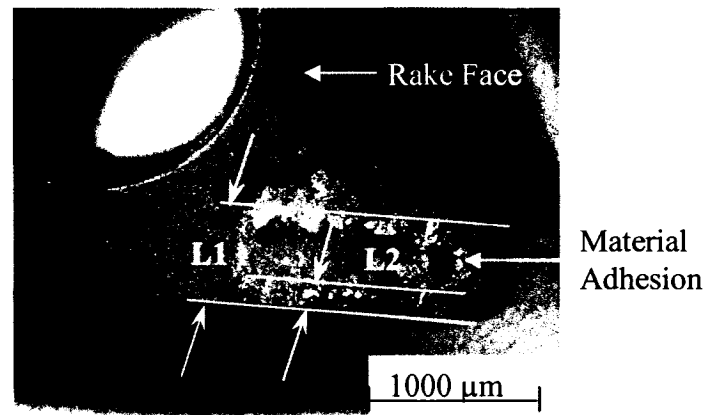


Figure 3.8: Contact length measurement

4.1 Introduction

Section one of this chapter deals with the generation of experimental data under two dimensional, plane strain orthogonal machining for the future identification of material behavior under high stress, stain, strain rate, and temperature. Cutting forces and chip thickness were measured and used to determine shear angle, shear stress, shear strain, and strain rate. The torque measurement is used in conjunction with other measured parameters such as forces, contact length, and shear angle [55]:

- (1) to determine the thickness of the primary shear zone
- (2) to identify the friction law at the tool chip interface
- (3) to validate FEM simulation for orthogonal cutting process.

In the second section, the experimental results obtained in oblique finish turning are discussed. Tool wear mechanisms are examined using three different tools as described in Chapter 3: uncoated, single layer PVD coated, and triple layer CVD coated tools. As well, analysis of the chip morphology, cutting forces, tool wear progression with respect to time, and surface finish of the material is performed.

4.2 Experimental Results Obtained in Orthogonal Machining

The orthogonal cutting tests were done for the cutting conditions given in Tables 3.2 and 3.3 in Chapter 3. The width of cut used is 2 mm and 3 mm. For width of cut $b = 2$ mm and $b/t \leq 10$ (where b represents the width of cut and t represents the feed), the effect of the width of cut on cutting speed and feed is investigated. For width of cut $b = 3$ mm, where $b/t \geq 10$, the problem can be considered to be two dimensional plane strain [56].

4.2.1 Experimental Results Obtained When Performing Orthogonal Machining With a 2 mm Width of Cut

4.2.1.1 Cutting Forces

The cutting force F_c and thrust force F_t were measured during each cutting test. Initially, two feeds were used to perform tests under dry cutting conditions. Figure 4.1 shows that while the cutting force and thrust force decrease with an increase in cutting speed, they increase with an increase in feed. From the thrust force and cutting force, the resultant force is computed, and, as expected, it also decreases with an increase in cutting speed, and increases with an increase in feed. The reduction in forces due to an increase in cutting speed can be attributed to the tool mean face temperature. As the cutting speed increases, the temperature increases, making the material softer. The mean shear-plane temperature (θ_s) and the mean temperature rise due to friction ($\Delta\theta_F$) were calculated for all cutting conditions, using the analytical approach given in [3]. Figure 4.1 (d) represents these values. From these temperatures, tool mean face temperature was computed ($\theta_T = \theta_s + \Delta\theta_F$). The results are shown in Figure 4.1(d), and, as expected, the tool mean temperature increases with an increase in the cutting speed and feed. This increase is approximately in accordance with the relation given in [3], which is given in equation (4.1). The variation is about 15% of the value computed in relation to equation (4.1).

$$\theta_T \sim V^{0.5} t^{0.3} \quad (4.1)$$

where θ_T represents the tool mean face temperature, V represents the cutting speed, and t represents feed. The calculated tool mean temperature at the cutting speed of 80 m/min and a feed of 0.3 mm/rev was found to be 1288°C, which is close to the melting temperature. The analytical approach used overpredicts the temperature, as during the experiment no sign of melting was observed. As expected, the cutting force and the thrust force increase with an increase in feed per revolution. This can be attributed to the chip thickness. The chip thickness increases with an increase in feed per revolution, leading to an increase of cutting area, which induces the cutting forces to increase [30]. The results for the chip thickness are shown in Figure 4.2.

The chips formed here were continuous for the following three cutting conditions: cutting speed 10 m/min and 20 m/min and feed 0.2 mm/rev, and cutting speed 10 m/min and feed 0.3 mm/rev. For the other conditions, the chips formed were continuous and in transition to segmental.

Three experiments were repeated to measure torque during continuous chip formation and to check the repeatability of the cutting forces. The results are represented in Figure 4.1. Figure 4.3 shows the effect of cutting speed and feed on torque for the repeated tests that were conducted for the 2 mm width of cut. As illustrated in Figure 4.3, the torque increases with the feed but practically remains unchanged with the increase of the cutting speed from 10 to 20 m/min.

4.2.1.2 Chip Analysis

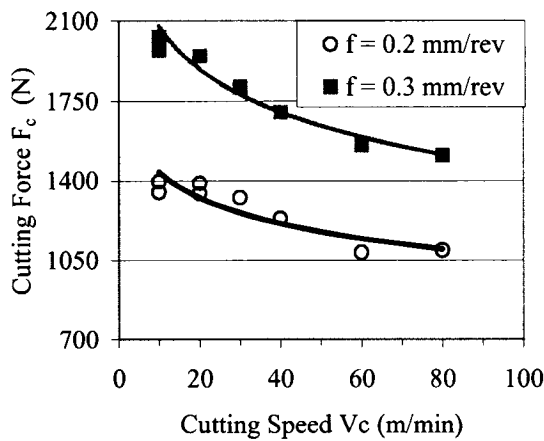
In the course of this investigation, the chip thickness and width of the chip were measured. Figure 4.2 shows the effect of the feed and cutting speed on the chip thickness for a width of cut of 2 mm. With the increase in the cutting speed, the chip thickness decreases. This can be attributed to the increase in the shear angle with an increase in the cutting speed as illustrated in Table 4.1.

The increase in the chip thickness (t_c) with the increase in the feed (t) is explained as follows. By definition, the chip thickness ratio, which is the ratio of chip thickness to the feed, is determined using equation (4.2) [57]

$$\frac{t_c}{t} = \frac{\cos(\phi - \alpha)}{\sin \phi} \quad (4.2)$$

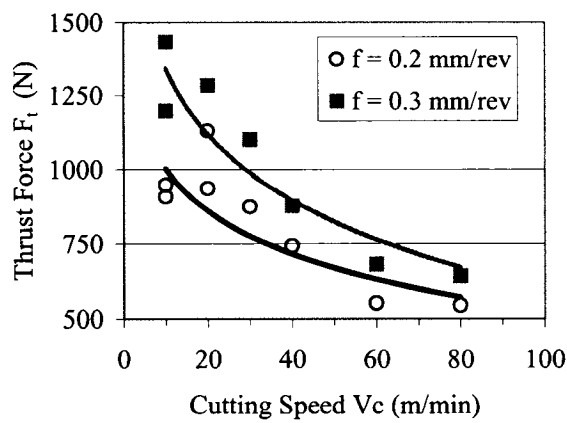
As rake angle (α) is zero, equation 4.2 can be written as equation (4.3)

$$t_c = \frac{t}{\tan \phi} \quad (4.3)$$



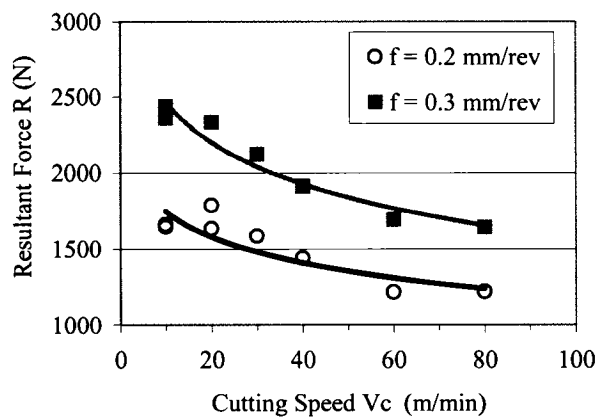
Cutting Speed V_c (m/min)	Cutting Force F_c (N)	
	Feed (mm/rev)	
	0.2	0.3
10	1395/1349	2031/1972
20	1343/1389	1947
30	1325	1813
40	1234	1702
60	1085	1554
80	1095	1512

(a) Cutting Force



Cutting Speed V_c (m/min)	Thrust Force F_t (N)	
	Feed (mm/rev)	
	0.2	0.3
10	910/949	1199/1434
20	937/1131	1285
30	874	1100
40	744	877
60	554	682
80	546	643

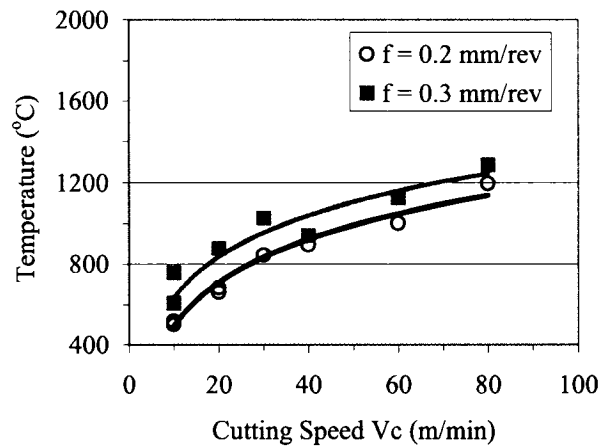
(b) Thrust Force



Cutting Speed V_c (m/min)	Resultant Force R (N)	
	Feed (mm/rev)	
	0.2	0.3
10	1665/1649	2358/2438
20	1638/1791	2333
30	1587	2121
40	1441	1915
60	1218	1697
80	1223	1643

(c) Resultant Force

Cutting Speed V_c (m/min)	Shear Plane Temperature θ_s ($^{\circ}\text{C}$)		Temperature Due to Friction $\Delta\theta_F$ ($^{\circ}\text{C}$)		Tool mean Face Temperature ($\theta_T = \theta_s + \Delta\theta_F$) ($^{\circ}\text{C}$)	
	0.2	0.3	0.2	0.3	Feed (mm/rev)	
					0.2	0.3
10	432.8/412	459.3/568	85.2/88	146.7/188	518/500	606/756
20	484/492	478.7	199/169	399.4	683/661	878
30	518	483.7	328	544.3	846	1028
40	516.3	516	379.6	426	896	942
60	489.6	495	513.4	632	1003	1127
80	506	494	692	794	1198	1288



(d) Mean Tool-Face Temperature

Figure 4.1: Effect of cutting speed and feed on cutting forces and mean tool-face temperature

As is evident from equation 4.3 and Table 4.1, the percentage increase in the feed is much greater than the percentage increase in $\tan \phi$. Hence, with an increase in the feed the chip thickness always increases. The chip thickness was also measured for the repeated test to check the repeatability. The results obtained for the repeated test are shown in Figure 4.2.

Figure 4.4 shows the values for the width of the chip. The width increases from 2 mm to a range of 2.2 to 2.6 mm. The width of the chip was also measured for the repeated test to check the repeatability. The results obtained for the repeated test are shown in Figure 4.4.

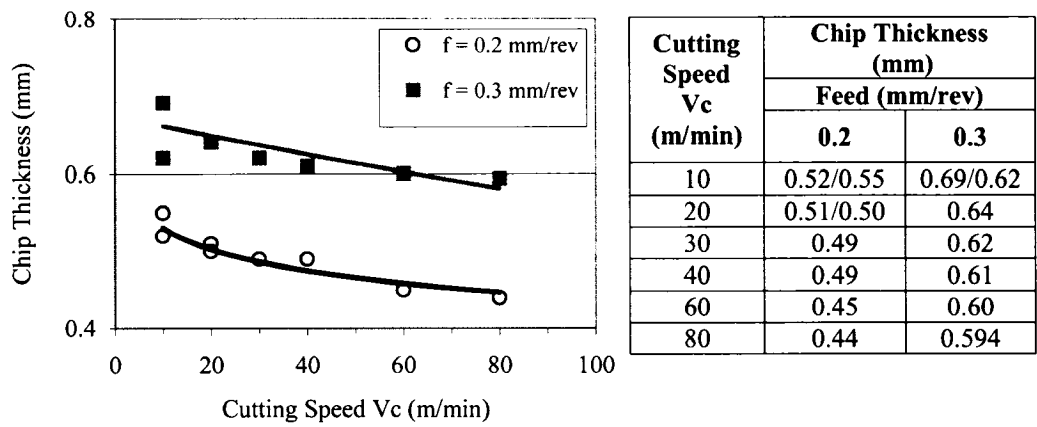


Figure 4.2: Effect of cutting speed and feed on chip thickness

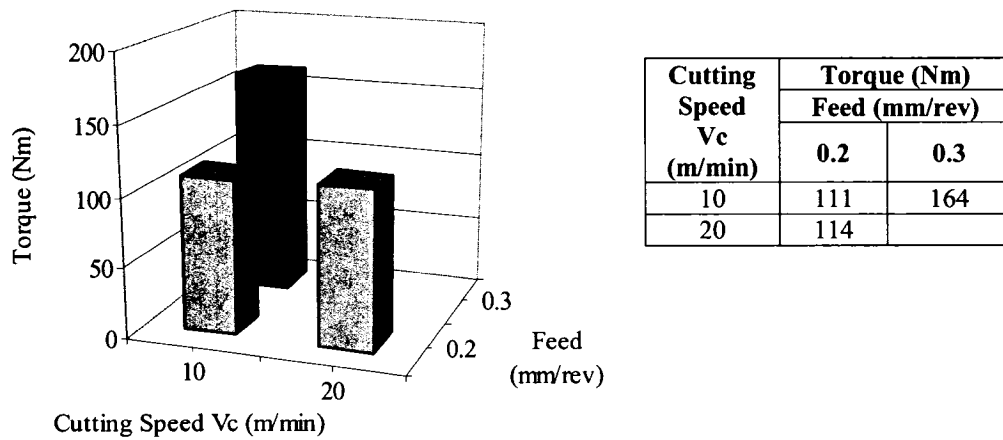


Figure 4.3: Effect of cutting speed and feed on torque

Table 4.1: Comparative Analysis of the percentage increase of $\tan \phi$ with the percentage increase of feed

Cutting Speed Vc (m/min)	Shear Angle (ϕ)		Percentage increase in Feed (%)	Percentage Increase in $\tan \phi$ (%)
	Feed (mm/rev)			
	0.2	0.3		
10	20.8	23.26	50	13.4
20	21.3	25.17	50	20.5
30	22.29	26.64	50	22.4
40	22.29	26.1	50	19.5
60	23.75	26.56	50	13.6
80	24.22	27.02	50	13.4

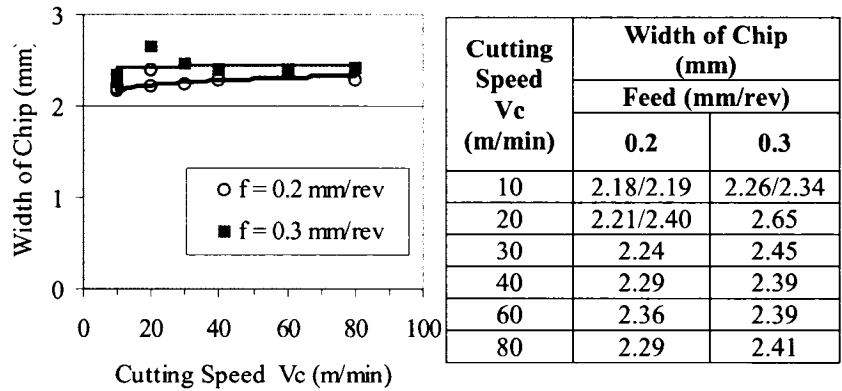
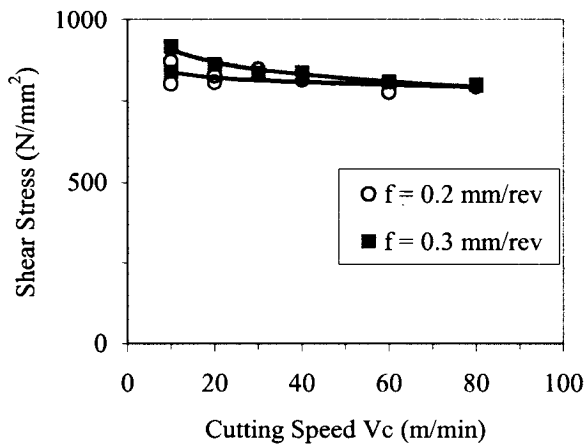


Figure 4.4: Effect of cutting speed and feed on width of chip

4.2.1.3 Evaluation of Shear Stress, Shear Strain, and Strain Rate

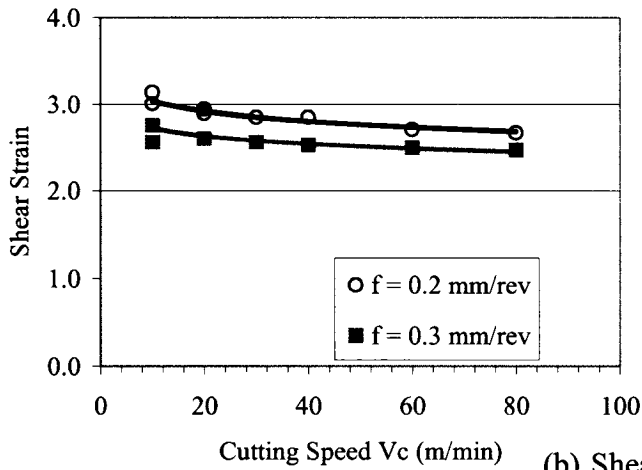
In this section, the shear stress, shear strain, and strain rate were calculated. The shear angle also was calculated using the experimentally measured chip thickness and equation 2.1 given in Chapter 2 [5]. By using the results of the calculation of shear angle, shear stress, shear strain and strain rate were calculated using the equations 2.3, 2.4 and 2.5. Figures 4.5 (a), (b), and (c) show the effect of cutting speed and feed on the shear stress, shear strain, and strain rate, respectively. Figure 4.5 (a) shows that the shear stress decreases with an increase in cutting speed, and is practically independent of feed. This decrease in shear stress can be attributed to the decrease in the cutting and thrust forces as cutting speed increases. The maximum shear stress found to be 916 N/mm^2 occurred at a low cutting speed of 10 m/min and feed 0.3 mm/rev . This is compared to a yield stress of approximately 1060 N/mm^2 at room temperature.

Figure 4.5 (b) shows that the shear strain decreases, as expected, with an increase in the cutting speed as also revealed in [27]. The decrease in shear strain with an increase in feed from 0.2 mm/rev to 0.3 mm/rev is attributed to the increase in the cutting ratio (r). With an increase in the cutting ratio, the shear angle increases, with consequent reduction in the shear strain, as illustrated in Table 4.2. Assuming a reasonable mean value of the shear zone thickness ($\sim 25 \mu\text{m}$) [3], strain rate was calculated using equation 2.5. The results in Figure 4.5 (c) show that the value of strain rate increases with an increase in the cutting speed and is independent of feed. Also, Figure 4.5 shows the results are repeatable within $\pm 5\%$ of the average value.



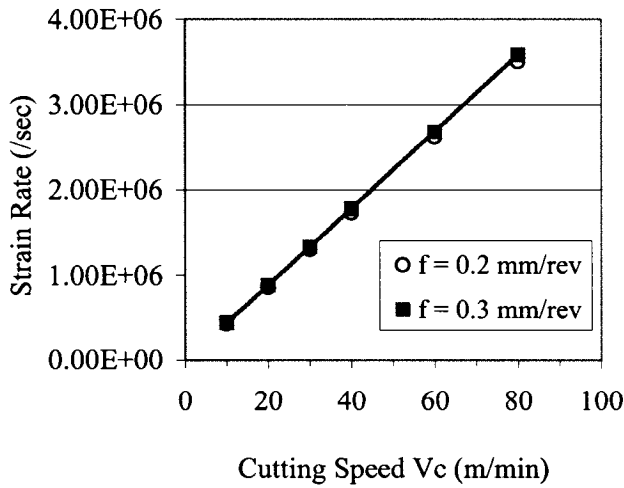
Cutting Speed Vc (m/min)	Shear Stress (N/mm ²)	
	Feed (mm/rev)	
	0.2	0.3
10	871/802	916/835
20	827/807	862
30	848	835
40	815	838
60	775	808
80	793	798

(a) Shear Stress



Cutting Speed Vc (m/min)	Shear Strain	
	Feed (mm/rev)	
	0.2	0.3
10	3.01/3.14	2.76/2.56
20	2.95/2.90	2.60
30	2.85	2.56
40	2.85	2.53
60	2.71	2.50
80	2.67	2.47

(b) Shear Strain



Cutting Speed Vc (m/min)	Strain Rate	
	Feed (mm/rev)	
	0.2	0.3
10	4.28E+05/4.25E+05	4.35E+05/4.44E+05
20	8.59E+05/8.62E+05	8.84E+05
30	1.30E+06	1.33E+06
40	1.73E+06	1.78E+06
60	2.62E+06	2.68E+06
80	3.51E+06	3.59E+06

(c) Strain Rate

Figure 4.5: Effect of cutting speed and feed on shear stress, strain, and strain rate

4.2.1.4 Contact Length

Since contact length is an important input to process modeling and simulation of the machining process [58, 59], in this set of experiments, it was measured for all the cutting conditions (see Figure 4.6). It is observed that the value of contact length decreases with an increase in the cutting speed and increases with increase in feed. This is in agreement with [60]. As shear angle is inversely proportional to the contact length [3], the increase in cutting speed will increase the shear angle, as illustrated in Table 4.2. Figure 4.7 shows the effect of shear angle on the chip-tool contact length. The value for contact length could not be measured at 30 m/min and 0.3 mm/rev feed, since the cutting edge was chipped off. The tests were repeated for the following conditions where continuous chips were obtained. Figure 4.6 shows the results are repeatable within $\pm 7.5\%$ of the average value.

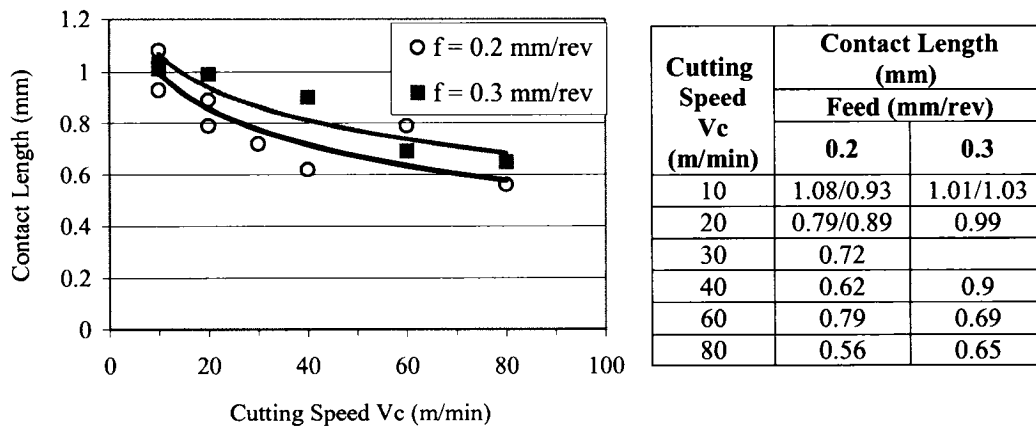


Figure 4.6: Effect of cutting speed and feed on chip-tool contact length with 2 mm width of cut

Table 4.2: Effect of shear angle with an increase in the cutting speed

Cutting Speed Vc (m/min)	Shear Angle (ϕ)		Shear Strain	
	Feed (mm/rev)		Feed (mm/rev)	
	0.2	0.3	0.2	0.3
10	20.8	23.26	3.01	2.76
20	21.3	25.17	2.95	2.60
30	22.29	26.64	2.85	2.56
40	22.29	26.10	2.85	2.53
60	23.75	26.56	2.71	2.50
80	24.22	27.02	2.67	2.47

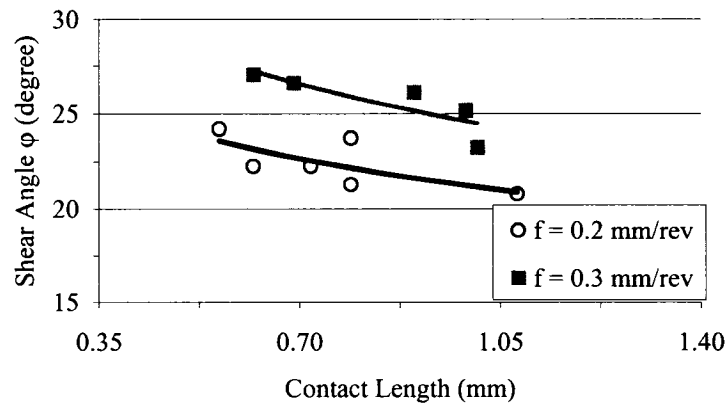


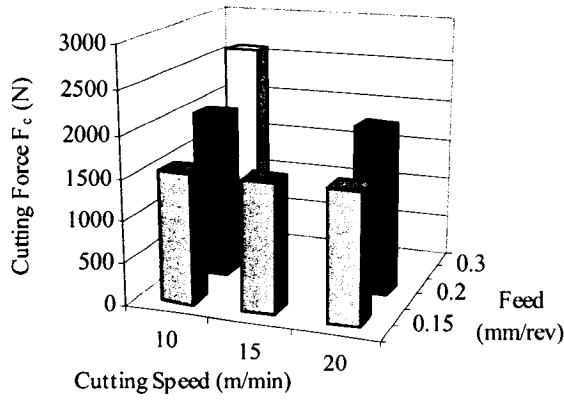
Figure 4.7: Effect of shear angle and chip-tool contact length with 2 mm width of cut

4.2.2 Experimental Results Obtained When Performing Orthogonal Machining With a 3 mm Width of Cut

4.2.2.1 Cutting Forces

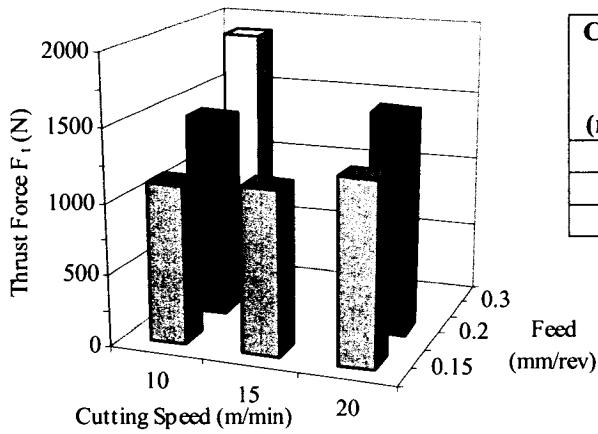
Cutting forces were measured in a way similar to the measurement of the 2 mm width of cut. The cutting parameters selected here assure the formation of continuous chips and to have a plane strain problem. The results presented in Figure 4.8 show that the value of the cutting force decreases marginally with an increase in cutting speed (similar to the results observed with a 2 mm width of cut), but the thrust force increases with the increase in cutting speed. Due to this, the resultant force also increases (approximately 2.8 to 4.6%). The mean tool-face temperature was also calculated (similar to the 2 mm width of cut) and presented in Figure 4.8 (d). Figure 4.9 shows the effect of cutting speed and feed on torque (similar results were obtained with a 2 mm width of cut).

By comparing the cutting force, thrust force, resultant force and torque at cutting speeds of 10 m/min and 20 m/min at a feed of 0.2 mm/rev, it can be seen that an increase in the width of cut from 2 mm to 3 mm causes all the components to increase. In spite of the increase in the cutting forces with the increase in the width of cut from 2 mm to 3 mm, the temperature rise is reduced due to the increase in the heated volume of the chip (thermal capacitance). The results are represented in Figure 4.10 (a), (b), (c), (d) and (e). The same results, as illustrated in Table 4.3 were obtained with a feed of 0.3 mm/rev.



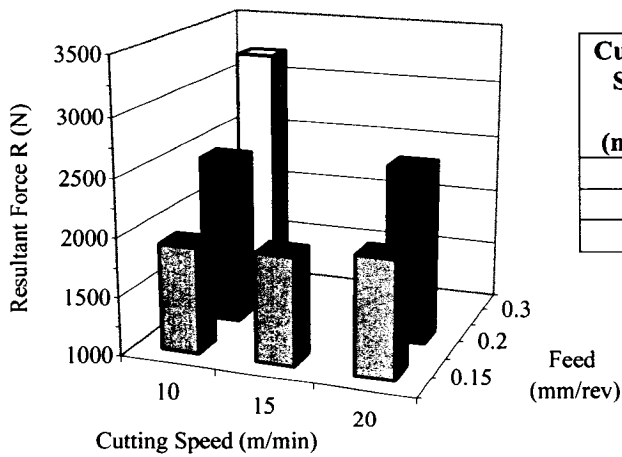
Cutting Speed V_c (m/min)	Cutting Force F_c (N)		
	Feed (mm/rev)		
	0.15	0.2	0.3
10	1549	1998	2589
15	1540		
20	1541	1989	

(a) Cutting Force



Cutting Speed V_c (m/min)	Thrust Force F_t (N)		
	Feed (mm/rev)		
	0.15	0.2	0.3
10	1118	1416	1893
15	1152		
20	1274	1545	

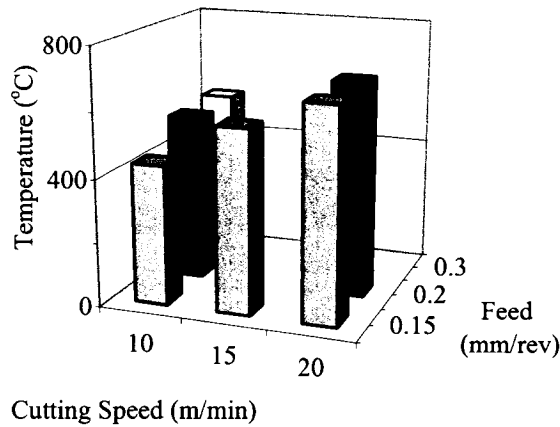
(b) Thrust Force



Cutting Speed V_c (m/min)	Resultant Force R (N)		
	Feed (mm/rev)		
	0.15	0.2	0.3
10	1911	2449	3207
15	1923		
20	1999	2519	

(c) Resultant Force

Cutting Speed V_c m/min	Shear Plane Temperature θ_s (°C)			Temperature Due to Friction $\Delta\theta_F$ (°C)			Tool Mean Face Temperature ($\theta_T = \theta_s + \Delta\theta_F$) (°C)		
	Feed (mm/rev)			Feed (mm/rev)			Feed (mm/rev)		
	0.15	0.2	0.3	0.15	0.2	0.3	0.15	0.2	0.3
10	419.5	411	383	18.4	104	153	438	515	536
15	436			138			574		
20	450	478.2		214	196.3		664	675	



(d) Mean Tool-Face Temperature

Figure 4.8: Effect of speed and feed on cutting forces and mean tool-face temperature for 3 mm width of cut

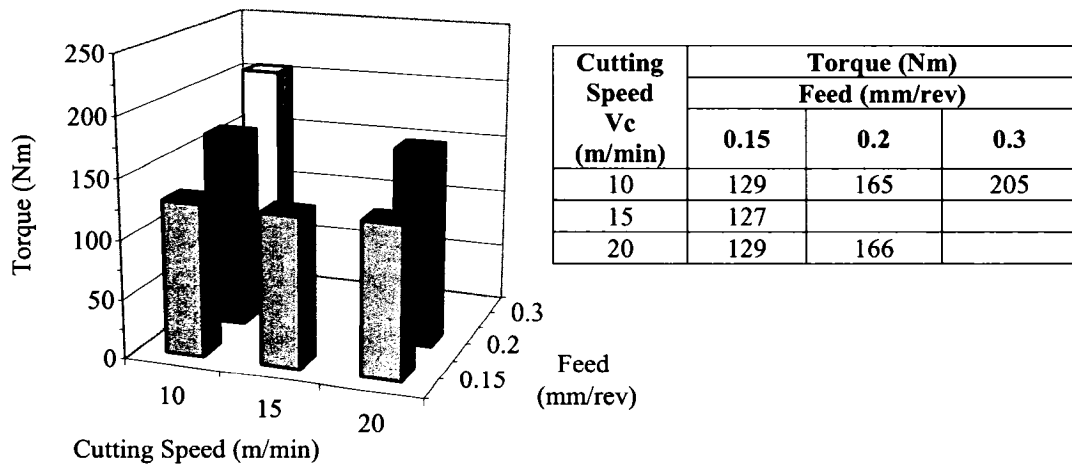
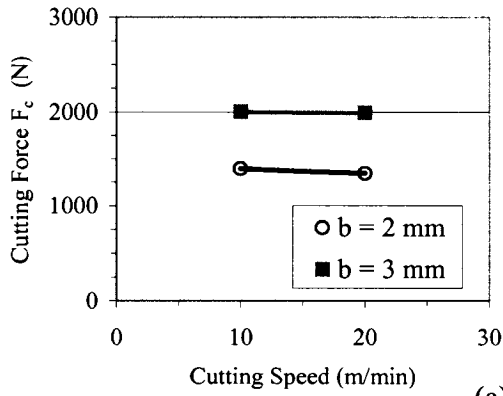
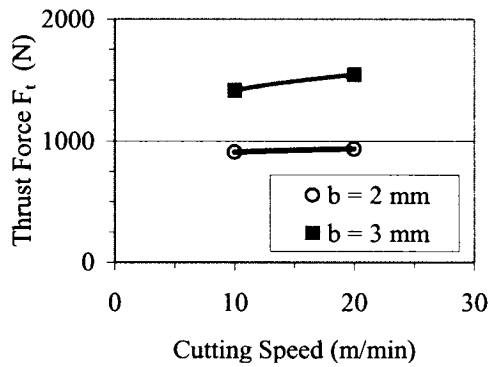


Figure 4.9: Effect of cutting speed and feed on torque for a 3 mm width of cut



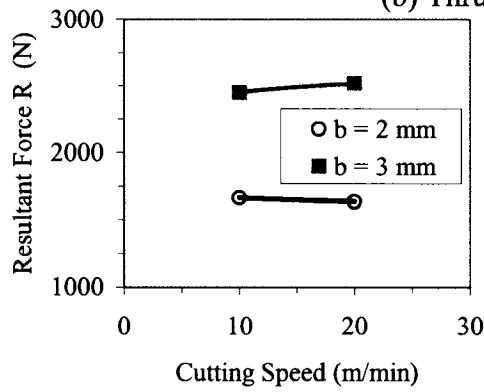
Cutting Speed V_c (m/min)	Cutting Force (N)	
	Width of Cut (mm)	
	2	3
10	1395	1998
20	1343	1898

(a) Cutting Force



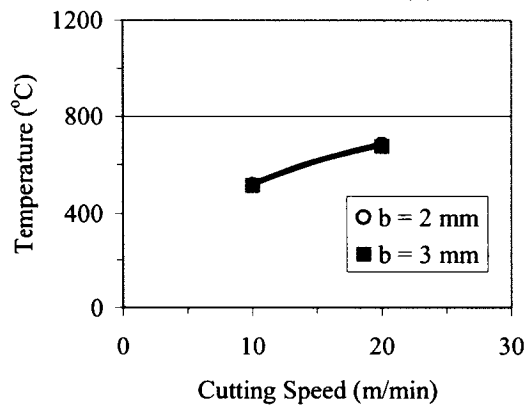
Cutting Speed V_c (m/min)	Thrust Force (N)	
	Width of Cut (mm)	
	2	3
10	910	1416
20	937	1545

(b) Thrust Force



Cutting Speed V_c (m/min)	Resultant Force (N)	
	Width of Cut (mm)	
	2	3
10	1665	2449
20	1638	2518

(c) Resultant Force



Cutting Speed V_c (m/min)	Tool Mean Face Temperature (°C)	
	Width of Cut (mm)	
	2	3
10	518	515
20	683	675

(d) Mean Tool-Face Temperature

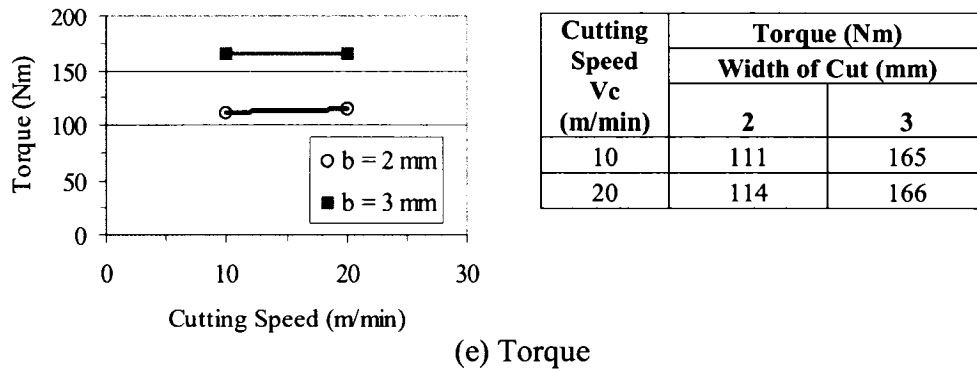


Figure 4.10: Effect of width of cut on forces, mean tool-face temperature, and torque with a feed of 0.2 mm/rev

Table 4.3: Effect of width of cut on forces, cutting temperature, and torque at a cutting speed of 10 m/min and feed of 0.3 mm/rev

Width of Cut (mm)	Cutting Force F_c (N)	Thrust Force F_t (N)	Resultant Force R (N)	Temperature ($^{\circ}$ C)	Torque (Nm)
2	2031	1199	2358	606	164
3	2589	1893	3207	536	205

4.2.2.2 Chip Analysis

The chip produced was continuous in all the cutting conditions. Figures 4.11 (a) and (b) show the effect of cutting speed and feed on the chip thickness and the width of chip. A similar trend is observed for chip thickness as with a 2 mm width of cut. The width of chip measured was in the range of 3 to 3.15 mm. The problem for the plane strain holds true where $b/t \geq 10$ [56] as compared to a 2 mm width of cut.

When compared to the tests where the width of cut was 2 mm and the combinations of the cutting speeds and feeds were (10 m/min, 0.2 mm/rev), (20 m/min, 0.2 mm/rev) and (10m/min, 0.3 mm/rev), it was observed that the chip thickness increases as the width of cut increases. The results are presented in Figure 4.12 (a) for a feed of 0.2 mm/rev and Table 4.4 for a feed of 0.3 mm/rev. The increase in the chip thickness can be dictated by the plastic incompressibility and how close the orthogonal cutting to plane-strain conditions. At similar cutting speed and feed, the material has higher tendency to flow outside the plane of motion (cutting speed and feed) when the width of cut is small.

Consequently the resulting chip thickness will be smaller in order to conserve the volume of the flowing material. It is also observed that as the width of cut, the width of chip also increases. As the width of cut increases and the orthogonal cutting conditions tend to be plane strain conditions ($b/t \geq 10$ [56]), the rate of variation in the width of chip will decrease and tend to be zero. The results are shown in Figures 4.12 (b) for a feed of 0.2 mm/rev and Table 4.4 for a feed of 0.3 mm/rev.

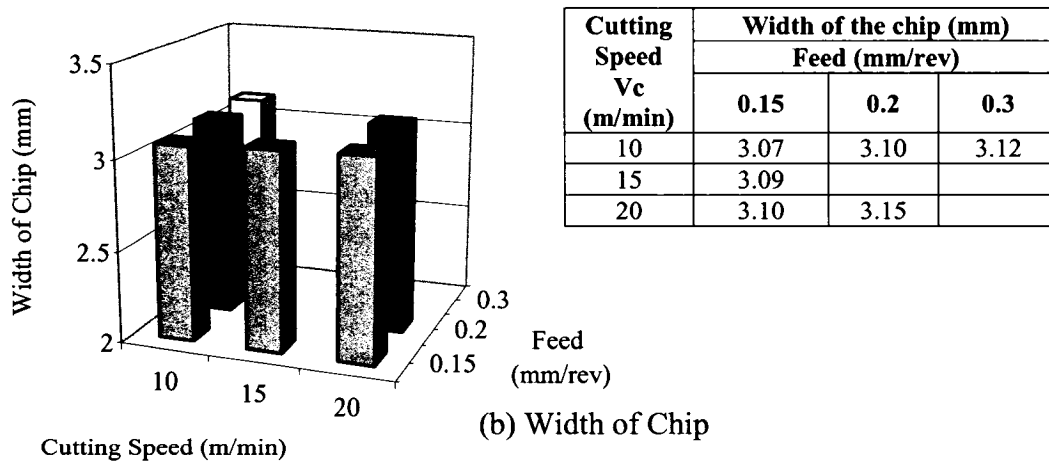
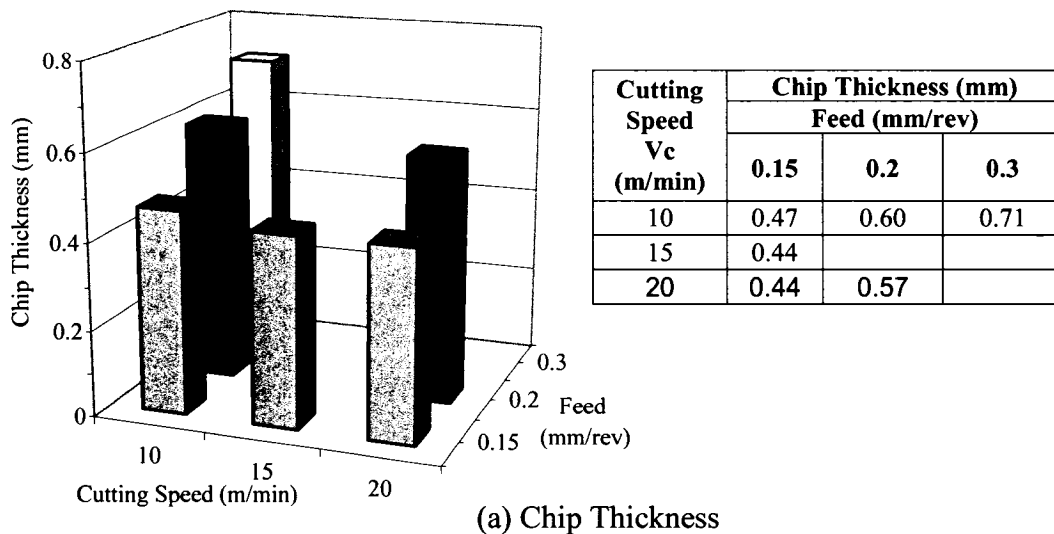
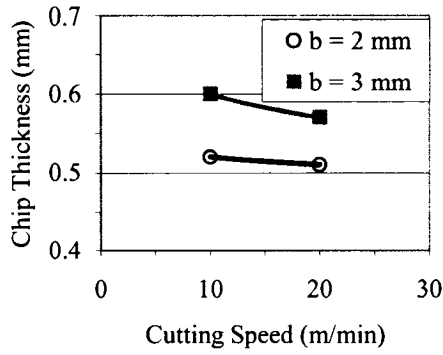
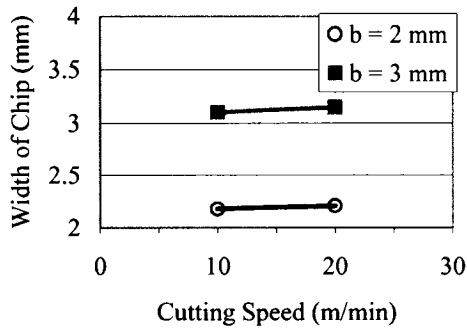


Figure 4.11: Effect of cutting speed and feed on (a) chip thickness and (b) width of chip for a 3 mm width of cut



Cutting Speed V_c (m/min)	Chip Thickness (mm)	
	Width of Cut (mm)	
	2	3
10	0.52	0.60
20	0.51	0.57

(a) Chip Thickness



Cutting Speed V_c (m/min)	Width of Chip (mm)	
	Width of Cut (mm)	
	2	3
10	2.18	3.10
20	2.21	3.15

(b) Width of Chip

Figure 4.12: Effect of width of cut on chip thickness and width of chip with a feed of 0.2 mm/rev

Table 4.4: Effect of width of cut on chip thickness and width of chip at a cutting speed of 10 m/min and feed of 0.3 mm/rev

Width of Cut (mm)	Chip Thickness (mm)	Width of Chip (mm)
2	0.69	2.26
3	0.71	3.12

4.2.2.3 Evaluation of Shear Stress, Strain and Strain Rate

Figure 4.13 (a), (b) and (c) shows the effect of cutting speed and feed on shear stress, shear strain, and strain rate, respectively. Figure 4.13 (a) shows a decrease in shear stress when the cutting speed increases except at cutting speed 15 m/min and feed 0.15 mm/rev where there is slight increase in shear stress, which is not significant (the increase is approximately 1.2%). The Figure 4.13 (a) shows also that the shear stress slightly decreases with an increase in the feed. Figure 4.13 (b) shows that shear strain decreases

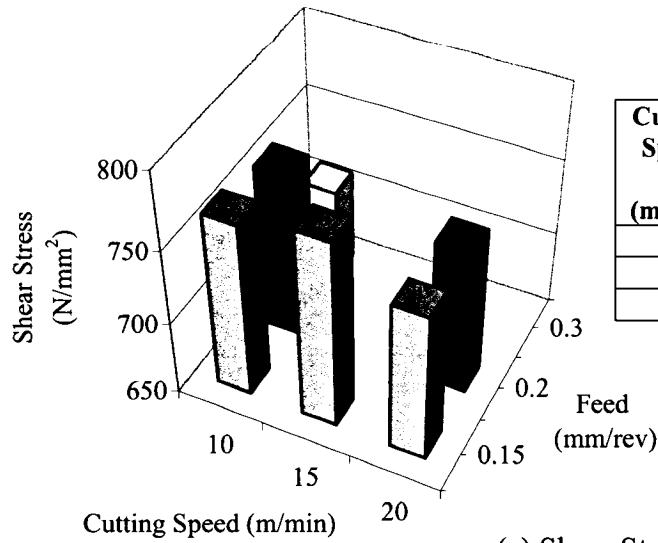
with an increase in feed, which is similar to the results observed with a 2 mm width of cut. Figure 4.13 (c) shows that the strain rate increases with the cutting speed and is practically independent of feed.

When compared to the values obtained with a 2 mm width of cut with a cutting speed of 10 m/min and 20 m/min at a feed of 0.2 mm/rev and 0.3 mm/rev, it is observed that increasing the width of cut decreases the shear stress. The results are shown in Figure 4.14 (a) and Table 4.5, respectively. Increasing the width of cut increases the shear strain. This increase is due to the increase of chip thickness, which decreases the cutting ratio and shear angle, which, in turn, increases the shear strain with relation to the equation 2.4. The results are shown in Figure 4.14 (b) and Table 4.5, respectively. The strain rate is independent of the increase in the width of cut at both feeds at 0.2 mm/rev and 0.3 mm/rev. The results are shown in Figure 4.14 (c) and Table 4.5, respectively.

4.2.2.4 Contact Length

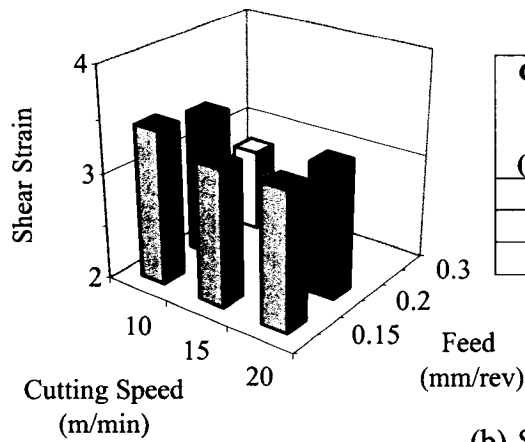
Figure 4.15 shows the measurement of contact length for all cutting conditions for a 3 mm width of cut. As expected, the contact length decreases with an increase in the cutting speed and increases with an increase in the feed [60]. This phenomenon has been explained earlier for the 2 mm width of cut. Table 4.6 represents the increase of shear angle as the cutting speed increases. Figure 4.16 represents the effect of shear angle on the chip-tool contact length.

When compared with the results obtained with the 2 mm width of cut with a cutting speed of 10 m/min and 20 m/min at a feed of 0.2 mm/rev, the contact length decreases with an increase in the width of cut. A similar trend also is observed with a feed of 0.3 mm/rev. The results are shown in Figure 4.17 and Table 4.7, respectively. This decrease in the contact length can be attributed to the curling effect of the chip. With an increase in the width of cut (from 2 mm to 3 mm), it has been observed that the curling effect is more pronounced, which leads to a decrease in the contact length. Figures 4.18 and 4.19 illustrate this effect for feeds of 0.2 mm/rev and 0.3 mm/rev, respectively.



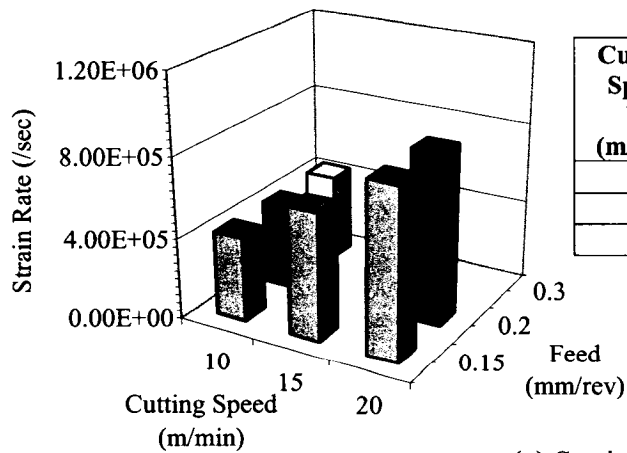
Cutting Speed Vc (m/min)	Shear Stress (N/mm ²)		
	Feed (mm/rev)		
	0.15	0.2	0.3
10	768	760	712
15	777		
20	750	749	

(a) Shear Stress



Cutting Speed Vc (m/min)	Shear Strain		
	Feed (mm/rev)		
	0.15	0.2	0.3
10	3.45	3.36	2.79
15	3.28		
20	3.28	3.23	

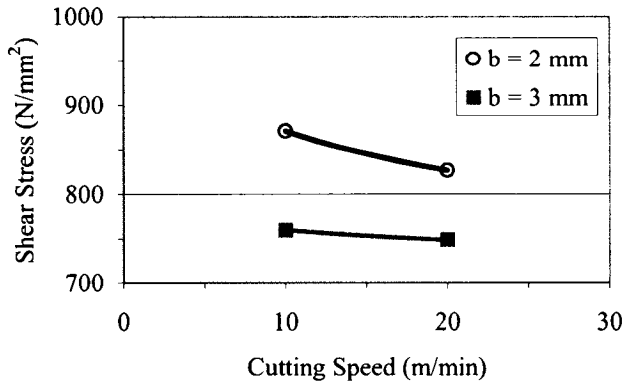
(b) Shear Strain



Cutting Speed Vc (m/min)	Strain Rate		
	Feed (mm/rev)		
	0.15	0.2	0.3
10	4.20E+05	4.21E+05	4.34E+05
15	6.34E+05		
20	8.42E+05	8.47E+05	

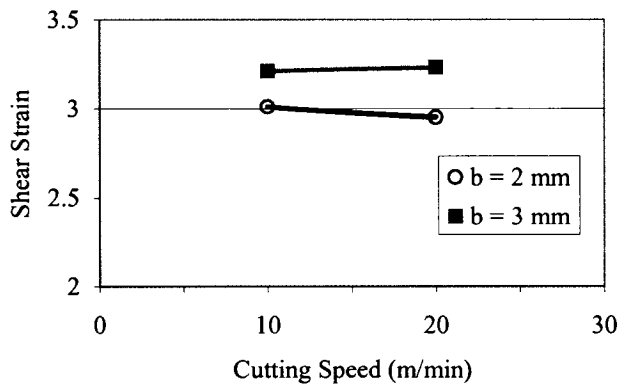
(c) Strain Rate

Figure 4.13: Effect of cutting speed and feed on shear stress, strain, and strain rate for a 3 mm width of cut



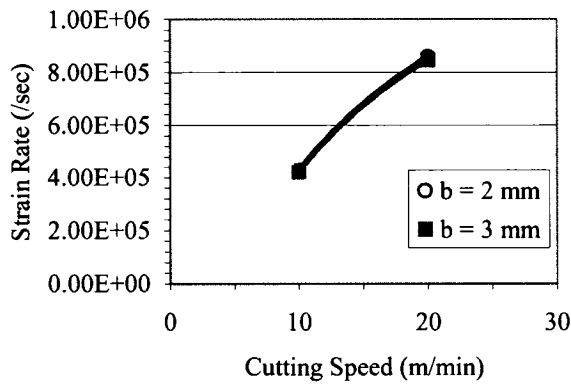
Cutting Speed V_c (m/min)	Shear Stress (N/mm^2)	
	Width of Cut (mm)	
	2	3
10	871	760
20	827	749

(a) Shear Stress



Cutting Speed V_c (m/min)	Shear Strain	
	Width of Cut (mm)	
	2	3
10	3.01	3.21
20	2.95	3.23

(b) Shear Strain



Cutting Speed V_c (m/min)	Strain Rate	
	Width of Cut (mm)	
	2	3
10	4.28E+05	4.21E+05
20	8.59E+05	8.47E+05

(c) Strain Rate

Figure 4.14: Effect of width of cut on shear stress, shear strain, and strain rate with a feed of 0.2 mm/rev

Table 4.5: Effect of width of cut on shear stress, shear strain, and strain rate at a cutting speed of 10 m/min and feed of 0.3 mm/rev

Width of Cut (mm)	Shear Stress (N/mm ²)	Shear Strain	Strain Rate
2	916	2.76	4.35E+05
3	712	2.79	4.34E+05

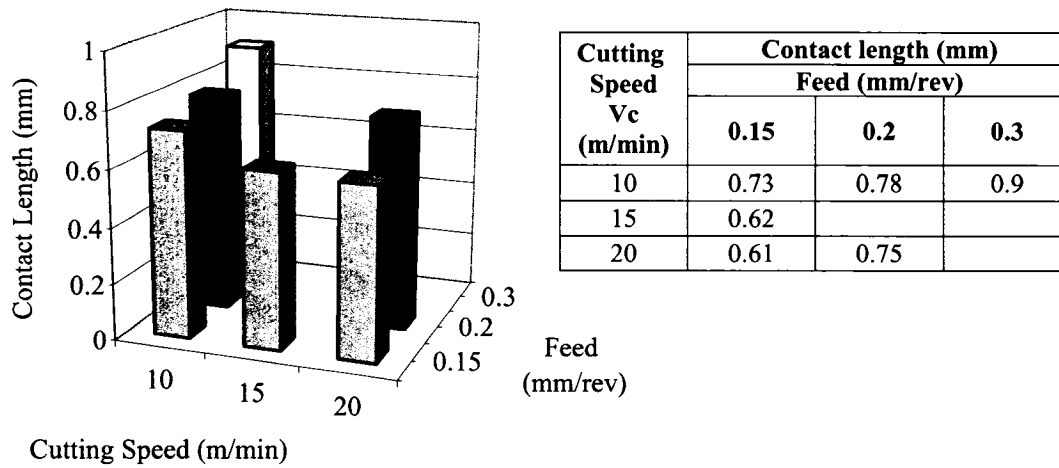


Figure 4.15: Effect of cutting speed and feed on contact length for a 3 mm width of cut

Table 4.6: Effect of shear angle with an increase in the cutting speed

Cutting Speed Vc (m/min)	Shear Angle (ϕ)		
	Feed (mm/rev)		
	0.15	0.2	0.3
10	17.74	18.29	22.90
15	18.77		
20	18.77	19.10	

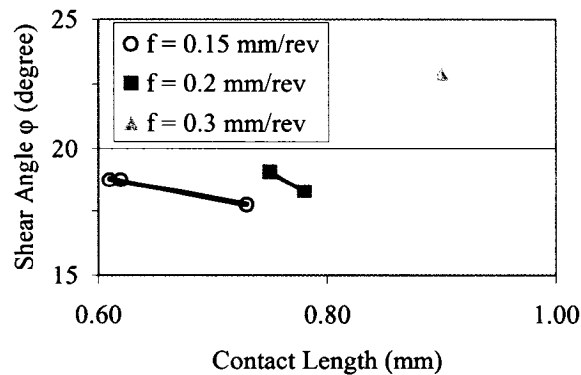
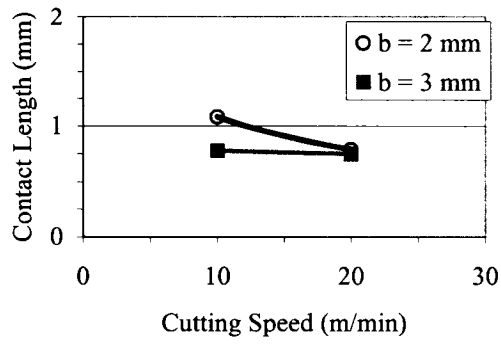


Figure 4.16: Effect of shear angle and chip-tool contact length with 2 mm width of cut



Cutting Speed V_c (m/min)	Contact Length (mm)	
	Width of Cut (mm)	
	2	3
10	1.08	0.78
20	0.79	0.75

Figure 4.17: Effect of width of cut on contact length with feed 0.2 mm/rev

Table 4.7: Effect of width of cut on contact length with feed 0.3 mm/rev

Cutting Speed V_c (m/min)	Contact Length (mm)	
	Width of Cut (mm)	
	2	3
10	1.01	0.9

Cutting Speed V_c (m/min)	Width of Cut (mm)	
	2	3
10		
20		

Figure 4.18: Effect of width of cut on the curling of chip with feed 0.2 mm/rev

Cutting Speed V_c (m/min)	Width of Cut (mm)	
	2	3
10		

Figure 4.19: Effect of width of cut on the curling of chip with feed 0.3 mm/rev

The results produced in the orthogonal machining process will lead to the development of the constitutive laws of material Inconel 718. However, the machinability of Inconel 718 in terms of tool wear need to be examined under oblique finish turning operation, which is explained in the next section.

4.3 Finish Turning Operation

The test matrix and the tools used during the finish turning operation are described in Chapter 3. The finish turning operation is an important process that is used in practice to achieve desired surface finish and dimensional accuracy. In orthogonal cutting, the cutting edge is perpendicular to the velocity vector, whereas in oblique turning, the straight cutting edge is inclined to the velocity vector. This section deals with (1) the effect of tool coating on tool wear mechanism and failure mode and (2) the effect of the cutting speed and feed on surface finish. In the first section, tool wear mechanisms and tool failure modes are discussed in relation to chip formation and chip morphology, cutting forces and tool life.

4.3.1 Tool Wear Mechanisms and Tool Failure Modes

In this section, the tool wear mechanisms have been studied for various cutting conditions. Figure 4.20 shows the different tool wear modes during the machining process. The causes for the types of tool wear that can be encountered are discussed in this section.

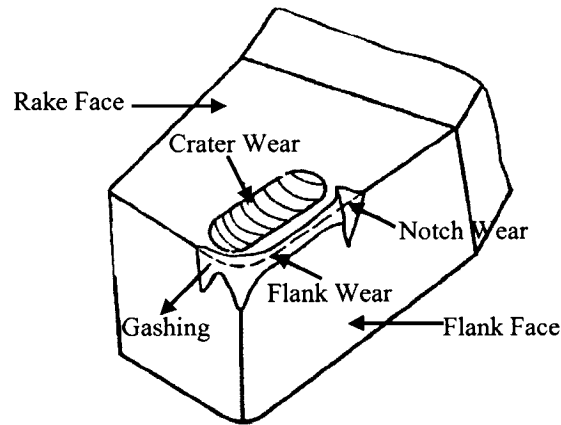


Figure 4.20: Different tool wear modes [61]

Wear on the flank face is called the flank wear and results in the formation of a wear land. It most commonly results from the abrasive wear of the cutting edge against the machined surface. Diffusion wear occurs by a process of chemical dissolution of the tool material, in the chip, particularly at the hottest points of contact on the top, rake face (called crater wear). This is also due to the severe friction between the chip and rake face, leaving a scar on the rake face, which usually parallels the major cutting edge. The gashing (or grooving, or gouging) at the outer edge of the wear land is an indication of a hard or abrasive skin on the work material. Depth of cut (DOC) notch wear is the result of an oxidation process whereby the carbide actually breaks down, leaving a void on the cutting edge [61].

4.3.1.1 Tool Wear Mechanism at Low Cutting Speed (50 m/min)

Figure 4.21 (a), (b) and (c) shows the SEM image for the wear mechanisms observed at a low cutting speed of 50 m/min and a feed of 0.075 mm/rev for three different types of tools when the tool life was 33.55, 24.34 and 2.5 min. respectively. The tool life was calculated when the average flank wear reaches 300 μm . The wear mechanisms observed were mainly abrasion and adhesion on the tool rake face and the flank face. This applies to all three tools. The abrasion wear is due to the impurities within the workpiece material, such as carbon, nitride, and oxide compounds, as well as, built up fragments [61]. The adhesion wear is due to the high temperature and pressure during cutting which cause welding to occur between the fresh surface of the chip and the rake face (chip flows on the rake face results in a chemically clean surface) [61].

Figure 4.22, which shows the chemical analysis for all three types of tools on the rake face before and after cutting, demonstrates the transfer of material and wear by adhesion. Flank wear is the common tool wear mode observed for all three different types of tools. However, as is shown in Figure 4.21 (c), with the triple layer CVD coated tools, another tool wear mode was observed—flaking of the coating. This is due to prolonged cutting, for example, when cutting was continued even after the tool wear criterion (of 300 μm of average flank wear) was met [34]. The DOC notch wear was seen only with the triple layer CVD (TiCN/Al₂O₃/TiN) coated tool, as illustrated in Figure 4.23. However, this is not a dominant tool failure mode.

The wear mechanisms were also studied with different feeds of 0.1 mm/rev and 0.125 mm/rev at a cutting speed of 50 m/min. As illustrated in Figures 4.24 and 4.25, no significant difference exists in the tool wear mechanisms when the feed rate is increased.

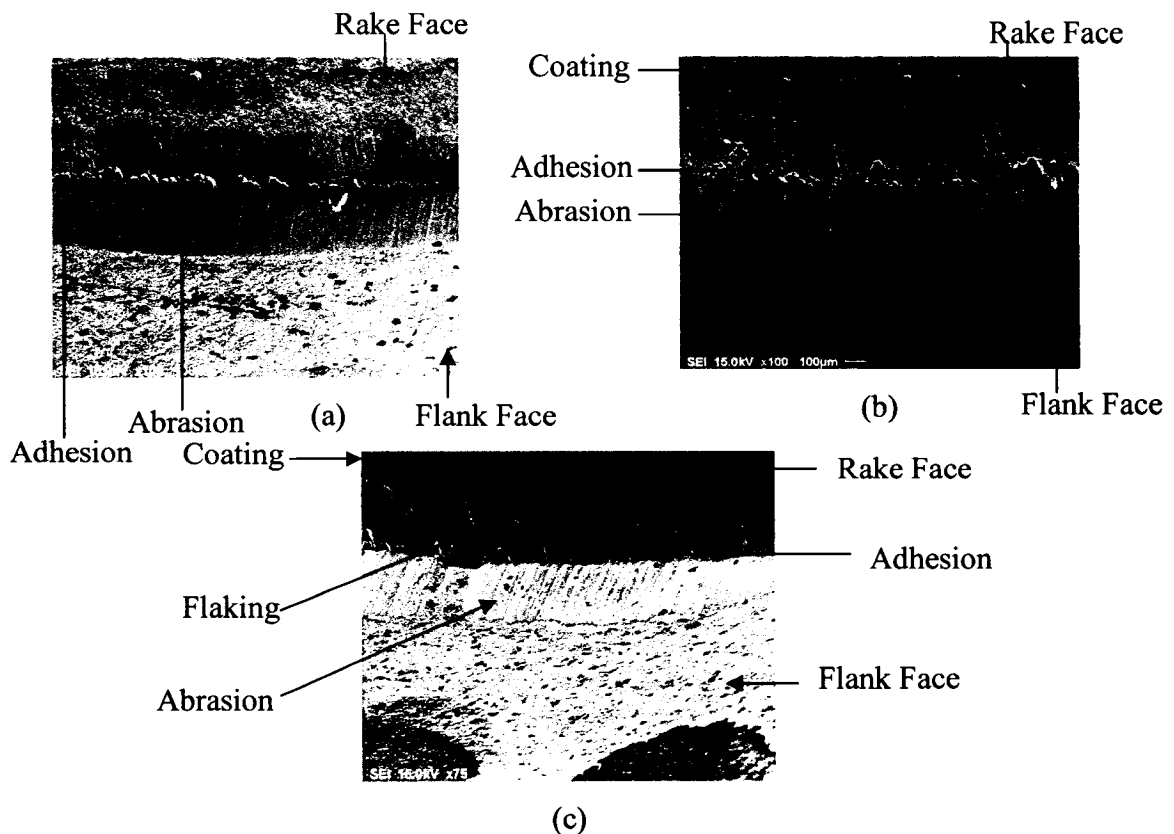


Figure 4.21: SEM images for a speed of 50 m/min and a feed of 0.075 mm/rev: (a) rake and flank face for an uncoated tool at 33.55 min., (b) rake and flank face for a single layer PVD coated tool at 24.34 min., and (c) rake and flank face for a triple layer CVD coated tool at 2.5 min.

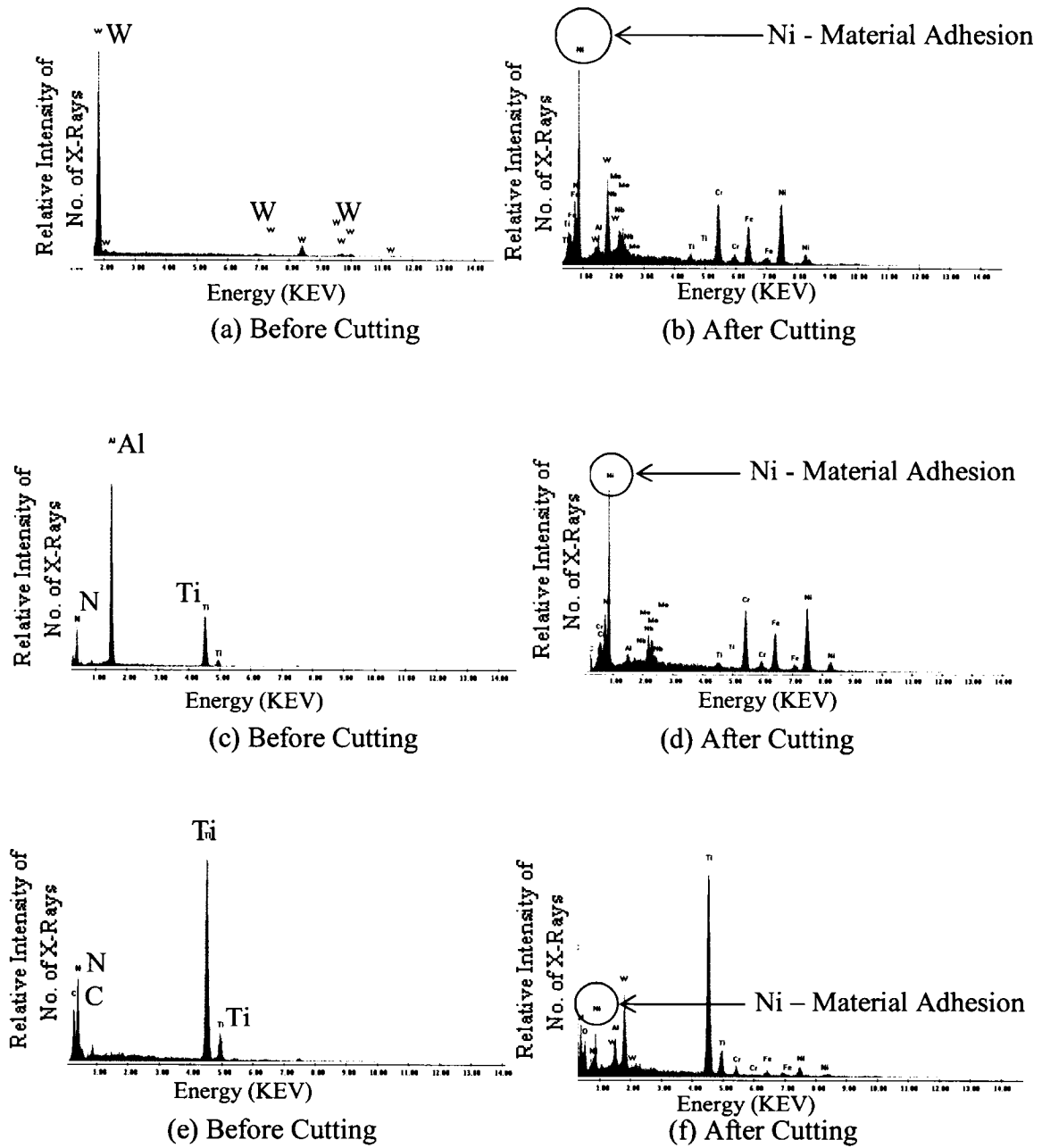
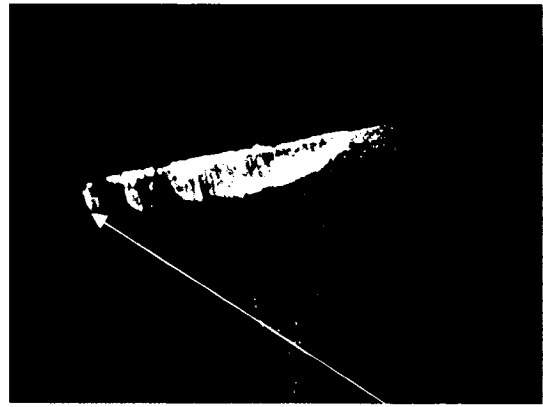


Figure 4.22: Chemical analysis of the tool rake face for an uncoated tool (a) Before Cutting and (b) After Cutting; Chemical analysis of the tool rake face for a single layer PVD TiAlN coated tool (c) Before Cutting and (d) After Cutting, and Chemical analysis of the tool rake face for a triple layer CVD TiCN/Al₂O₃/TiN coated tool (e) Before Cutting and (f) After Cutting.

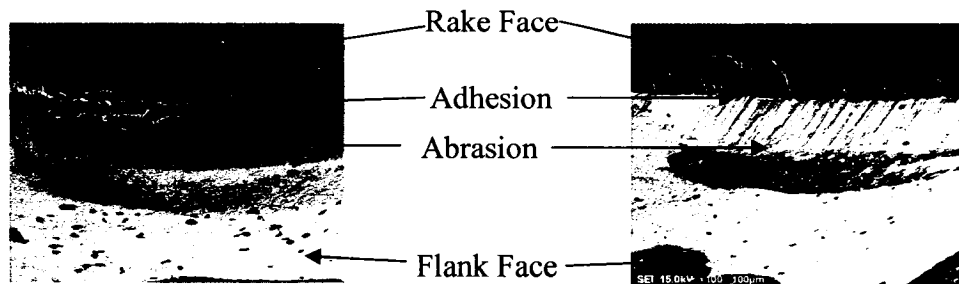


DOC Notch Wear (a)



(b) DOC Notch Wear

Figure 4.23: Triple layer CVD (TiCN/Al₂O₃/TiN) coated tool (a) rake face (b) flank face



(a)

(b)



(c)

Figure 4.24: SEM images for a speed of 50 m/min and a feed of 0.1 mm/rev: (a) rake and flank face for an uncoated tool at 38.85 min., (b) rake and flank face for a single layer PVD coated tool at 19.75 min., and (c) rake and flank face for a triple layer CVD coated tool at 11.60 min.

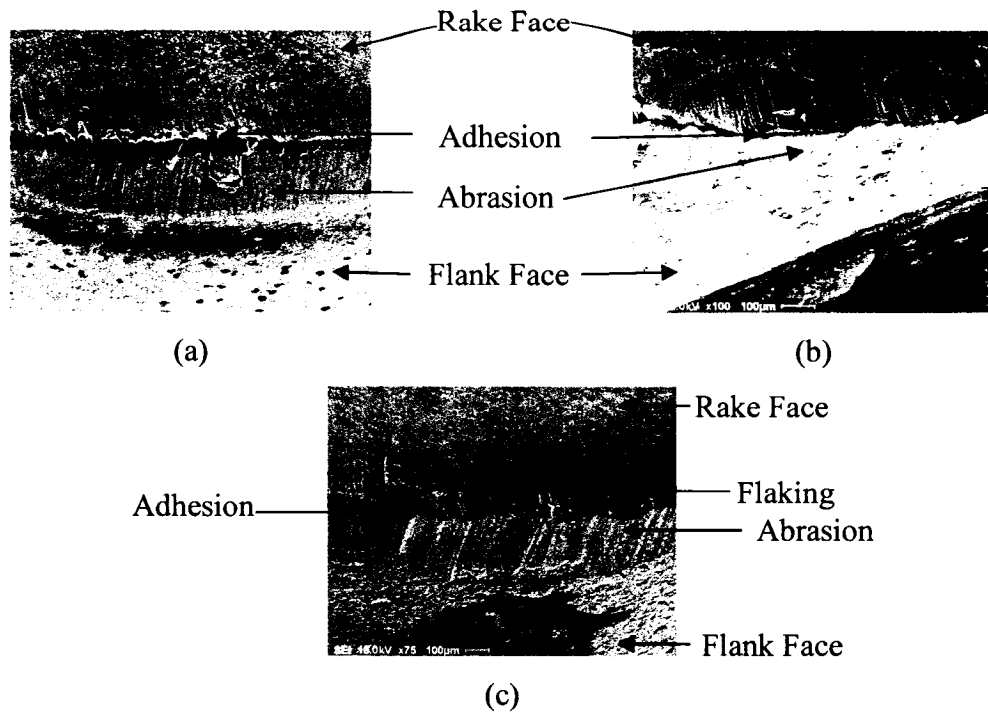


Figure 4.25: SEM images for a speed of 50 m/min and a feed of 0.125 mm/rev: (a) rake and flank face for an uncoated tool at 27.42 min., (b) rake and flank face for a single layer PVD coated tool at 20.32, and (c) rake and flank face for a triple layer CVD coated tool at 8.19 min.

4.3.1.1.1 Chip Morphology and Metallurgical Analysis at a Low Cutting Speed (50 m/min)

The metallurgical aspect was studied for the material as well as for the chips formed during cutting conditions. Figure 4.26 shows the SEM image with chemical analysis for the material Inconel 718 used for the machining test. The chemical analysis was done at different areas as shown in Figure 4.26 (a), and at these different areas, the same chemical composition was observed. The micro-hardness was measured at different areas, and an average value of 301 HV was obtained.

The metallographic study of the chip shown in Figure 4.27 was done to reveal the structure of the chip for the uncoated tool at a feed of 0.075 mm/rev. The chemical analysis was carried out at three different areas, as illustrated in the Figure 4.28. The chemical composition was observed to be similar to that of the base material. No phase

transformation was observed on the chip. In some of the analysis, the carbon content was observed to be high, which is due to the bakelite powder on which the chips were mounted. A similar study of the chip formed by single layer PVD coated tool at a feed of 0.1 mm/rev was carried out, as illustrated in Figures 4.29 and 4.30, and again, the same kinds of observations were made.

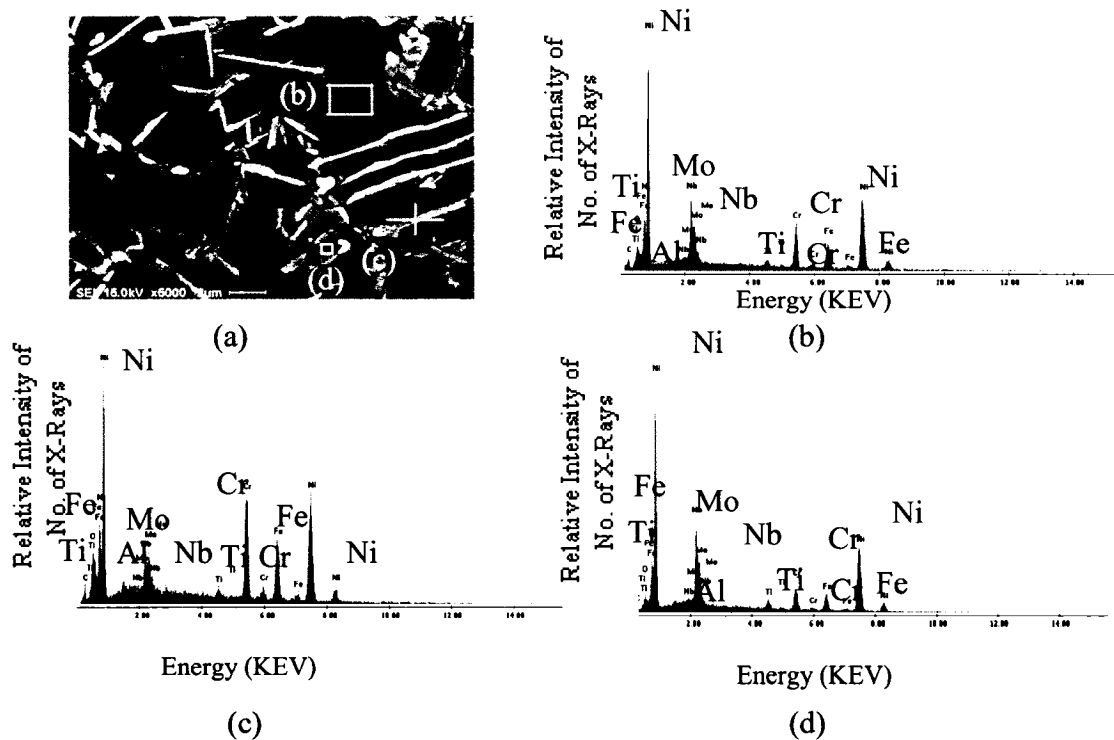


Figure 4.26: SEM Image for Inconel 718 with the spot marked (a) where the chemical analysis is done (b, c, d) using SEM

The micro-hardness was measured at three sections on the chip (section A = at the top section of the chip, section B = in the middle of the chip, and section C = near the secondary shear zone), as illustrated in the Figure 4.31, to check the strain hardening effect of the chips formed by the uncoated and single layer PVD coated tools during the oblique finish turning operation. Table 4.8 represents the values for micro-hardness. An increase in the micro-hardness of the chip due to the strain-hardening effect was observed as compared with the initial value of hardness, which is 301 HV. It also is observed that the value of micro-hardness is high at the top section (free surface) of the chip.

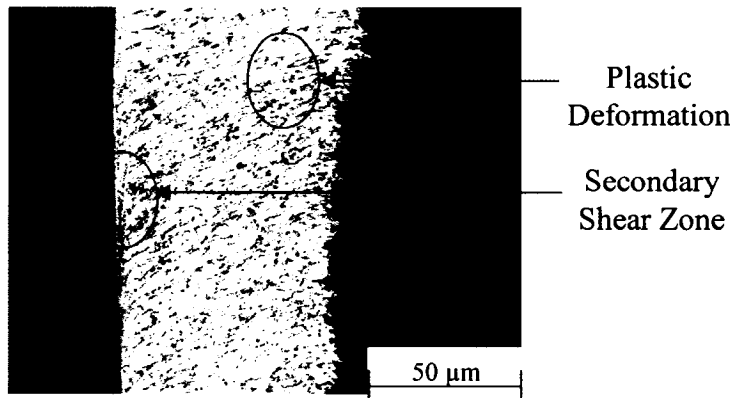


Figure 4.27: Chip image for the uncoated tool at a cutting speed of 50 m/min and a feed of 0.075 mm/rev

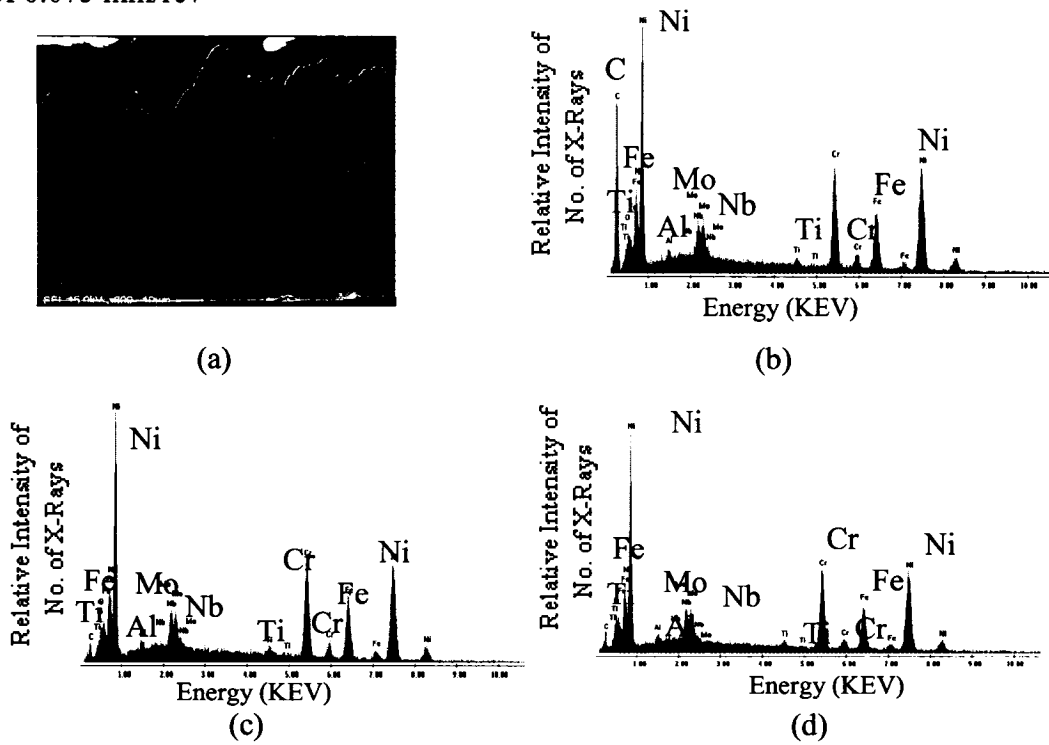


Figure 4.28: Chip image with the spot marked where the chemical analysis is done (a); chemical analysis using SEM (b, c, d) for a speed of 50 m/min and a feed of 0.075 mm/rev with an uncoated tool showing no phase transformation

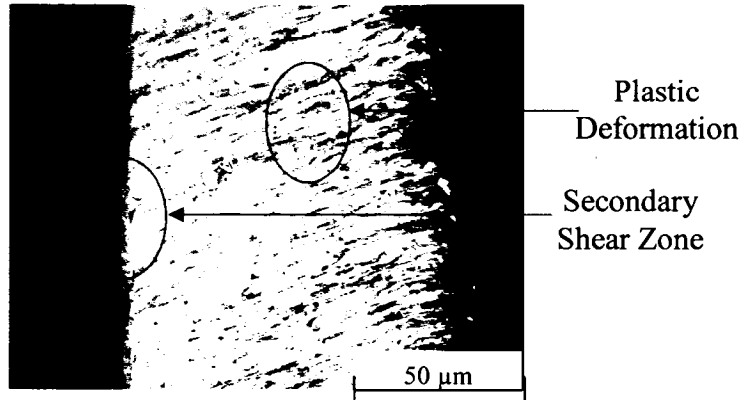


Figure 4.29: Chip image at a cutting speed of 50 m/min and a feed of 0.1 mm/rev for a single layer PVD coated tool

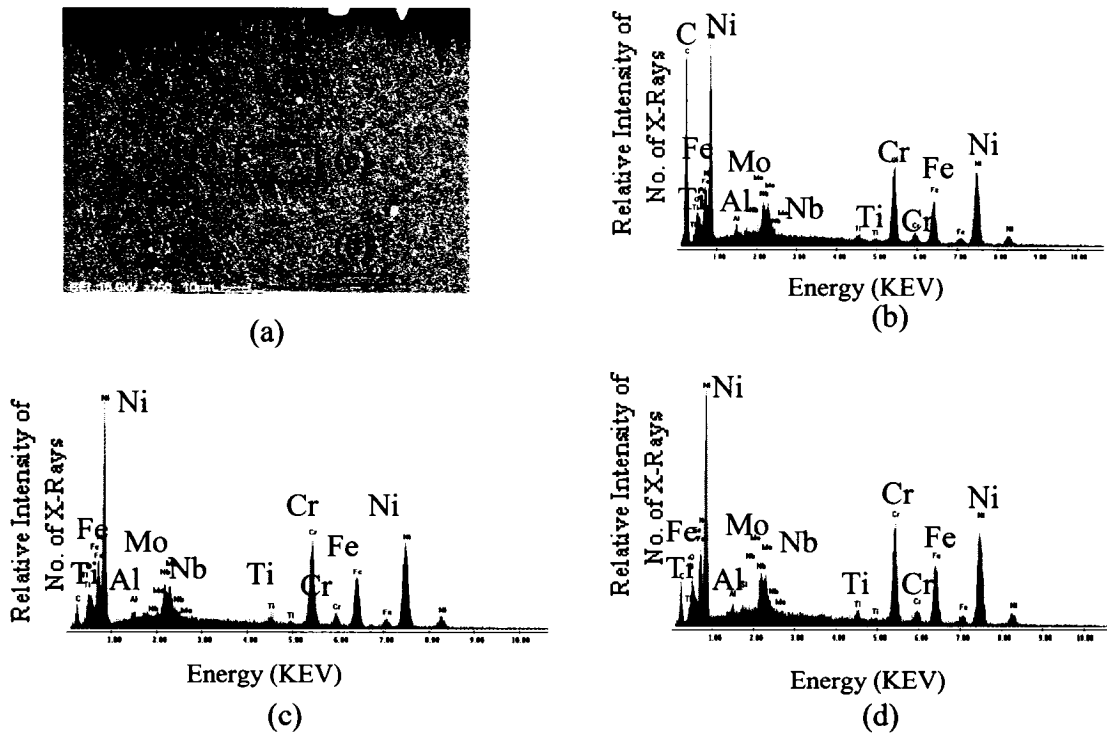


Figure 4.30: Chip image with the spot marked where the chemical analysis is done (a); chemical analysis using SEM (b, c, d) for a speed of 50 m/min and a feed of 0.1 mm/rev with a single layer PVD TiAlN coated tool showing no phase transformation

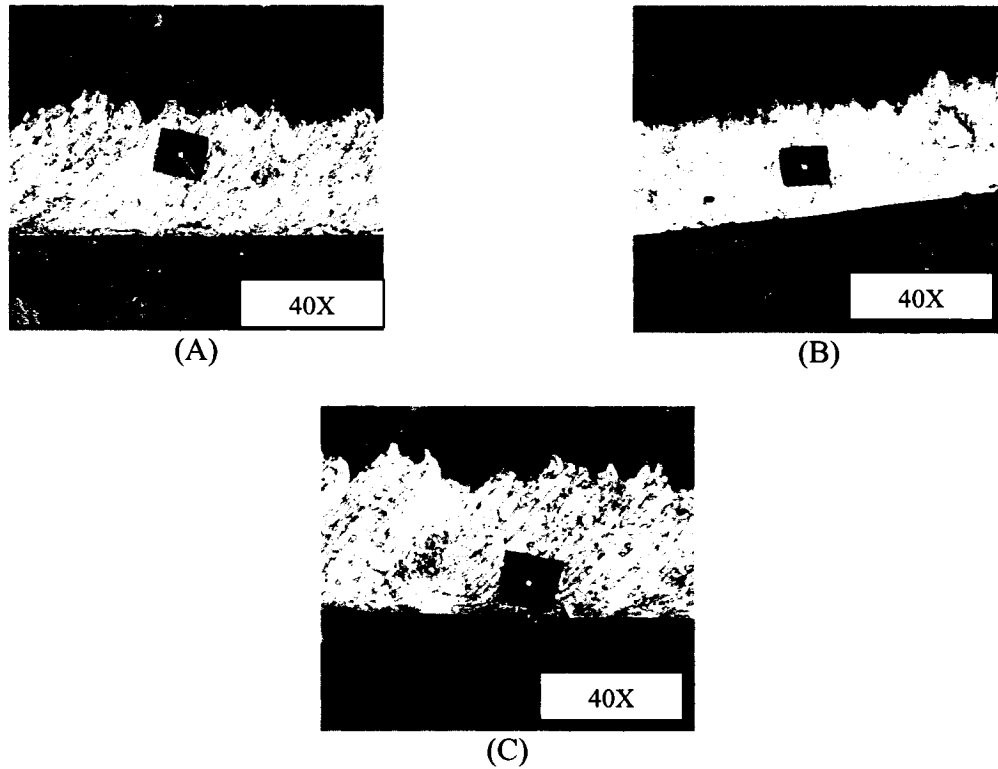


Figure 4.31: Micro-hardness measurement done at three areas (A, B, C)

Table 4.8: Micro-hardness measurement for a cutting speed of 50 m/min

Tool	Cutting Conditions			Micro-Hardness (HV)		
	Vc (m/min)	F (mm/rev)	DOC (mm)	A	B	C
Uncoated	50	0.075	0.25	509	506	432
Single Layer PVD Coated	50	0.1	0.25	534	509	503

4.3.1.1.2 Forces at Low Cutting speed (50 m/min)

Figure 4.32 shows the thrust force, feed force, and cutting force for three different tools at three different feeds when the tool edge is sharp. The direction of these forces in oblique finish turning operation is shown in Figure 3.6. All three forces increase with an increase in feed per revolution with both the uncoated and single layer PVD TiAlN tools, except for PVD coated tool there is a slight decrease in the feed force (Figure 4.32 (b)) and cutting force (Figure 4.32 (c)) at feed 0.1 mm/rev (the decrease is approximately 4.2 to 7.6 %), which is not significant.. The reason for this can be attributed to the increase in the chip thickness. An increase in chip thickness with an increase in the feed rate per revolution leads to an increase of the cutting area, which induces the cutting forces to increase [30]. Contrary to this, for the triple layer CVD coated tool, all three forces

decrease or remain practically unchanged with an increase in feed per revolution. This can be attributed to the properties of the intermediate coating (Al_2O_3), which is high hot hardness (hardness of the material at elevated temperature), excellent chemical stability, and low thermal conductivity at elevated temperatures [44], which permit more heat flow towards the material and chip as compared to the substrate. This will result in the softening of the material, thus reducing the cutting forces.

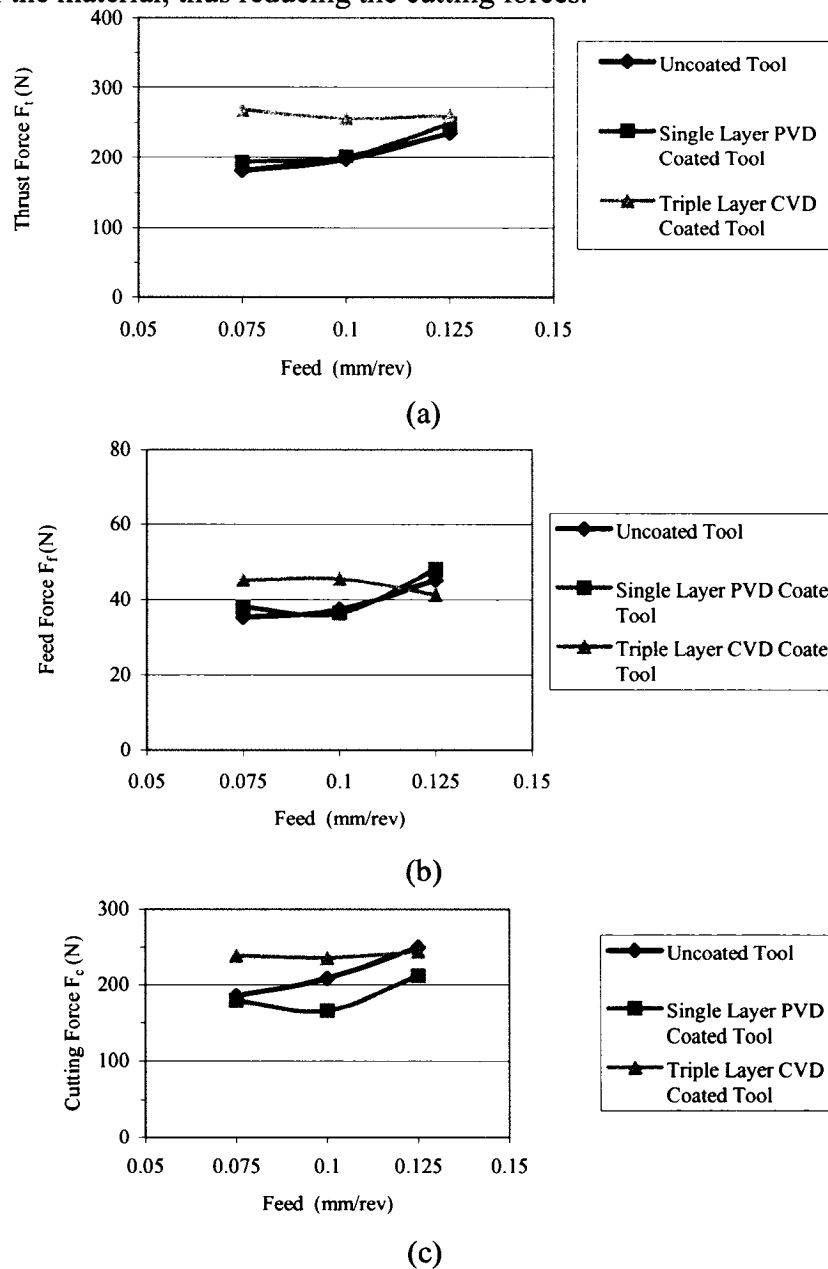


Figure 4.32: Forces with three different tools when the tool edge is sharp at speed 50 m/min and three different feeds (a) thrust force, (b) feed force, and (c) cutting force

4.3.1.1.3 Tool Life at a Low Cutting Speed (50 m/min)

As shown in Figure 4.34, the tool wear progression with respect to time was studied for all three different types of tools, at three different feeds—0.075 mm/rev, 0.1 mm/rev, and 0.125 mm/rev. Average flank wear was found to be the dominant tool failure mode at all feeds. The three regions of the flank wear were also shown in Figure 4.34 for all three different tools. The tool life was calculated by regression analysis when the average flank wear was 300 μm .

There are three regions of flank wear, as illustrated in Figure 4.33, are described as follows [61]:

(A) Initial (or preliminary) Wear Region: This region is caused by micro-cracking, surface oxidation and carbon loss layer, at the cutting tool tip. For the new cutting edge, due to the small contact area and high contact pressure, it will result in high wear rate.

(B) Steady Wear Region: After the initial (or preliminary) wear (cutting edge rounding), the micro-roughness improved in this region, and the wear size is proportional to the cutting time. The wear rate is relatively constant.

(C) Severe (or ultimate or catastrophic) Wear Region: When the wear size increases to a critical value, the surface roughness of the machined surface decreased, the cutting force and temperature increase rapidly, and as a result the wear rate increases. Then the tool loses its cutting ability.

The three regions are shown in Figure 4.34 (a), (b), (c) for the uncoated tool only when compared with Figure 4.33, for the sake of clarity. The time duration for this regions for all the three different tools are shown in Table 4.9. At low speed of 50 m/min the wear pattern for uncoated tool is uniform as compared to single layer PVD coated and triple layer CVD coated tools.

Figure 4.34 also shows that in terms of tool life, the performance of the uncoated tool was superior at low cutting speed and at all three different feeds. The excellent resistance to flank wear of the uncoated tools was noted at a low speed of 50 m/min. It was also observed that the uncoated tool gives the best tool life of 53 min. at 0.1 mm/rev. The test was discontinued for the uncoated tool at 0.1 mm/rev when the wear reached 283 μm due to the chipping of the cutting edge, and loss on the material condition (*i.e.* hardness value). The value for the tool life at a feed of 0.1 mm/rev was extrapolated to 300 μm average flank wear using regression analysis.

The single layer PVD coated tool performed better than the triple layer CVD coated tool. The best tool life of 23 min. was found at a feed of 0.075 mm/rev. As the PVD coated TiAlN tool has the lowest thermal conductivity [36, 61], this should result in lower tool tip temperatures, since much of the heat generated during machining would be carried away by the chip. As a result, the TiAlN coating imparts excellent resistance to crater wear and consequently increases tool life [36]. With the increase in feed, the average flanks wear increases, results in decreasing the tool life.

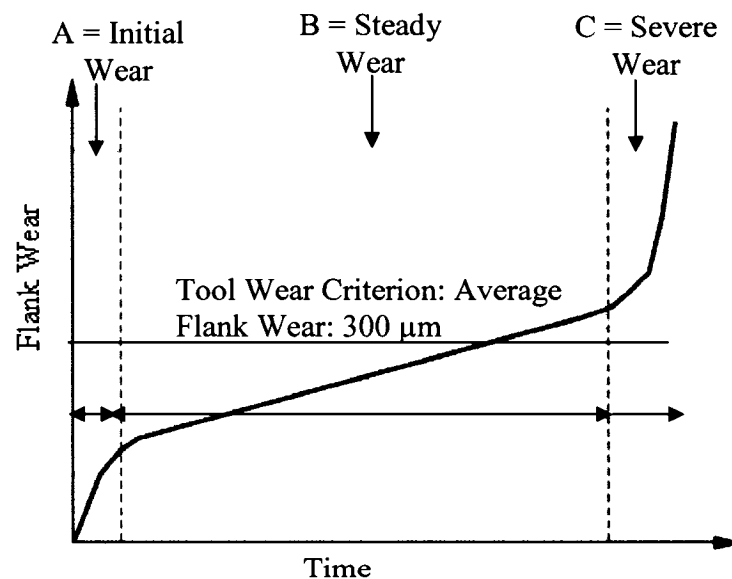


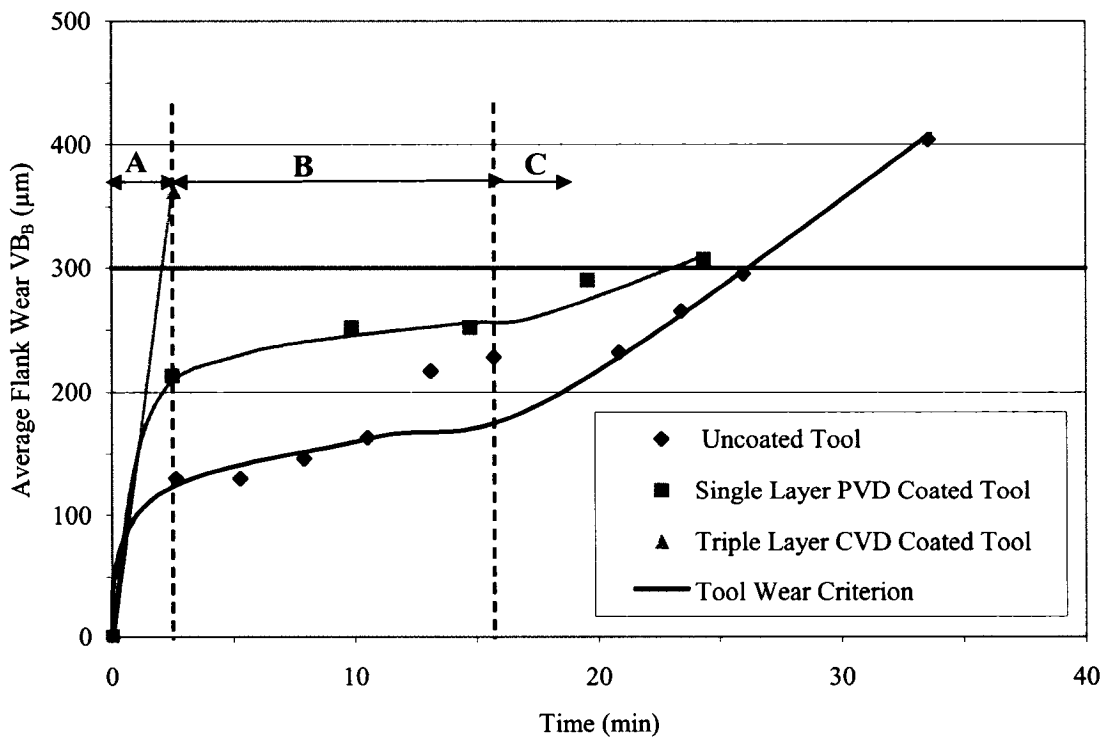
Figure 4.33: Variation of flank wear rate with cutting time, showing the initial wear, steady wear, and severe wear periods

The triple layer CVD coated tool had the worst tool life at only 2 min. at a low feed of 0.075 mm/rev. This tool fails at the first pass and did not withstand the mechanical load.

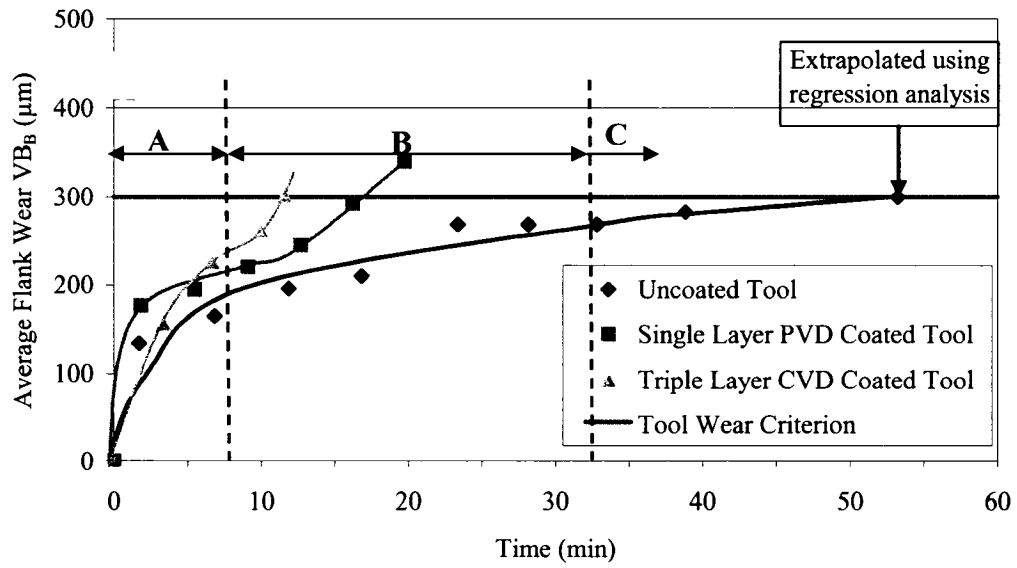
However, with an increase in feed, the triple layer performs better and gives a better tool life. This can be attributed to the properties of the intermediate coating (Al_2O_3), which is high hot hardness, excellent chemical stability, and low thermal conductivity at elevated temperatures, which permit less heat flow to the substrate, thus ensuring improved wear resistance [44]. Although the CVD coated tools showed a tendency for depth of cut notching, the end of tool life was reached by average flank wear.

Table 4.9: Time duration at which three regions formed at cutting speed of 50 m/min

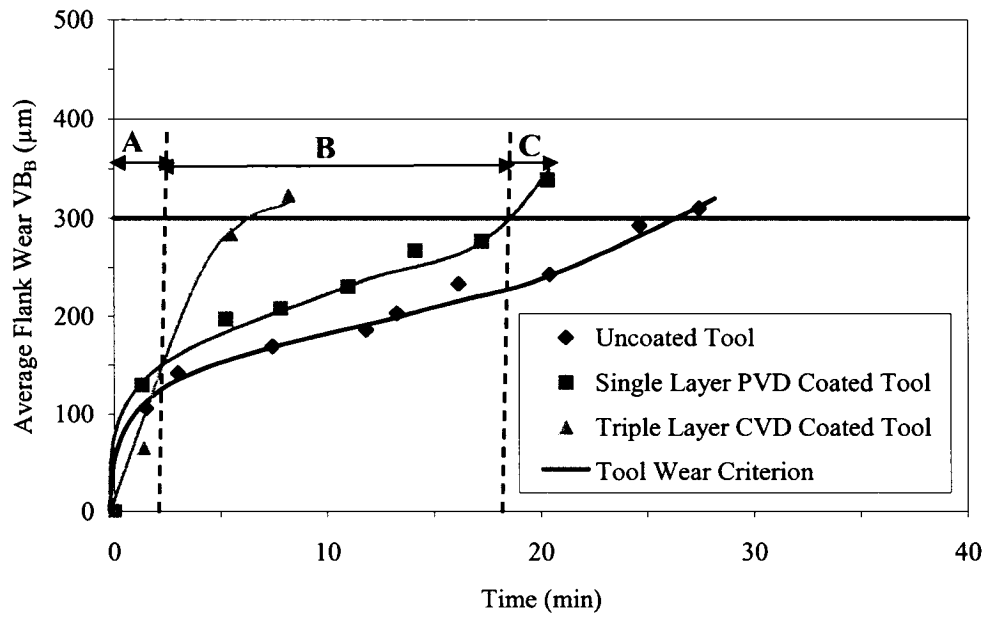
Tool	Time (min.)								
	Feed 0.075 mm/rev			Feed 0.1 mm/rev			Feed 0.125 mm/rev		
	Duration of Region								
	A	B	C	A	B	C	A	B	C
Uncoated	0-5.28	5.28-18.29	18.29-33.55	0-6.83	6.83-28.16	28.16-38.85	0-3	3-17.58	17.58-27.42
PVD Coated Single Layer	0-2.56	2.56-17.14	17.14-24.34	0-1.83	1.83-12	12-19.75	0-1.31	1.31-15.2	15.2-20.32
CVD Coated Triple Layer	-	-	2.56	0-1.68	1.68-9.97	9.97-11.60	0-4.12	4.12-6.84	6.84-8.19



(a)



(b)



(c)

Figure 4.34: Tool wear progression for three different tools at cutting speed of 50 m/min and feeds of (a) 0.075 mm/rev (b) 0.1 mm/rev (c) 0.125 mm/rev

4.3.1.2 Tool Wear Mechanism at a Medium Cutting Speed (75 m/min)

The wear mechanism also was studied at a medium speed of 75 m/min—similar to the discussion shown in Section 4.2.1.2 at a slow speed of 50 m/min—at three different feeds of 0.075 mm/rev, 0.1 mm/rev, and 0.125 mm/rev. Figure 4.35 shows the SEM image for the wear mechanisms for the three different types of tools used at a medium cutting speed of 75 m/min and a feed of 0.075 mm/rev when tool life was, 8.56 13.91 and 10.39 min. respectively

The wear mechanisms seen for all three different types of tools were similar to those observed at a low speed of 50 m/min and a feed of 0.075 mm/rev. As expected, the wear mechanisms were influenced by the cutting speed. The tool failure mode was similar to that found with a speed of 50 m/min and a feed of 0.075 mm/rev. However, with the triple layer CVD coated insert, another wear mechanism, namely, diffusion wear, was seen, and the tool failure mode of this tool was crater wear. The crater wear can be attributed to the diffusion and dissolution wear mechanism. Also, excessive chipping of the cutting edge was observed, which may be due to the observed increase in vibration level, possibly due to the tangling of the chips. As well, a similar observation can be made about an increase in feed from 0.1 mm/rev to 0.125 mm/rev. However, with an increase in feed, crater wear was not seen in the triple layer CVD coated tool. This is again due to the intermediate coating (Al_2O_3), which has an excellent chemical stability at an elevated temperature [44]. Figures 4.36 and 4.37 illustrate the SEM image for all three different types of tools at a feed of 0.1 mm/rev and 0.125 mm/rev.

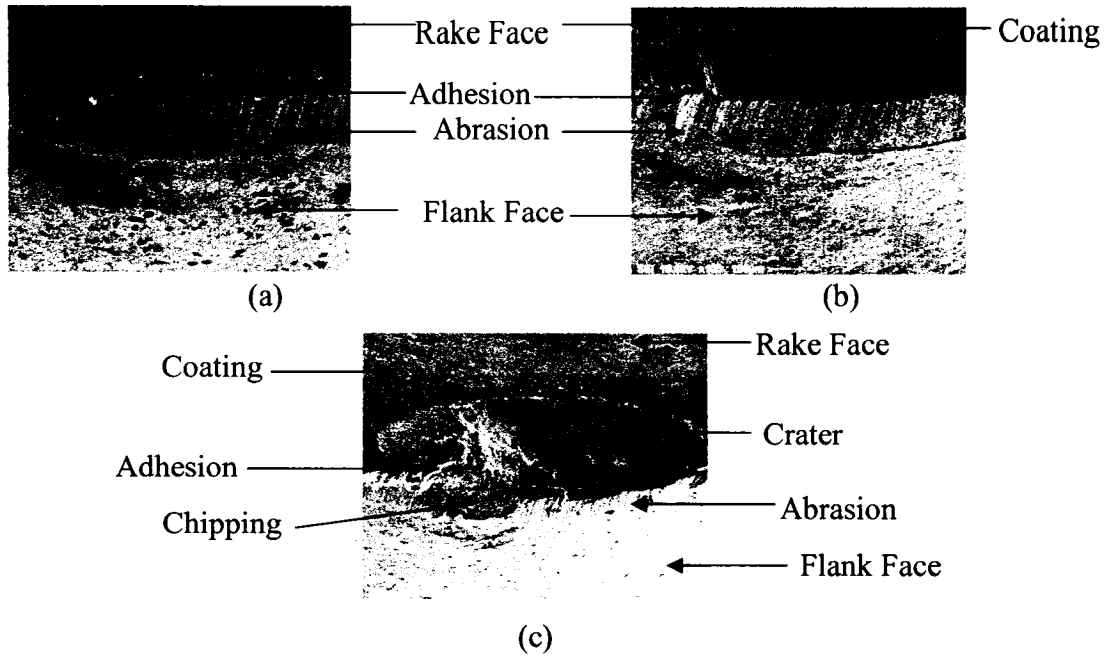


Figure 4.35: SEM images for a speed of 75 m/min and a feed of 0.075 mm/rev: (a) rake and flank face for an uncoated tool at 8.56 min., (b) rake and flank face for a single layer PVD coated tool at 13.91 min., and (c) rake and flank face for a triple layer CVD coated tool at 10.39 min.

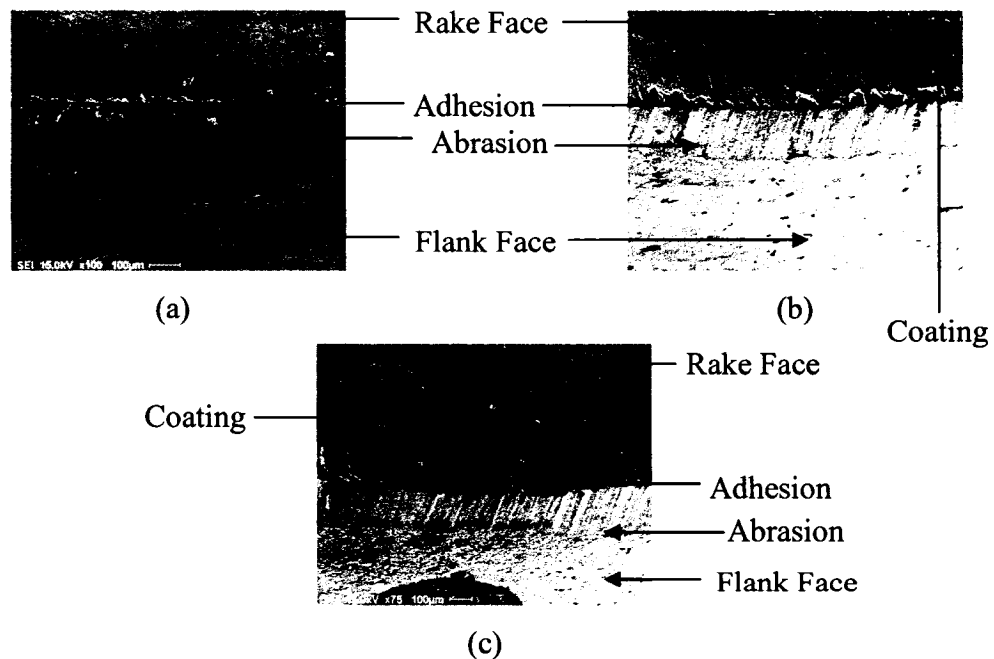


Figure 4.36: SEM images for a speed of 75 m/min and a feed of 0.1 mm/rev: (a) rake and flank face for an uncoated tool at 6.67 min., (b) rake and flank face for a single layer PVD coated tool at 13.63 min., and (c) rake and flank face for a triple layer CVD coated tool at 6.34 min.

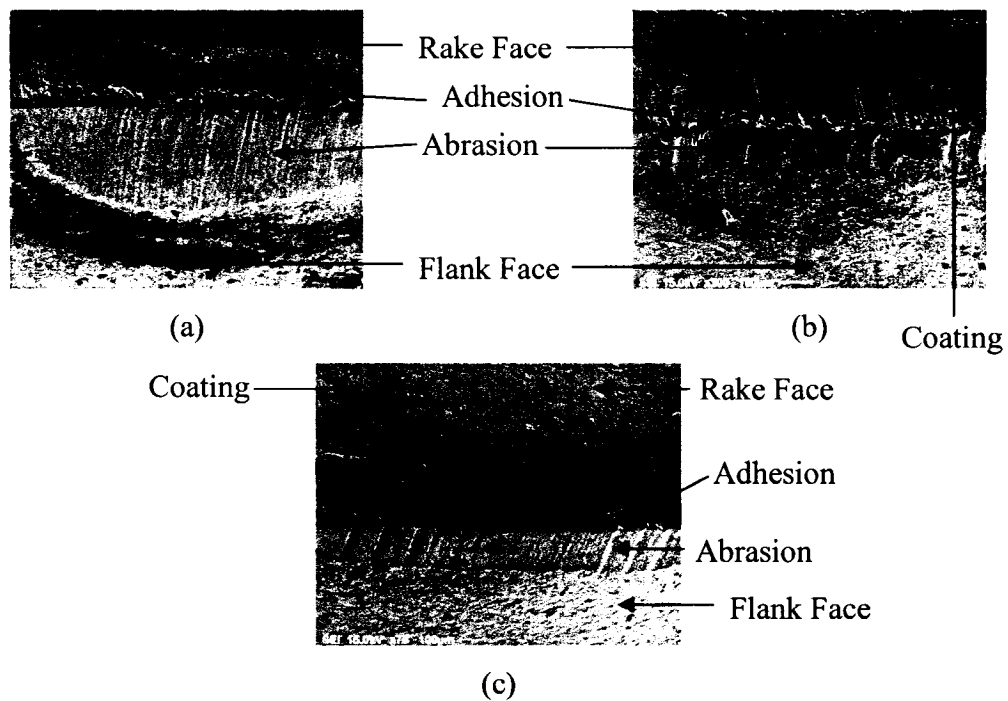


Figure 4.37: SEM images for a speed of 75 m/min and a feed of 0.125 mm/rev: (a) rake and flank face for an uncoated tool at 5.94 min., (b) rake and flank face for a single layer PVD coated tool at 8.31 min., and (c) rake and flank face for a triple layer CVD coated tool at 8.61 min.

4.3.1.2.1 Chip Morphology and Metallurgical Analysis at a Medium Cutting Speed (75 m/min)

Chip morphology was studied for an uncoated tool at a cutting speed of 75 m/min and three different feeds. Figures 4.38, 4.40, and 4.42 show the chip images, and Figures 4.39, 4.41, and 4.43 shows the metallurgical analysis, similar to the discussion shown in Section 4.2.1.1.1. Again, the chip that is formed here is continuous and ribbon-like but showing a transition, (*i.e.*, from a continuous to a shear localized chip) where shear localization is beginning to take place. This is consistent with the observation made in [12]. As before, the chip structure is plastically deformed at the top section of the chip, along with bending on the secondary shear zone. As expected, the chip thickness increases with an increase in feed per revolution [30]. The chemical analysis, which was conducted on the chips at a cutting speed of 75 m/min, was similar to the one conducted at a cutting speed of 50 m/min. No phase transformation was observed. A similar analysis

was done for the single layer PVD coated tool at a feed of 0.1 mm/rev, and again, the same kinds of observations were made. The results are shown in Figures 4.44 and 4.45.

A similar analysis was carried out for the triple layer CVD coated tool at a three different feeds, and again, the same kinds of observations were made. Figures 4.44, 4.46, and 4.48 show the chip images, and Figures 4.45, 4.47, and 4.49 shows the chemical analysis. Again, the chip deformation was similar to the one seen with uncoated and single layer PVD coated tools. The micro-hardness was measured at three sections in a way similar to the measurement done for the cutting speed of 50 m/min. The results are represented in Table 4.10 for three different tools. Again, an increase in micro-hardness was observed similar to the one observed with the cutting speed of 50 m/min. Again, an increase in the micro-hardness of the chip due to the strain-hardening effect was observed. It also is observed that the value of micro-hardness is high at the top section (free surface) of the chip.

Table 4.10: Micro-hardness measurement for a cutting speed of 75 m/min

Tool	Cutting Conditions			Micro-Hardness (HV)		
	Vc (m/min)	F (mm/rev)	DOC (mm)	A	B	C
Uncoated	75	0.075	0.25	475	452	407
Uncoated	75	0.1	0.25	515	495	444
Uncoated	75	0.125	0.25	503	497	447
Single Layer PVD Coated	75	0.1	0.25	545	537	521
Triple Layer CVD Coated	75	0.075	0.25	452	442	407
Triple Layer CVD Coated	75	0.1	0.25	495	486	478
Triple Layer CVD Coated	75	0.125	0.25	506	503	427

4.3.1.2.2 Forces at Medium Cutting Speed (75 m/min)

Figure 4.52 shows the thrust force, feed force, and cutting force for three different types of tools at three different feeds. As expected, all three forces increase or practically remain unchanged with feed per revolution [30] when using an uncoated and a single layer PVD TiAlN coated tool. Contrary to this, forces decrease with the triple layer CVD coated tool from 0.075 mm/rev to 0.1 mm/rev, which is due to the decrease in the thickness of secondary shear zone from 3.6 μm to 2.5 μm . But with the further increase in the feed from 0.1 mm/rev to 0.125 mm/rev the forces increases. This may be attributed

to an increase in the thickness of the secondary shear zone as observed in Figures 4.48 and 4.50. It has been reported in [3] that an increase in the thickness of the secondary shear zone will decrease the rake angle and will result in an increase in the cutting forces. The thickness of secondary shear zone increased from 2.5 μm to 3.97 μm with an increase in feed from 0.1 mm/rev to 0.125 mm/rev.

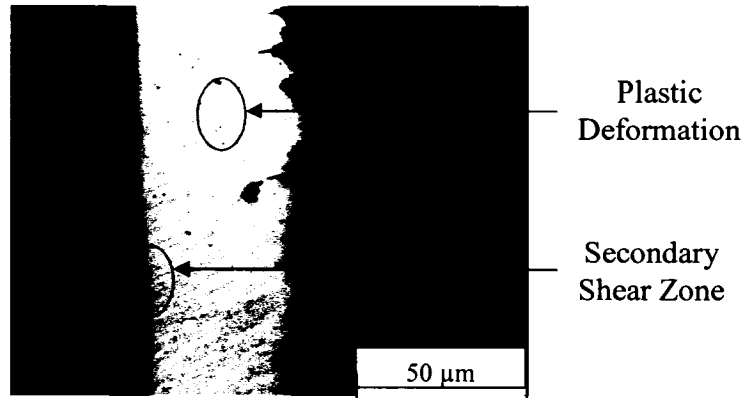


Figure 4.38: Chip image for an uncoated tool at a cutting speed of 75 m/min and a feed of 0.075 mm/rev

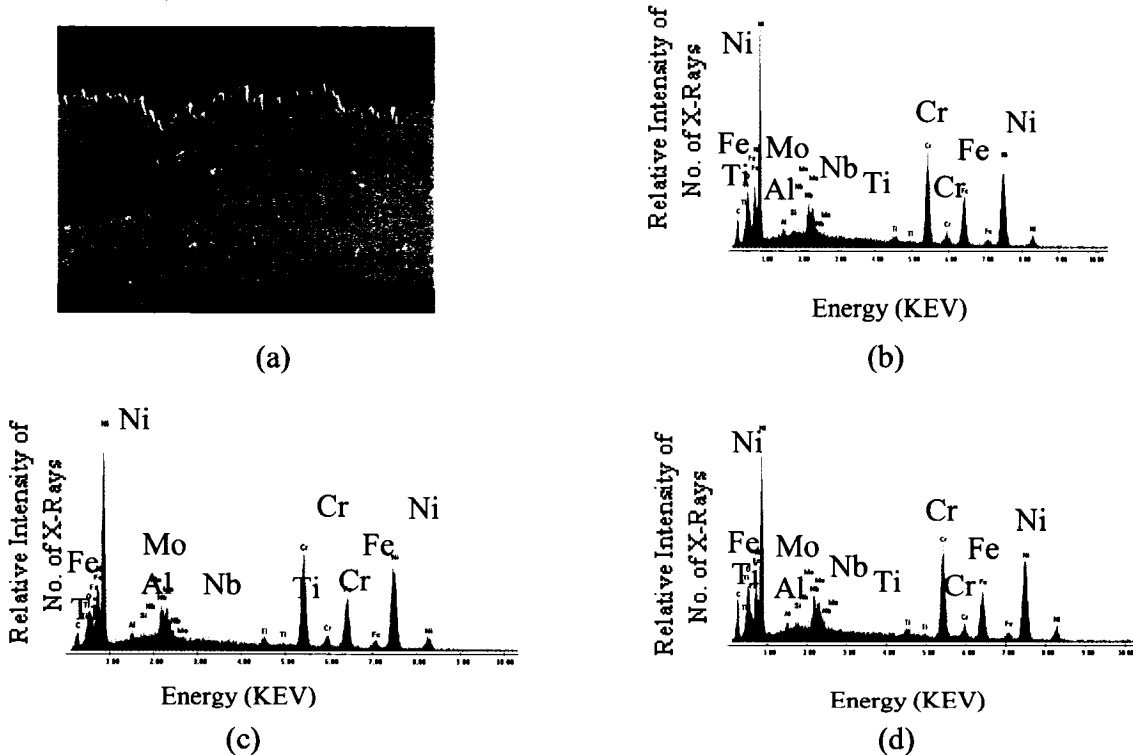


Figure 4.39: Chip image with the spot marked where the chemical analysis is done (a) chemical analysis using SEM (b, c, d) for a speed of 75 m/min and a feed of 0.075 mm/rev with an uncoated tool showing no phase transformation

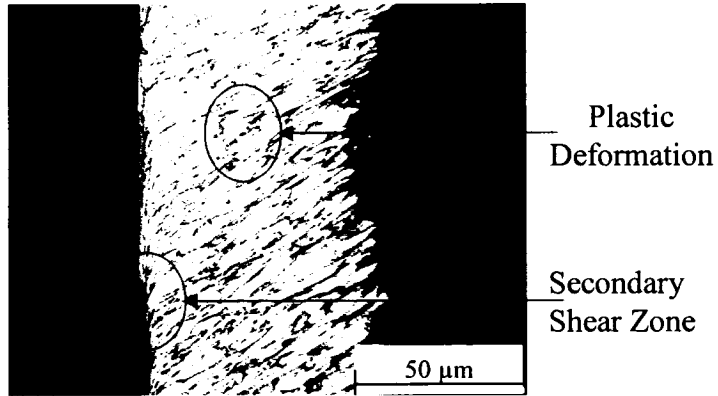


Figure 4.40: Chip image for uncoated tool at a cutting speed of 75 m/min and a feed of 0.1 mm/rev

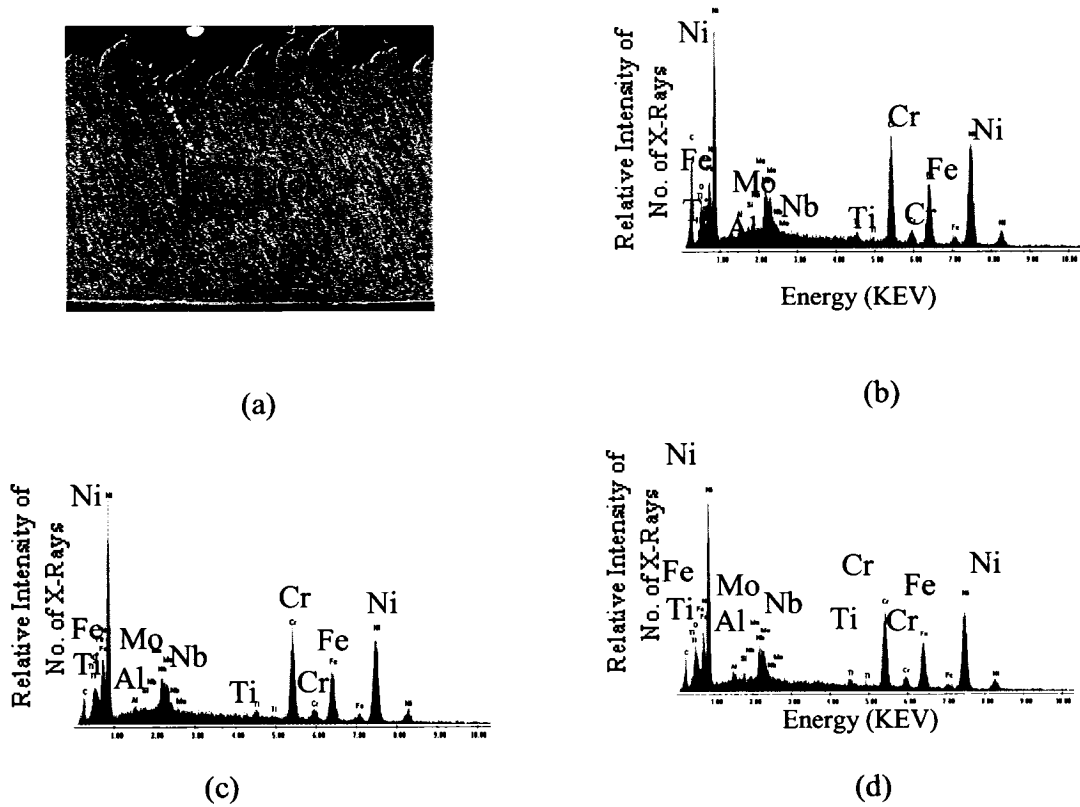


Figure 4.41: Chip image with the spot marked where the chemical analysis is done (a); chemical analysis using SEM (b, c, d) for a speed of 75 m/min and a feed of 0.1 mm/rev with an uncoated tool showing no phase transformation

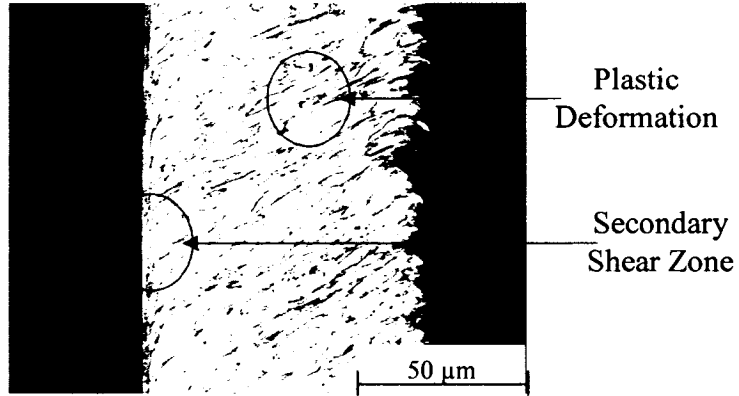


Figure 4.42: Chip image for uncoated tool at a cutting speed of 75 m/min and a feed of 0.1 mm/rev

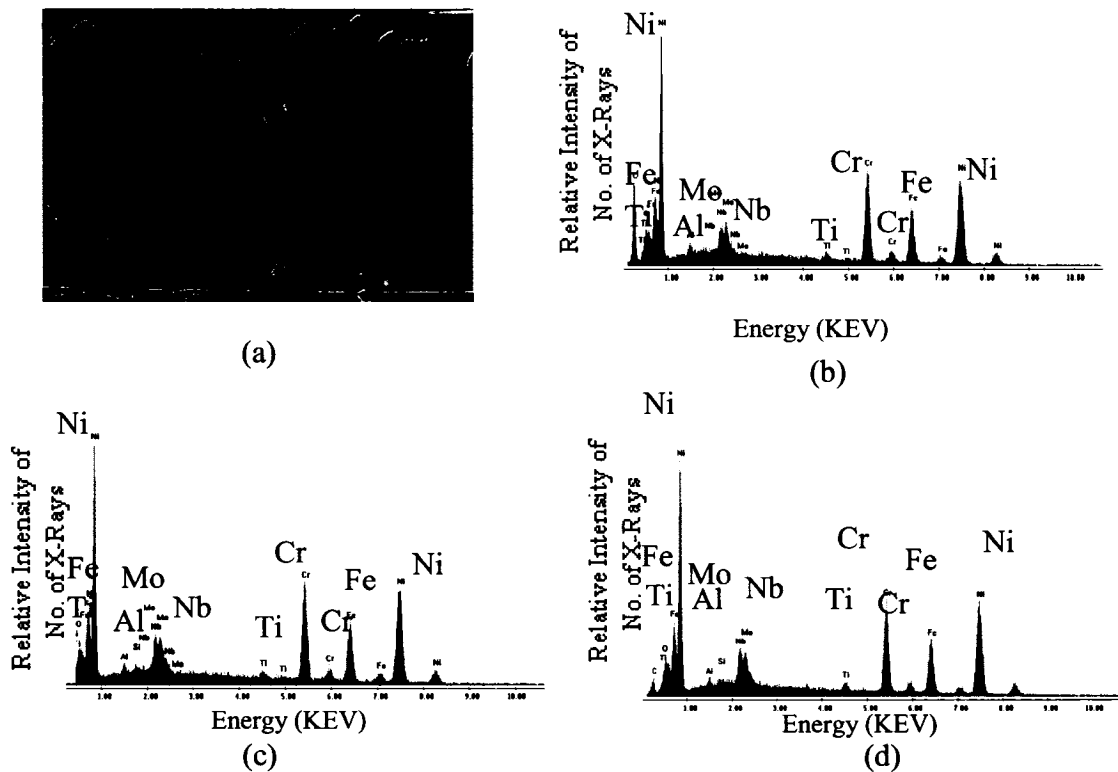


Figure 4.43: Chip image with the spot marked where the chemical analysis is done (a); chemical analysis using SEM (b, c, d) for a speed of 75 m/min and a feed of 0.125 mm/rev with an uncoated tool showing no phase transformation

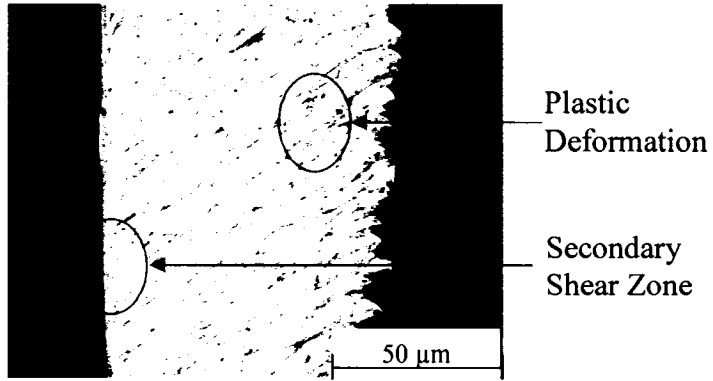


Figure 4.44: Chip image for single layer PVD coated tool at a cutting speed of 75 m/min and a feed of 0.1 mm/rev

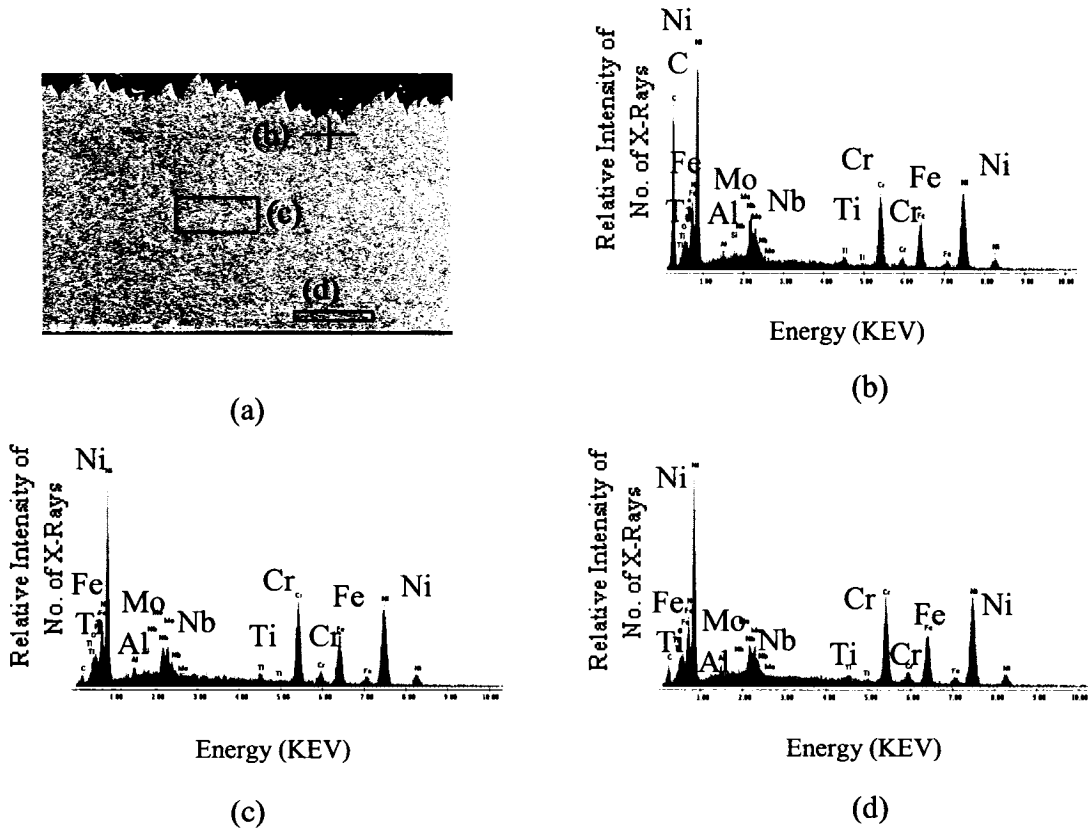


Figure 4.45: Chip image with the spot marked where the chemical analysis is done (a); chemical analysis using SEM (b, c, d) for a speed of 75 m/min and a feed of 0.1 mm/rev with a single layer PVD TiAlN coated tool showing no phase transformation

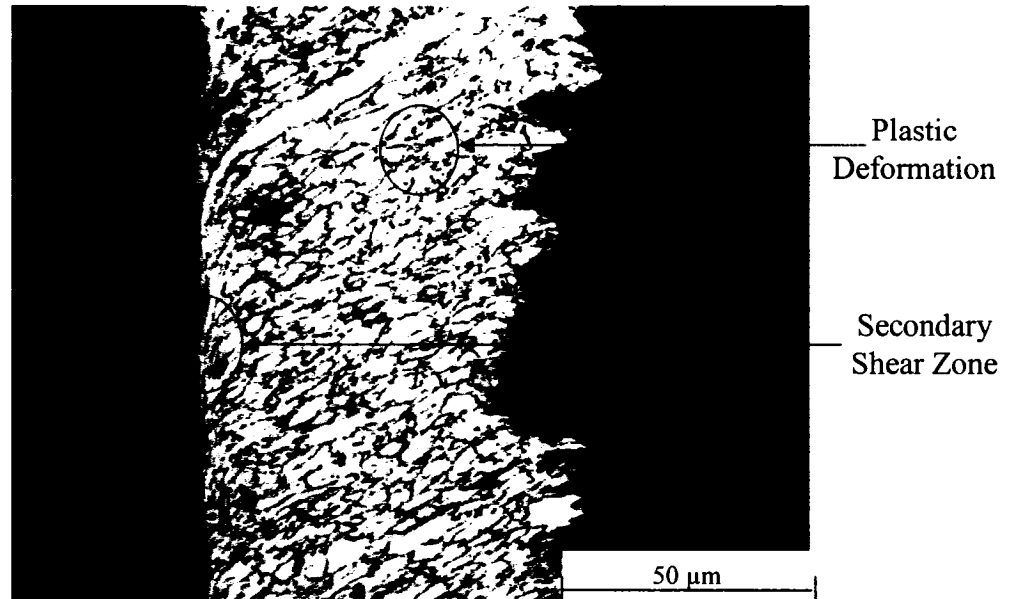


Figure 4.46: Chip image for a triple layer CVD coated tool at a cutting speed of 75 m/min and a feed of 0.075 mm/rev

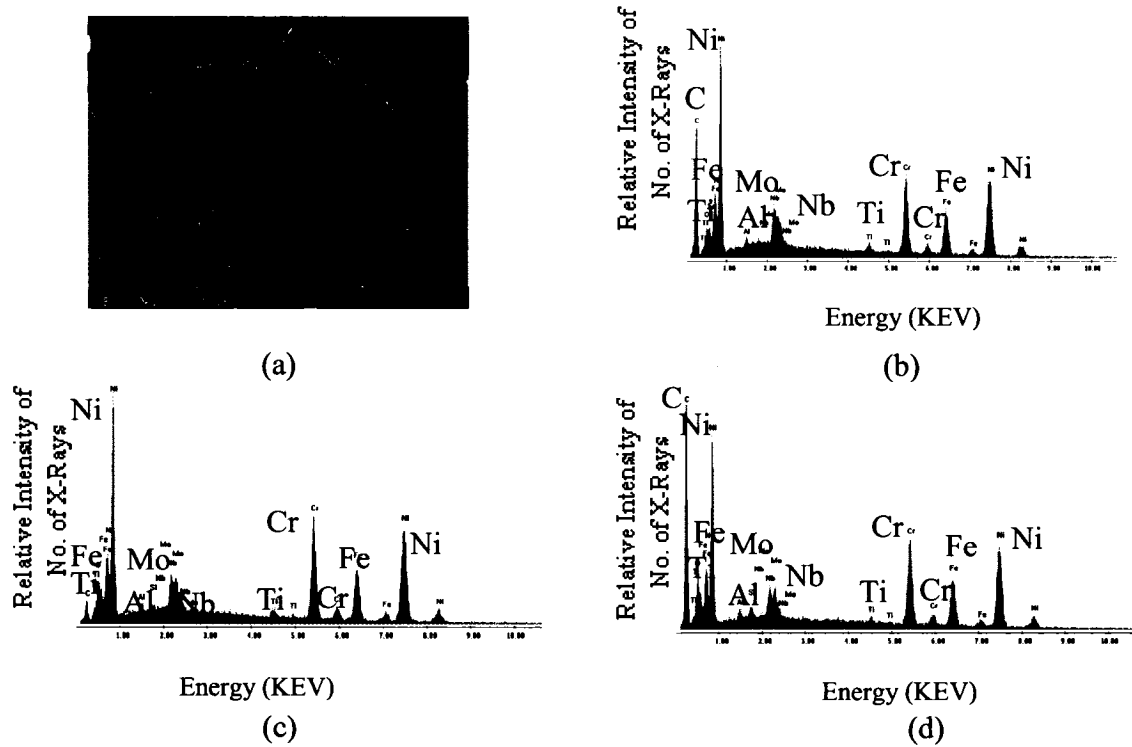


Figure 4.47: Chip image with the spot marked where the chemical analysis is done (a); chemical analysis using SEM (b, c, d) for a speed of 75 m/min and a feed of 0.075 mm/rev with a triple layer CVD (TiCN/Al₂O₃/TiN) coated tool showing no phase transformation

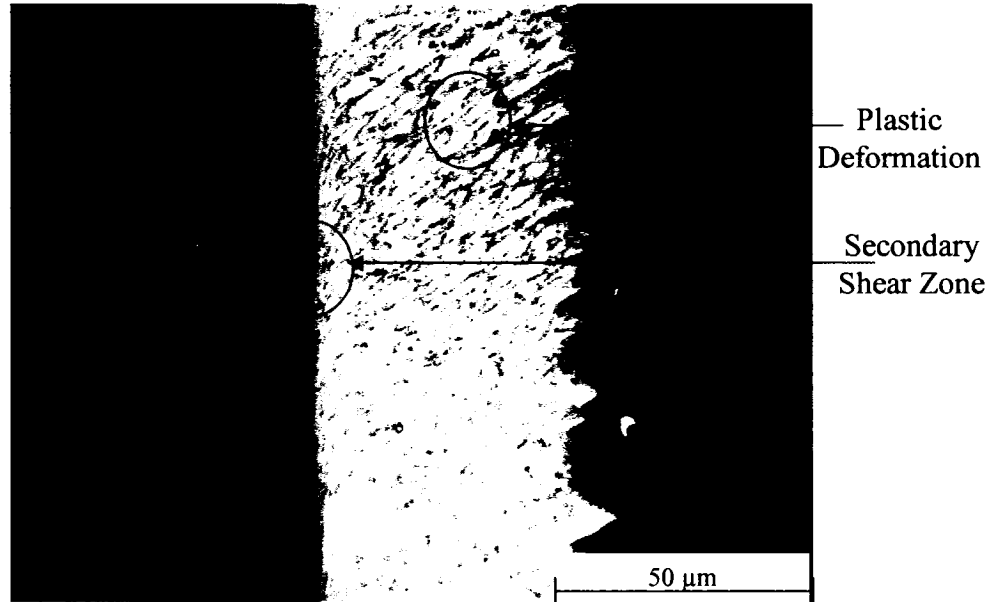


Figure 4.48: Chip image for a triple layer CVD coated tool at a cutting speed of 75 m/min and a feed of 0.1 mm/rev

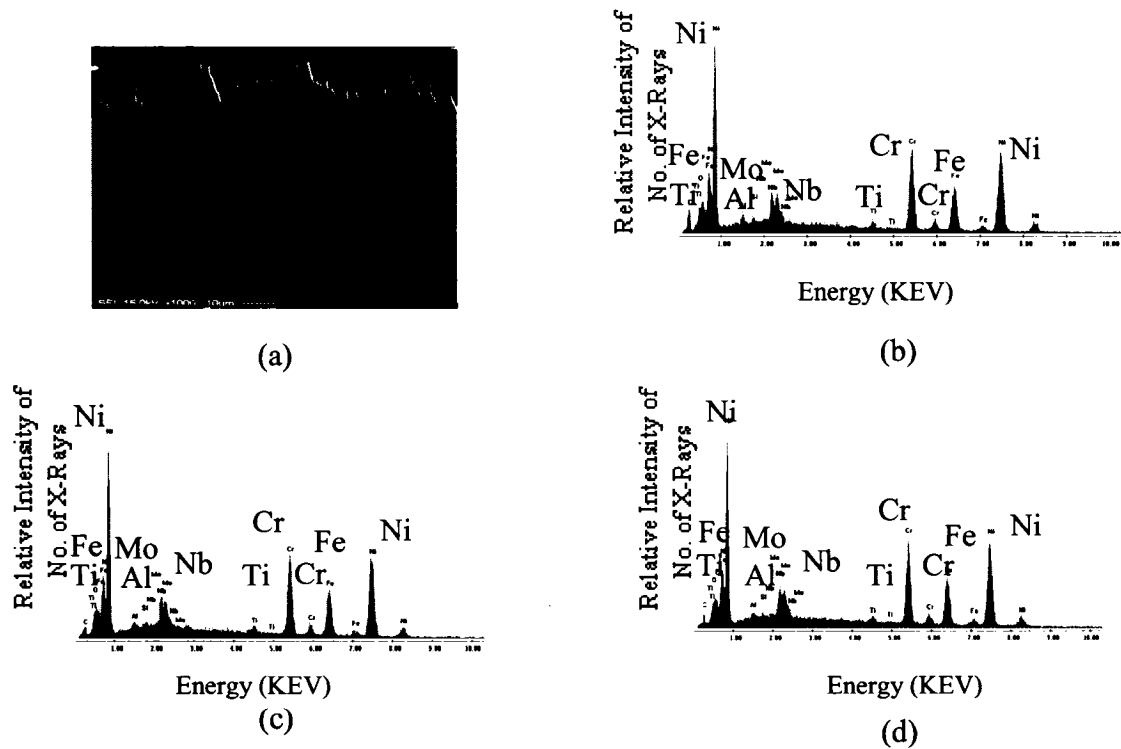


Figure 4.49: Chip image with the spot marked where the chemical analysis is done (a); chemical analysis using SEM (b, c, d) for a speed of 75 m/min and a feed of 0.1 mm/rev with a three layer CVD (TiCN/Al₂O₃/TiN) coated tool showing no phase transformation

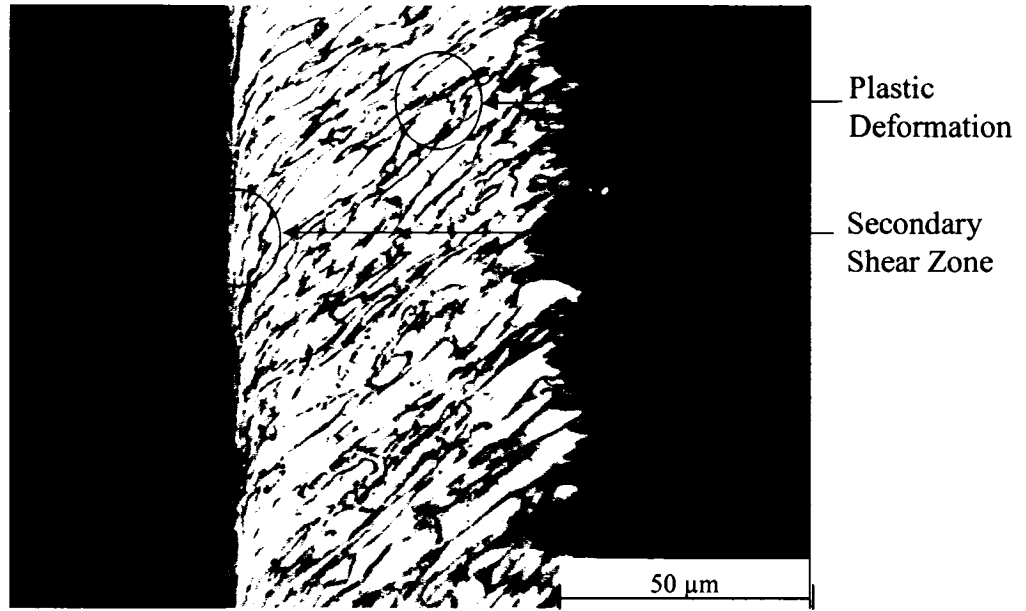


Figure 4.50: Chip image for a triple layer CVD coated tool at a cutting speed of 75 m/min and a feed of 0.125 mm/rev

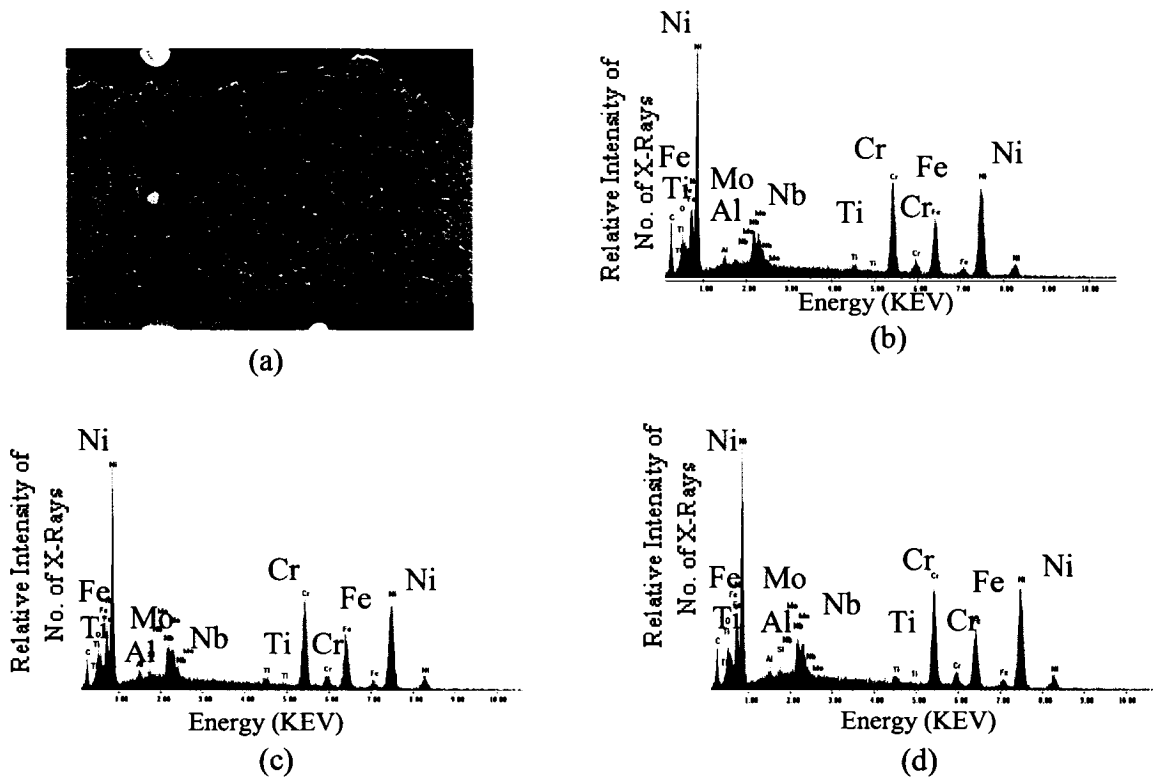


Figure 4.51: Chip image with the spot marked where the chemical analysis is done (a); chemical analysis using SEM using (b, c, d) for a speed of 75 m/min and a feed of 0.125 mm/rev with a three layer CVD (TiCN/Al₂O₃/TiN) coated tool showing no phase transformation

4.3.1.2.3 Tool Life at a Medium Cutting Speed (75 m/min)

Tool wear progression was studied with respect to time, and the results are shown with the three region of flank wear in Figure 4.53. The time duration for this regions for all the three different tools are shown in Table 4.11. The three regions shown in Figure 4.53 (a), (b), (c) is for the uncoated tool only, for the sake of clarity. At medium cutting speed of 75 m/min the wear pattern for PVD coated tool is uniform as compared to uncoated and triple layer CVD coated tools.

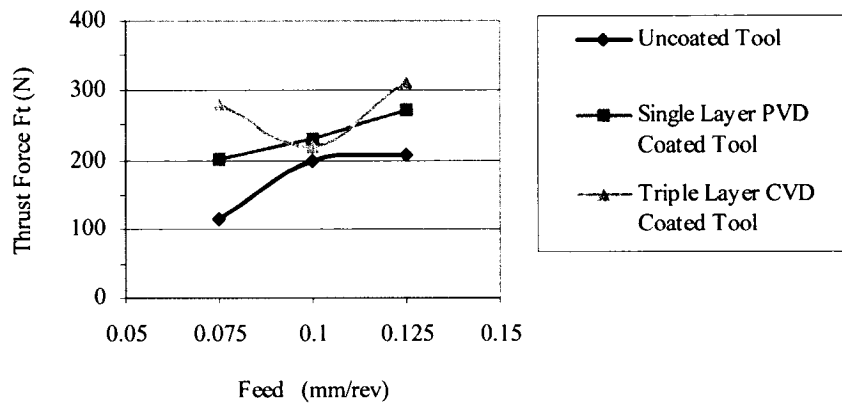
As expected, for an uncoated tool, tool life was strongly influenced by the cutting speed. An increase in feed rate also decreased tool life, but not as sharply as the increase in cutting speed. The cutting edge could not withstand the mechanical and thermal loads generated at the cutting speed of 75 m/min, which caused the decrease in tool life.

The single layer PVD coated tool performed better than the uncoated and the triple layer CVD coated tool. The best tool life of 12 min. was found at 0.075 mm/rev. This is due to the TiAlN coating film that provides better heat isolation from the tool cutting edge in comparison with most coating materials [32].

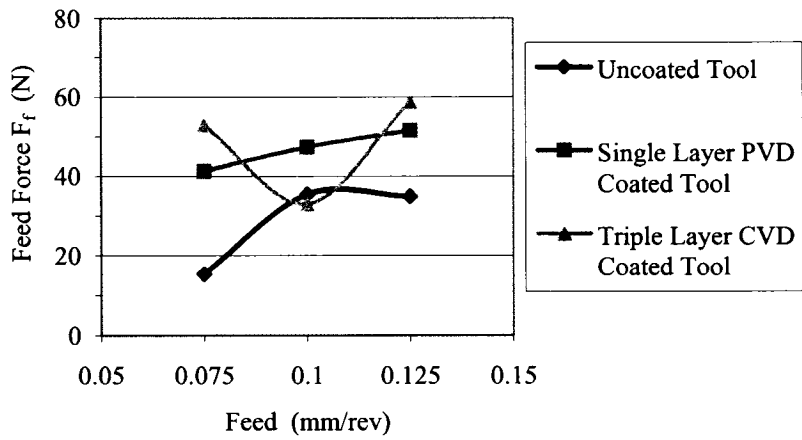
The triple layer CVD coated tool performed better than the uncoated tool. With an increase in the cutting speed from 50 m/min to 75 m/min, the triple layer tool has a longer tool life. This is again due to the intermediate coating (Al_2O_3), as explained earlier [44].

Table 4.11: Time duration at which three regions formed at cutting speed of 75 m/min

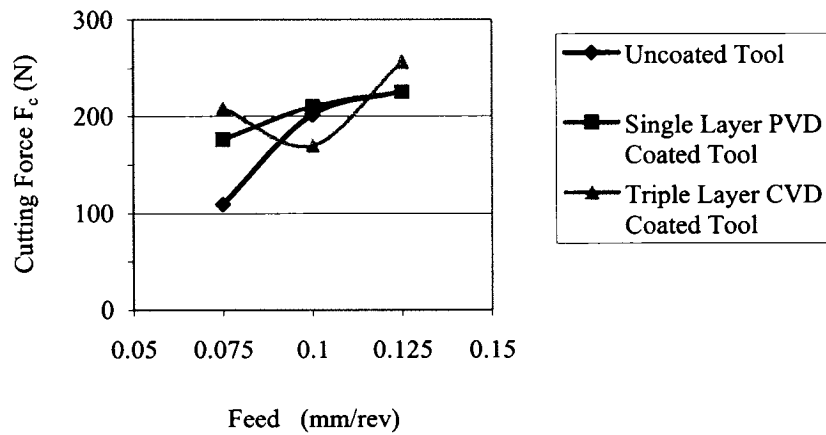
Tool	Time (min.)								
	Feed 0.075 mm/rev			Feed 0.1 mm/rev			Feed 0.125 mm/rev		
	Duration of Region								
	A	B	C	A	B	C	A	B	C
Uncoated	0- 1.72	1.72- 6.68	6.68- 8.56	0- 1.12	1.12- 5.57	5.57- 6.67	0- 1.72	1.72- 4.8	4.8- 5.94
PVD Coated Single Layer	0- 1.78	1.78- 13	13- 13.91	0-2	2- 12.52	12.52- 13.63	0- 0.98	0.98- 7.40	7.40- 8.31
CVD Coated Triple Layer	0- 1.75	1.75- 10.3	10.3- 10.39	0-1	1- 5.09	5.09- 6.34	0- 1.2	1.2- 6.73	6.73- 8.61



(a)

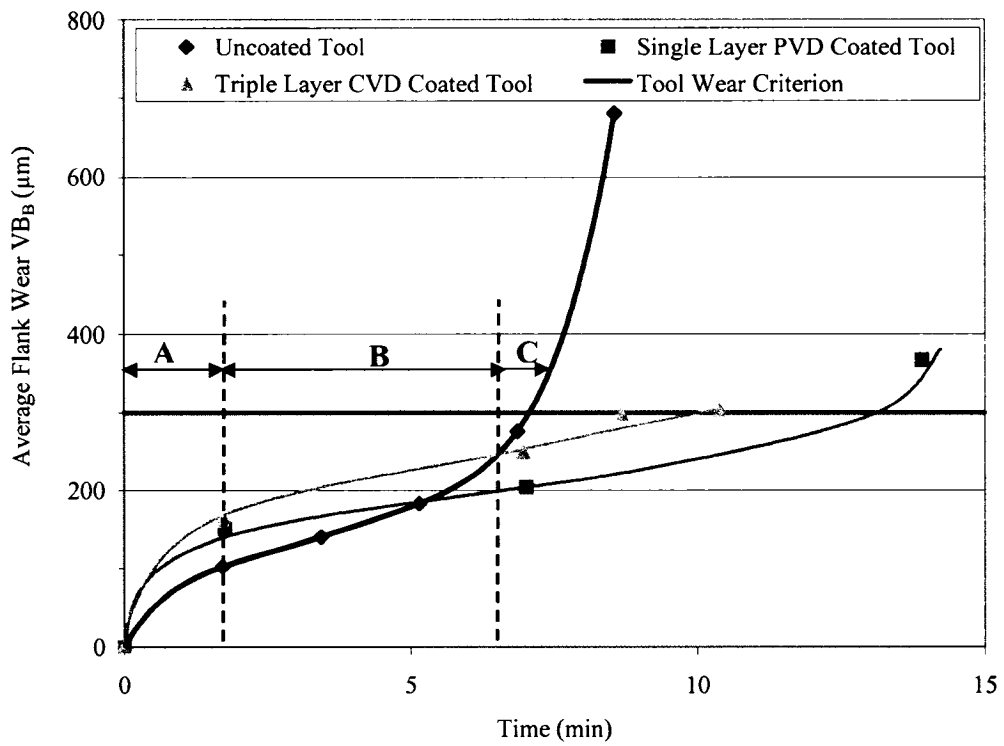


(b)

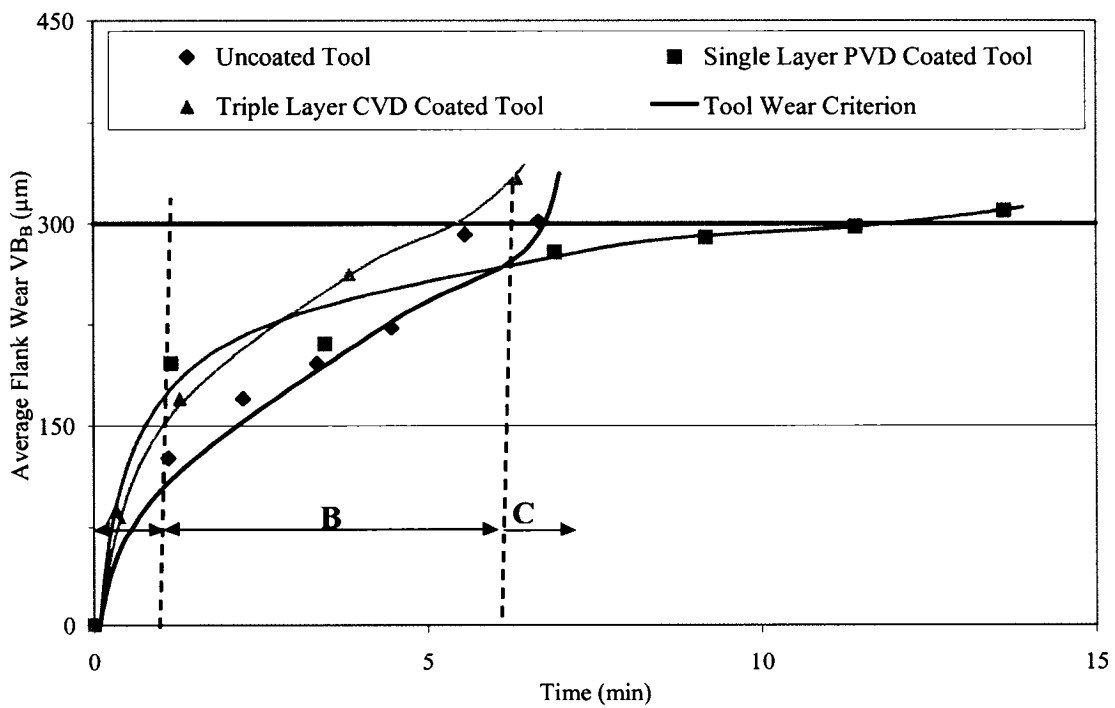


(c)

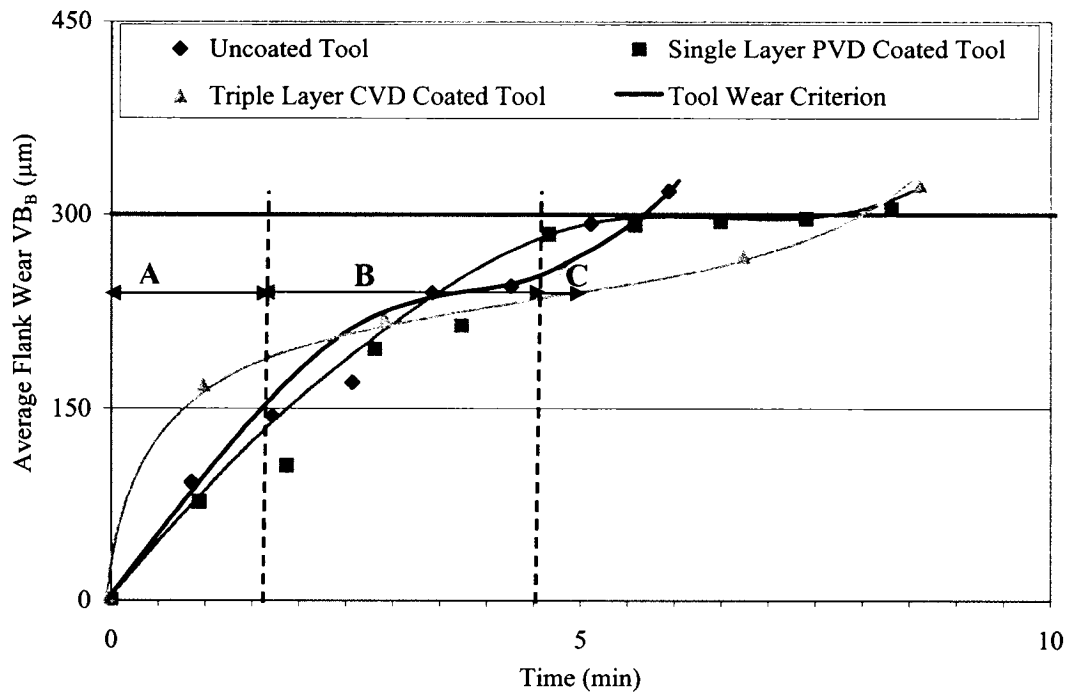
Figure 4.52: Forces with three different tools when the tool edge is sharp at speed 75 m/min and three different feeds (a) thrust force, (b) feed force, and (c) cutting force



(a)



(b)



(c)

Figure 4.53: Tool wear progression for three different tools at a speed of 75 m/min and feeds of (a) 0.075 mm/rev, (b) 0.1 mm/rev, and (c) 0.125 mm/rev

4.3.1.3 Tool Wear Mechanism at a High Cutting Speed (100 m/min)

The wear mechanism was also studied at a high cutting speed of 100 m/min and at feeds of 0.075 mm/rev, 0.1 mm/rev, and 0.125 mm/rev. The results are shown with the three regions of the flank wear in Figures 4.54, 4.55 and 4.56.

As expected, the tool wear rate was highly influenced by the cutting speed. Again, the mechanisms observed with all three different types of tools are abrasion and adhesion. Similar to the earlier trend, the main tool failure mode was flank wear. However, with the single layer PVD coated tool, chipping was observed. This is due to the observed increase in vibration level, possibly due to the tangling of the chips. Also, with the triple layer CVD coated tool, a crater is observed due to the diffusion wear mechanism, which also is explained earlier.

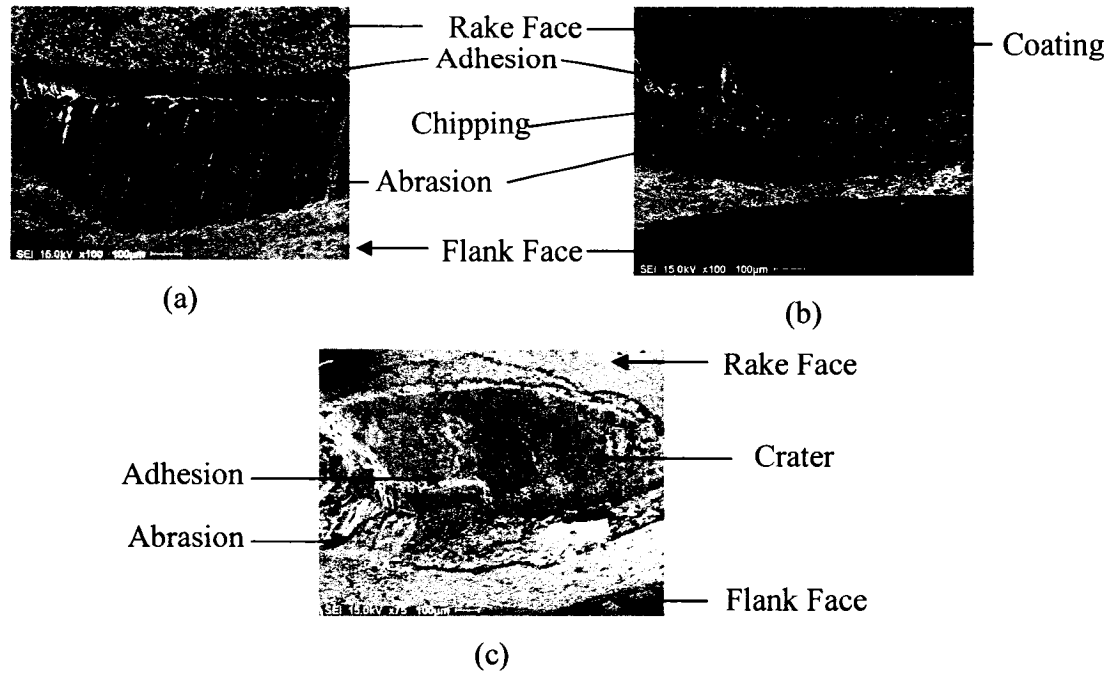


Figure 4.54: SEM images for a speed of 100 m/min and a feed of 0.075 mm/rev: (a) rake and flank face for an uncoated tool at 2.18 min., (b) rake and flank face for a single layer PVD coated tool at 7.57 min., and (c) rake and flank face for a triple layer CVD coated tool at 8.83 min.

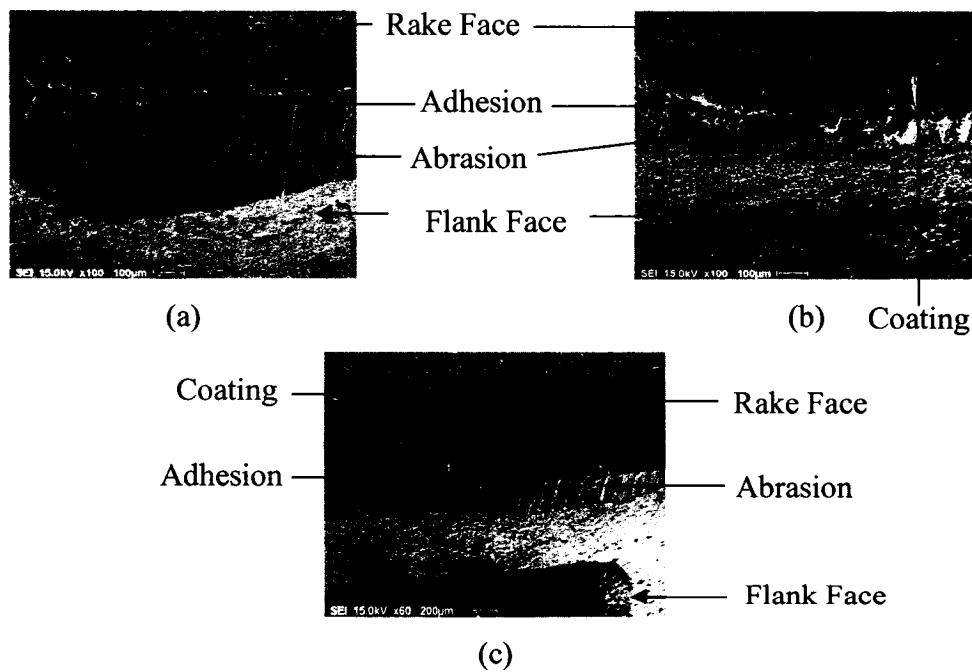


Figure 4.55: SEM images for a speed of 100 m/min and a feed of 0.1 mm/rev: (a) rake and flank face for an uncoated tool at 1.98 min., (b) rake and flank face for a single layer PVD coated tool at 6.51 min., and (c) rake and flank face for a triple layer CVD coated tool at 8.41 min.

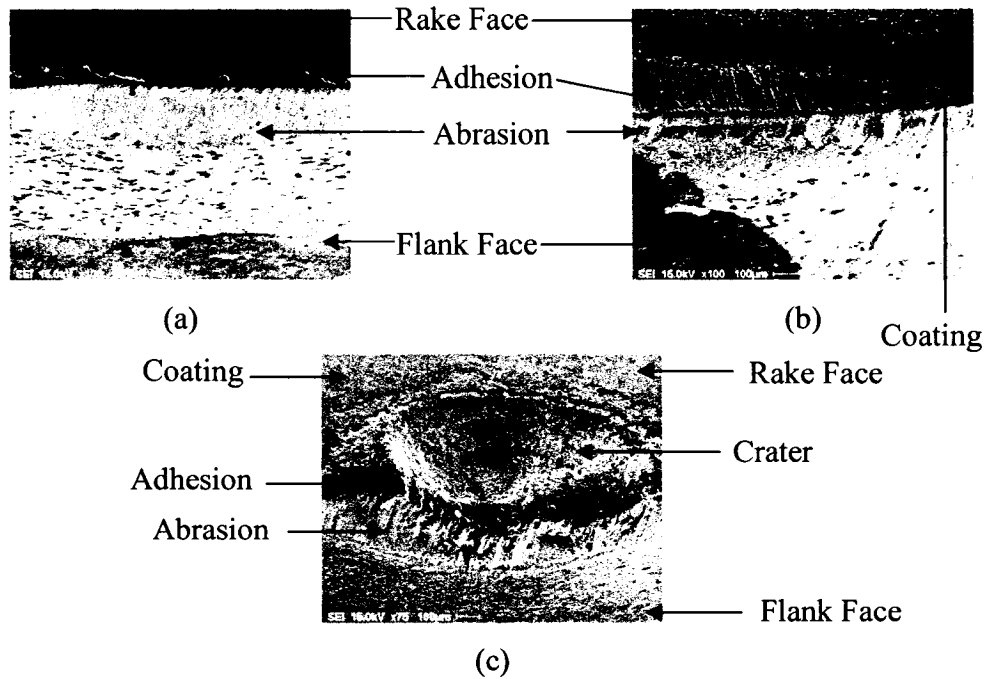


Figure 4.56: SEM images for a speed of 100 m/min and a feed of 0.1 mm/rev: (a) rake and flank face for an uncoated tool at 1.56 min., (b) rake and flank face for a single layer PVD coated tool at 3.80 min., and (c) rake and flank face for a triple layer CVD coated tool at 7.64 min.

4.3.1.3.1 Chip Morphology and Metallurgical Analysis at a High Cutting Speed (100 m/min)

The chip morphology was studied for uncoated tool at a cutting speed of 100 m/min and a feed of 0.075 mm/rev, and for a single layer PVD coated tool at a cutting speed of 100 m/min and a feed 0.1 mm/rev. Figures 4.57 and 4.59 show the chip images. A similar kind of deformation is seen again with both of the tools at this cutting speed. The chip that is formed is again continuous and ribbon-like, and in transition. This observation was in contradiction to the one made in [12]. This may be due to the larger depth of cut used by the latter. Figures 4.58 and 4.60 show the chemical analysis for the chips for the uncoated and single layer PVD coated tools shown in Figure 4.57 and 4.59. The analysis was similar to that observed before. The carbon content seen in Figure 4.57 (b) is due to the bakelite mounting of the chip. Also, a high chromium content is observed, which is due to the etching solution used on the chip.

The micro-hardness was measured at three sections in a way similar to the measurement done for the cutting speed of 50 m/min and 75 m/min. The results are represented in

Table 4.12 for uncoated and single layer PVD coated tools. As before, the micro-hardness increases due to the strain hardening effect. Again, it also is observed that the value of micro-hardness is high at the top section (free surface) of the chip

Table 4.12: Micro-hardness measurement for a cutting speed of 100 m/min

Tool	Cutting Conditions			Micro-Hardness (HV)		
	Vc (m/min)	F (mm/rev)	DOC (mm)	A	B	C
Uncoated	100	0.075	0.25	518	509	457
Single Layer PVD Coated	100	0.1	0.25	541	531	509

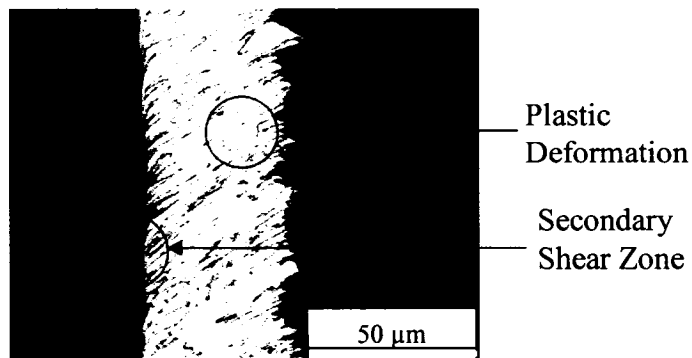


Figure 4.57: Chip images for the uncoated tool at a speed of 100 m/min and a feed of 0.075 mm/rev

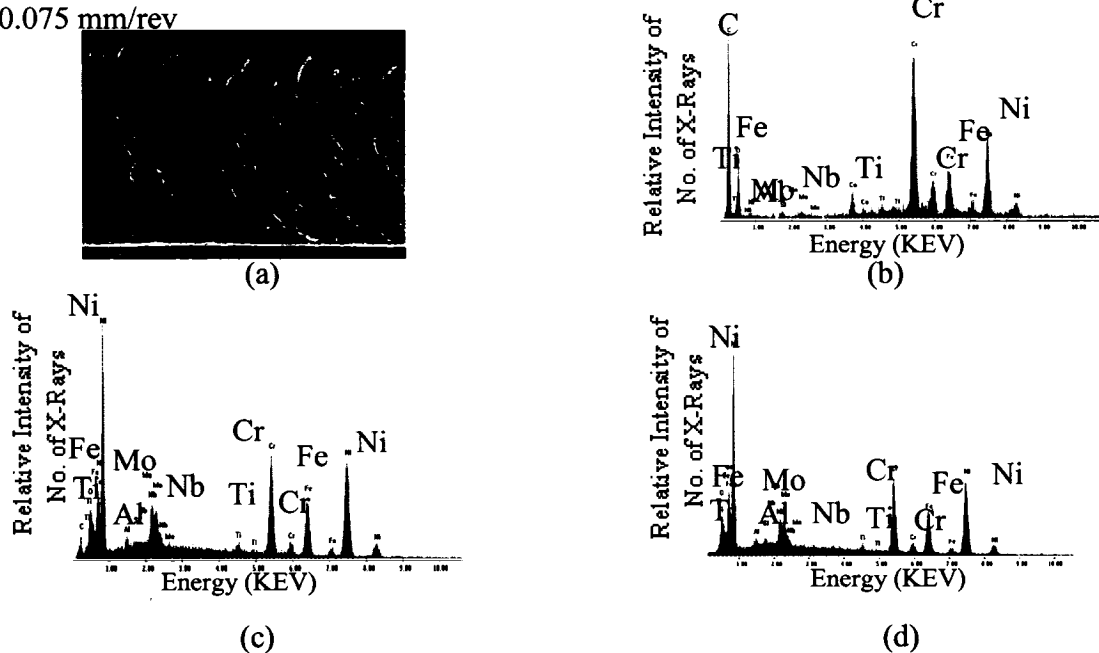


Figure 4.58: Chip image with the spot marked where the chemical analysis is done (a); chemical analysis using SEM (b, c, d) for a speed of 100 m/min and a feed of 0.075 mm/rev with an uncoated tool showing no phase transformation

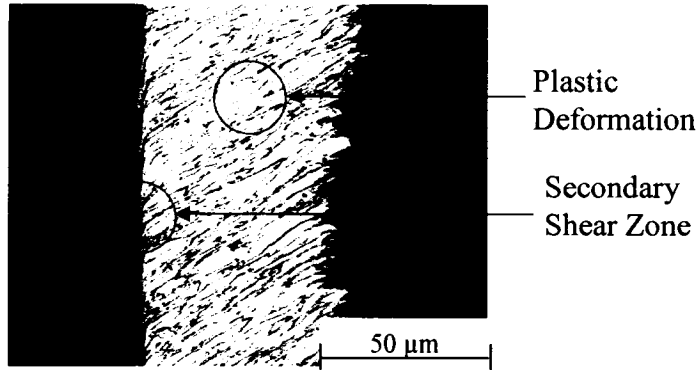


Figure 4.59: Chip images for a single layer PVD tool at a speed of 100 m/min and a feed of 0.1 mm/rev

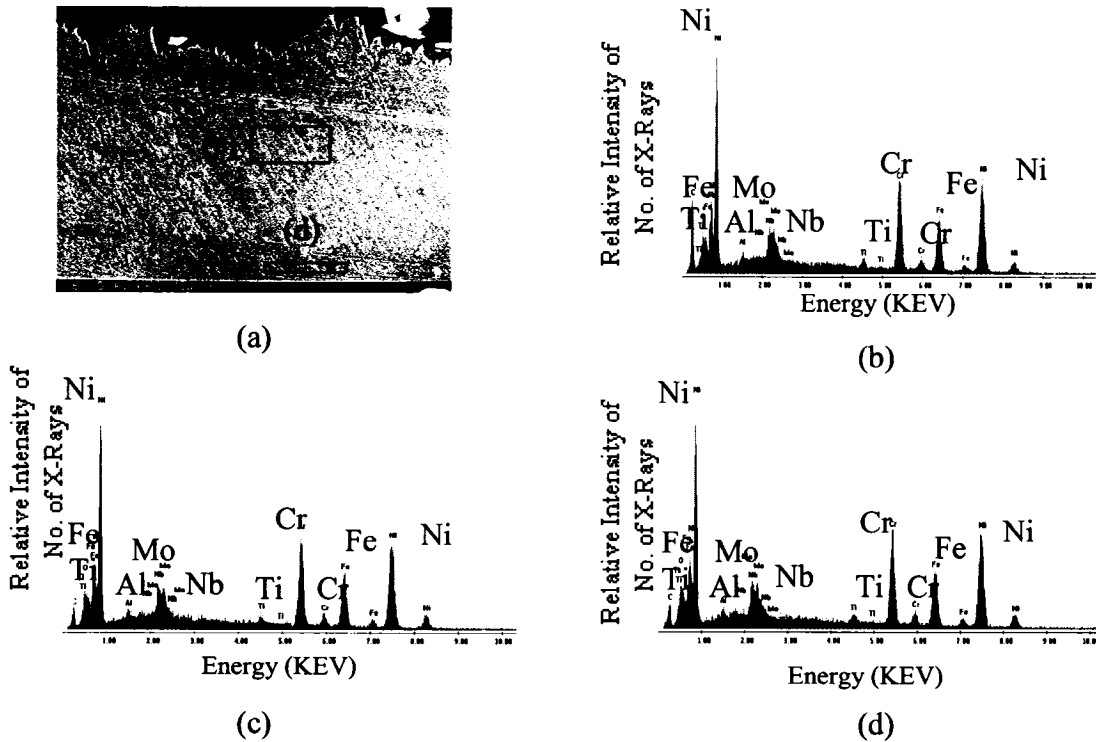


Figure 4.60: Chip image with the spot marked where the chemical analysis is done (a); chemical analysis using SEM (b, c, d) for a speed of 100 m/min and a feed of 0.1 mm/rev with a single layer PVD TiAlN coated tool showing no phase transformation

4.3.1.3.2 Forces at a High Cutting Speed (100 m/min)

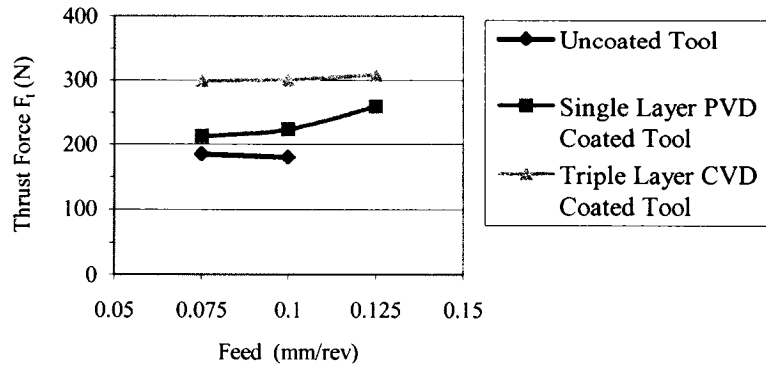
Figure 4.61 shows the thrust force, feed force and cutting force for three different types of tools at three different feeds. With the triple layer CVD coated tool, all the three forces increase with an increase in feed per revolution [30], except for feed force at feed 0.1 mm/rev there is a slight decrease in force by less than 5%. Also for single layer PVD coated tool, all the three forces show an increasing tendency as shown in Figure 4.61 (the

increase is approximately between 18 % to 22 %), although there is a insignificant decrease in the feed force (Figure 4.61 (b)) and cutting force (Figure 4.61 (c)) at 0.1 mm/rev (the decrease is approximately between 2.5 to 7.5 %). A similar trend was observed for uncoated tool for all the three forces at feed of 0.1 mm/rev (the decrease is approximately between 2.7 to 6.6 %). The slightly higher values of forces noted at feed 0.075 mm/rev for uncoated and single layer PVD coated tools can be attributed to the coolant flow not directed properly towards the tip of the tool. As shown in Figure 4.61, the forces could not be reported for the uncoated tool at 0.125 mm/rev due to human error.

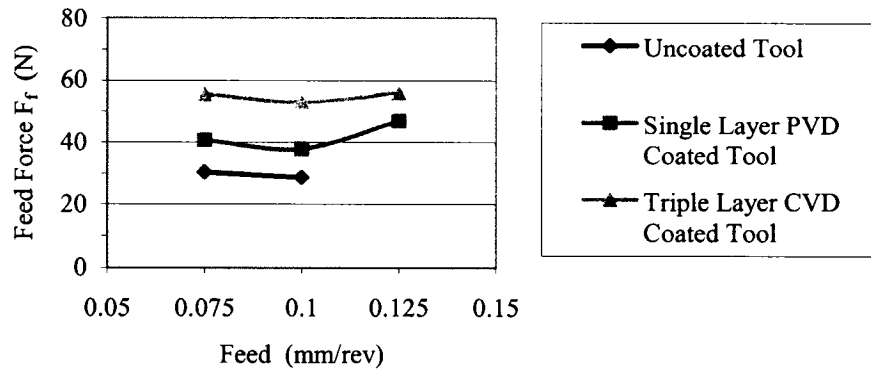
When comparing the forces in relation to the cutting speed, it is seen that the cutting forces decrease or practically remain unchanged for uncoated tool when the cutting speed increases from 50 m/min to 75 m/min at all three feeds, as illustrated in Figures 4.32 and 4.52. This decrease is attributed to the decrease in the strain hardening effect, as illustrated in Table 4.13. When the cutting speed increases from 75 m/min to 100 m/min, as illustrated in Figures 4.52 and 4.61 at feed of 0.1 mm/rev, there is a decrease in forces. This is due to the decrease in strain hardening effect, as illustrated in Table 4.13. However, at feed of 0.075 mm/rev it is observed that the forces increase. This can be attributed to the increase in the strain hardening effect, as illustrated in Table 4.13.

Table 4.13: Comparison of the micro-hardness values of the chip at three different cutting speeds and feeds for uncoated tool

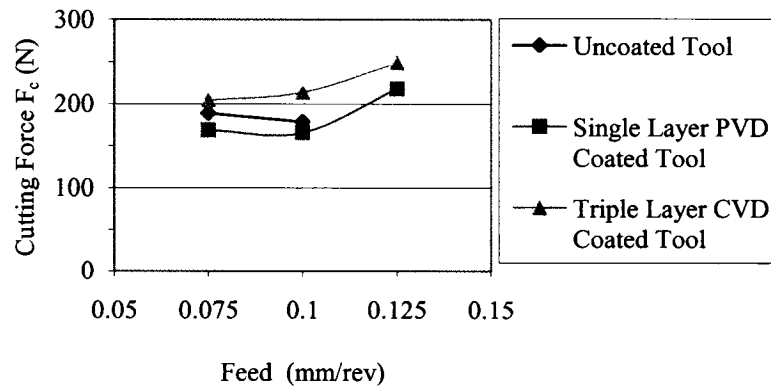
Cutting Conditions			Micro-Hardness (HV)		
Vc (m/min)	F (mm/rev)	DOC (mm)	A	B	C
50	0.075	0.25	509	506	432
75	0.075	0.25	475	452	407
100	0.075	0.25	518	509	457
50	0.1	0.25	515	512	489
75	0.1	0.25	515	495	444
100	0.1	0.25	497	467	414
50	0.125	0.25	500	495	472
75	0.125	0.25	503	497	447
100	0.125	0.25	537	472	447



(a)



(b)



(c)

Figure 4.61: Forces with three different tools when the tool edge is sharp at speed 100 m/min and three different feeds (a) thrust force, (b) feed force, and (c) cutting force

When comparing all the forces for single layer PVD coated tool, as illustrated in Figures 4.32, 4.52, and 4.61, it is observed that an increase in the cutting speed from 50 m/min to 75 m/min, results in an increase in all the three forces. This result can be attributed to the increase in the strain hardening effect as illustrated in Table 4.14. With a further increase

in the cutting speed from 75 m/min to 100 m/min, all the three forces decrease slightly. This result can be attributed to the decrease in the strain hardening effect, as illustrated in Table 4.14.

Table 4.14: Comparison of the micro-hardness values of the chip at three different cutting speeds and feeds for single layer PVD coated tool

Cutting Conditions			Micro-Hardness (HV)		
Vc (m/min)	F (mm/rev)	DOC (mm)	A	B	C
50	0.075	0.25	532	509	462
75	0.075	0.25	537	503	489
100	0.075	0.25	521	501	492
50	0.1	0.25	534	509	503
75	0.1	0.25	545	537	521
100	0.1	0.25	541	531	509
50	0.125	0.25	495	489	475
75	0.125	0.25	506	495	480
100	0.125	0.25	505	492	479

When comparing all the forces for CVD coated tool, as illustrated in Figures 4.32, 4.52, and 4.61, there is an increase in the forces with an increase in the cutting speed from 50 m/min to 100 m/min. This can be attributed to the increase in the strain hardening effect, as shown in Table 4.15. However, at a cutting speed of 75 m/min and feed of 0.1 mm/rev there is decrease in forces. This is due to the effect of the thickness of the secondary shear zone as explained in Section 4.3.1.2.2.

Table 4.15: Comparison of the micro-hardness values of the chip at three different cutting speeds and feeds for triple layer CVD coated tool

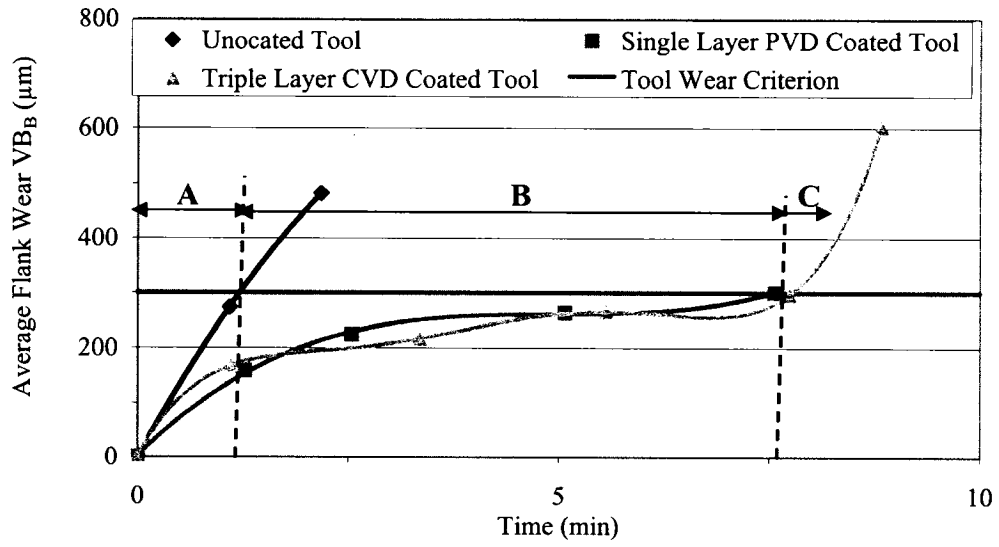
Cutting Conditions			Micro-Hardness (HV)		
Vc (m/min)	F (mm/rev)	DOC (mm)	A	B	C
50	0.075	0.25	446	434	397
75	0.075	0.25	452	442	407
100	0.075	0.25	464	449	421
50	0.1	0.25	464	459	447
75	0.1	0.25	495	486	478
100	0.1	0.25	501	492	486
50	0.125	0.25	506	495	416
75	0.125	0.25	506	503	427
100	0.125	0.25	511	507	442

4.3.1.3.3 Tool Life at a High Cutting Speed (100/min)

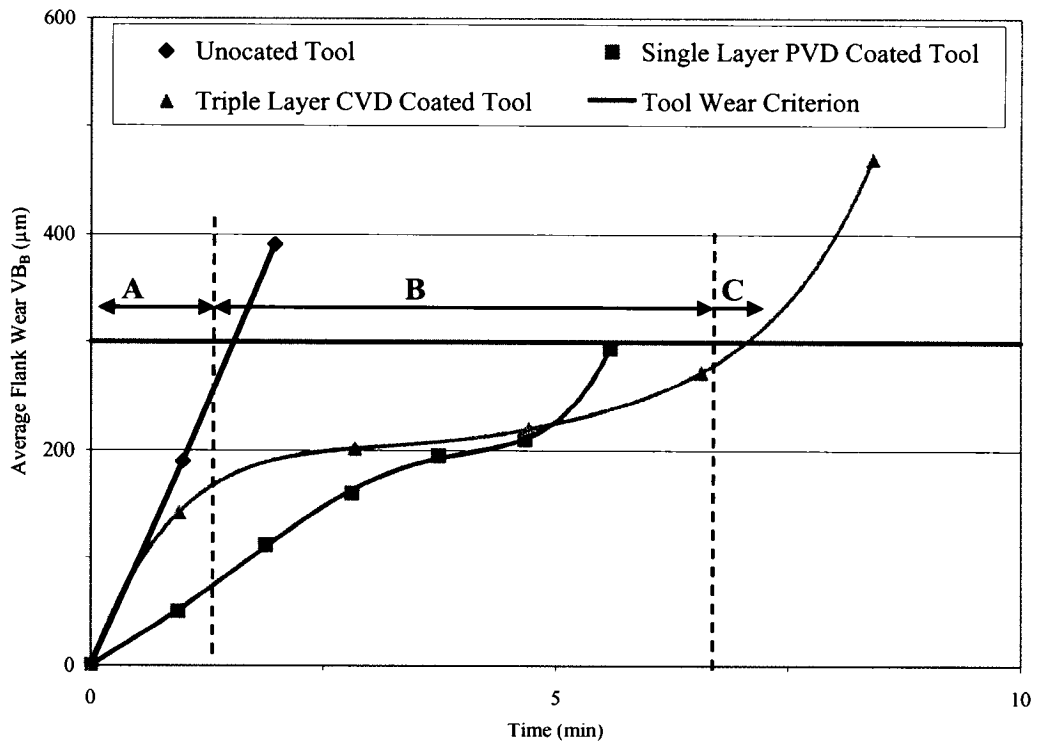
Tool wear progression was studied again at a high cutting speed of 100 m/min. Figure 4.62 shows the wear progression for three different types of tools at three different feeds of 0.075 mm/rev, 0.1 mm/rev, and 0.125 mm/rev with the three region of flank wear. The duration at which this region occurs is shown in Table 4.16. The three regions are shown in Figure 4.62 (a), (b), (c) for the triple layer CVD coated tool only, for the sake of clarity. At high cutting speed of 100 m/min the wear pattern for CVD coated tool is uniform as compared to uncoated and single layer PVD coated tools. Again, the tool wear progression is highly influenced by the cutting speed. The tool life for the uncoated tool is much less at the three different feeds (less than 2 min.) when compared to the other two tools. The single layer PVD coated tool performs better than the uncoated tool, with a tool life of approximately 7 min. at a feed of 0.075 mm/rev. The triple layer CVD coated tool exhibits the best performance when compared to the other two tools, with a tool life of approximately 8 min. at a feed of 0.075 mm/rev. With the single layer PVD TiAlN tool, the hot hardness increased due to the solid solution strengthening effect of either carbon or aluminum present in the TiN lattice [63], giving better tool life. For the triple layer CVD coated (TiCN/Al₂O₃/TiN) tool, the Al₂O₃ coating imparts a higher chemical stability to the tool at elevated temperature, which provides higher resistance to abrasive wear, thereby providing longer tool life and a higher speed capability on a workpiece material [44].

Table 4.16: Time duration at which three regions formed at cutting speed of 100 m/min

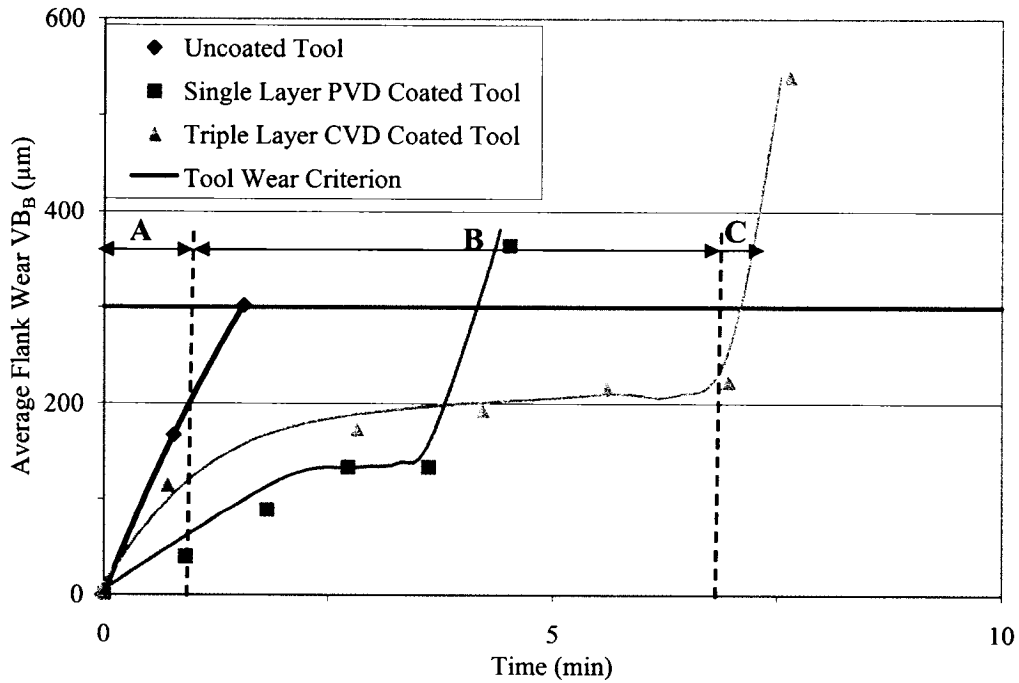
Tool	Time (min.)								
	Feed 0.075 mm/rev			Feed 0.1 mm/rev			Feed 0.125 mm/rev		
	Duration of Region								
	A	B	C	A	B	C	A	B	C
Uncoated	-	-	2.18	-	-	1.98	-	-	1.56
PVD Coated Single Layer	0-2	2-6	6- 7.57	0- 2.81	2.81- 3.8	3.8- 6.51	0- 1.64	1.64- 3.08	3.08- 3.80
CVD Coated Triple Layer	0-1.2	1.2- 7.74	7.74- 8.83	0-1.2	1.2- 7.52	7.52- 8.41	0-1	1- 6.96	6.96- 7.64



(a)



(b)



(c)

Figure 4.62: Tool wear progression for three different tools at a 100 m/min speed and feeds of (a) 0.075 mm/rev, (b) 0.1 mm/rev, and (c) 0.125 mm/rev

4.3.2 Surface Finish

Average surface roughness Ra values were recorded as the tool deterioration progressed until it met the tool failure criterion. The measurement trace was done throughout the surface in a direction perpendicular to the feed mark. As stated in Chapter 3, a cut off length of 0.8 mm and an evaluation length of 4 mm were used in the measurements.

The ideal surface roughness value is caused by the given tool shape and feed rate, and for turning operation, is expressed as a function of the feed rate (t) and nose radius (r) of a tool [44, 64].

$$Ra = (0.0321 * t^2)/r \quad (4.4)$$

The ideal surface roughness values were obtained using equation 4.4 and are presented in Table 4.17 for the three different feeds which were used during the cutting tests. When

the ideal surface roughness values are compared with those obtained during the cutting test when the cutting tool is sharp, as illustrated in Figure 4.63, these results indicate that lower surface roughness values can be expected for the radius/feed combination evaluated. This increase in the surface roughness is caused by the irregularities in the cutting operation such as the occurrence of vibration, as mention in Sections 4.3.1.2 and 4.3.1.3, defects in the structure of the workpiece and inaccuracies in the machine tool movement.

Table 4.17: Ideal Surface Roughness values for three different feeds

Ideal Surface Roughness	Feed (mm/rev)		
	0.075	0.1	0.125
Ra (μm)	0.03	0.054	0.084

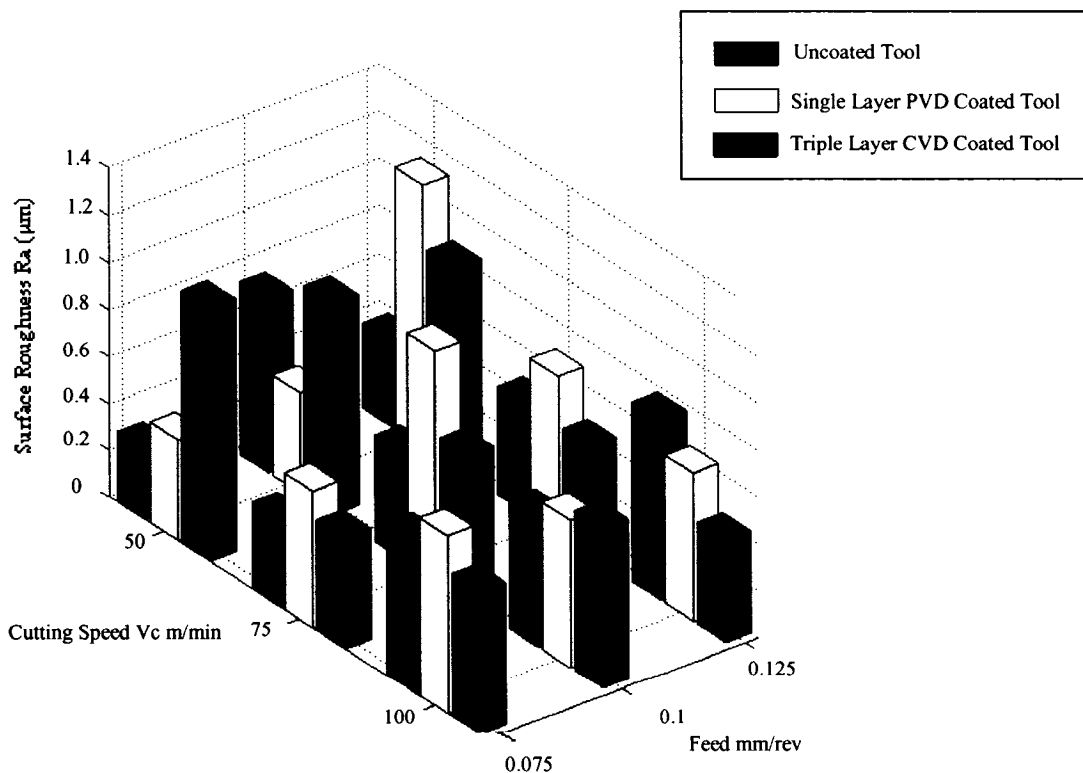


Figure 4.63: Effect of cutting speed and feed on surface roughness when the tool edge is sharp

Figure 4.64 shows the values of surface roughness for all the cutting conditions tested at the end of tool life according to tool failure criteria.

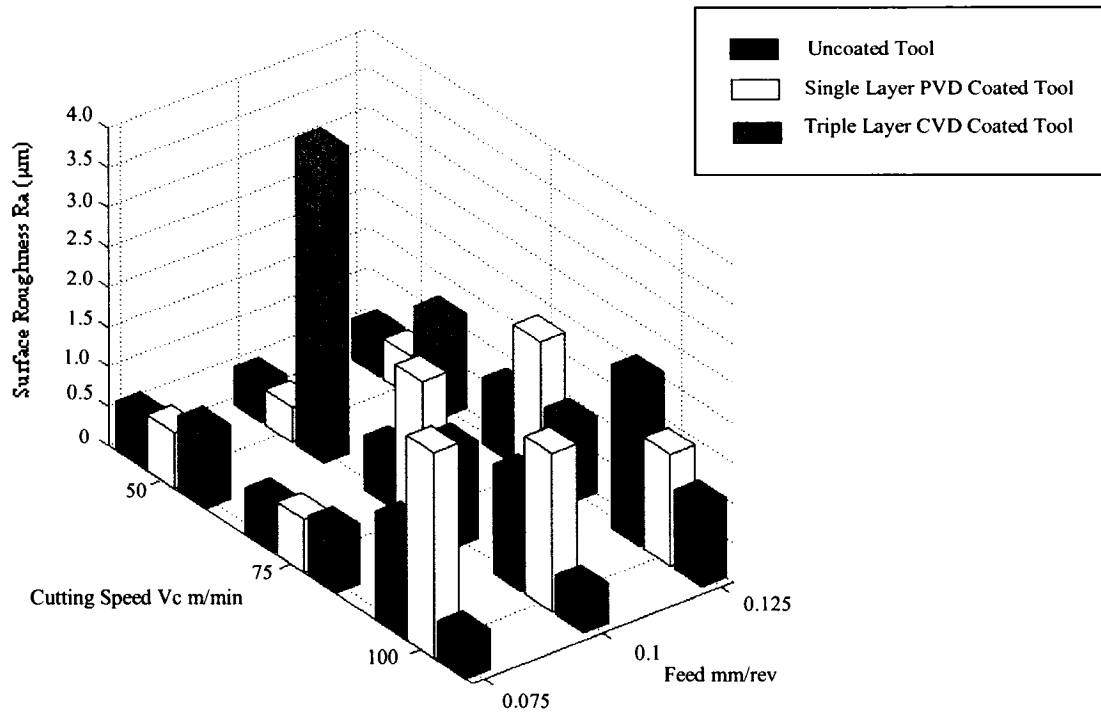


Figure 4.64: Effect of cutting speed and feed on surface roughness when the tool edge reaches tool failure criteria

In general, low values ($<1 \mu\text{m}$) of surface roughness (Ra) at the end of tool life were obtained even for high tool wear, except for some conditions where the surface roughness was more than $1 \mu\text{m}$. This can be attributed to the round tool geometry, since the contact length of the tool is large; the height of the feed marks is reduced, resulting in lower values of surface roughness. The worst surface roughness ($3.87 \mu\text{m}$) was found with the CVD coated triple layer ($\text{TiCN}/\text{Al}_2\text{O}_3/\text{TiN}$) tool at a speed of 50 m/min and a feed of 0.1 mm/rev. This is due to the pronounced nose wear at the tool nose, which tends to channel the metal in the opposite direction on the machined surface, as illustrated in the Figure 4.65.



(a) Flank Face



(b) Rake Face

Figure 4.65: Showing nose wear for CVD coated triple layer (TiCN/Al₂O₃/TiN) at a speed of 50 m/min and a feed of 0.1 mm/rev.

Chapter 5 Conclusions and Future Recommendations

5.1 Conclusions

The machinability of nickel-based super alloy Inconel 718 has been evaluated and described through cutting forces, tool wear, chip morphology, and surface roughness in relation to three different tools. The three tools used during the machining tests were: (1) an uncoated WC tool, (2) a single layer PVD TiAlN coated carbide tool, and (3) a triple layer CVD (TiCN/Al₂O₃/TiN) coated carbide tool.

Tool wear mechanisms have been studied for all three tools at all different cutting conditions. Several wear mechanisms also were identified which were responsible for tool deterioration, including adhesion, abrasion, diffusion, oxidation, flaking and chipping off the cutting edge. Figure 5.1 depicts the wear mechanisms for all three types of tools.

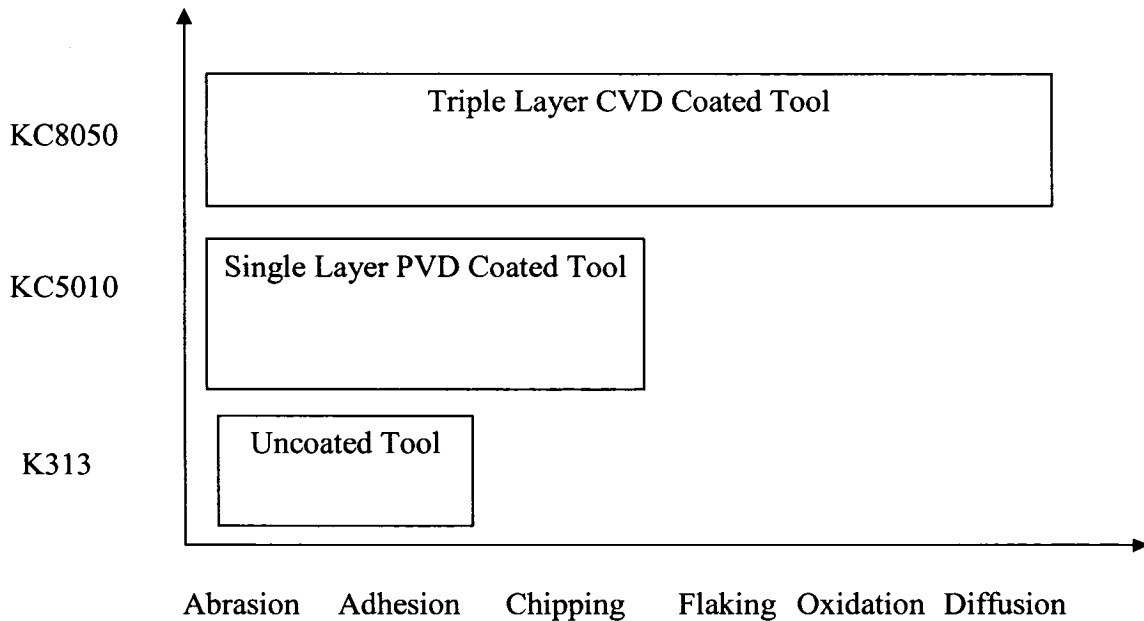


Figure 5.1: Tool wear mechanisms for all three tools

In general, with all three types of tools, the cutting forces increase with feed and decrease with cutting speed, although a few unexpected results were observed, which were due to temperature rise [25], as explained in Chapter 4. In general, the values of cutting forces are low for the uncoated tool, and high for the triple layer coated tool.

The chip SEM chemical analysis reveals no microstructure change (Figures 4.28, 4.30, 4.39, 4.41, 4.43, 4.45, 4.47, 4.49, 4.51, 4.59, 4.61) when compared to the base microstructure (Figure 4.26) after going through deformation during machining. The shear localized chips that form are continuous and ribbon-like with a deformation of the primary shear zone and a bending of the secondary shear zone. The analysis also confirms (through measurement of the micro-hardness of the chips) the existence of strain hardening when machining Inconel 718.

Tool life results confirmed that the uncoated WC tool material with a small grain size ($<1 \mu\text{m}$) performs better at a low cutting speed of 50 m/min and a feed of 0.1 mm/rev, giving a tool life of 53 min. In terms of tool life, the PVD single layer TiAlN coated carbide tool performs better at a slightly higher cutting speed of 75 m/min and a feed of 0.075 mm/rev, giving a tool life of 12 min. The CVD triple layer (TiCN/Al₂O₃/TiN) coated carbide tool performs better than the other tools at a higher cutting speed of 100 m/min and a feed of 0.075 mm/rev, giving a tool life of approximately 8 min. Figure 5.2 depicts the best optimum cutting conditions in terms of tool life for all three tools.

For surface roughness, optimum cutting conditions also were found as shown in Figure 5.3. The roughness values ranging between 0.5 μm to 1 μm were achieved in most of the cutting conditions at the end of tool life.

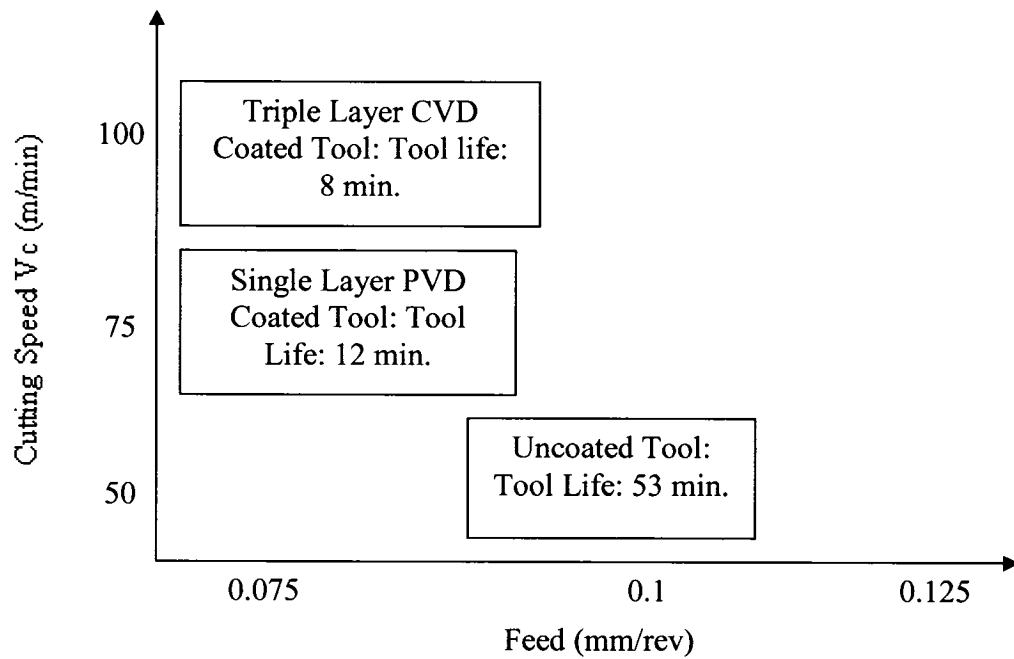


Figure 5.2: Optimum cutting conditions in terms of tool life for all three tools

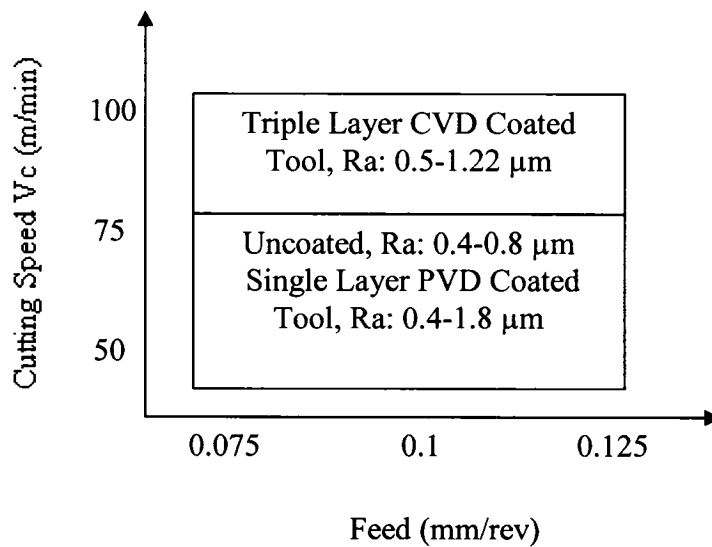


Figure 5.3: Optimum cutting conditions in terms of surface roughness R_a (μm) for all three tools

5.2 Recommendations for Future Work

In the present study, orthogonal tests were carried out for future identification of material behavior (constitutive laws) under high stress, strain, strain rate, and temperature.

In future research, temperature should be measured for all cutting conditions tested to establish its effect in the machining test, and to understand its impact on material behavior on tool wear mechanisms.

Further work is also needed for the finite element simulation of the finish turning operation, and to optimize the process performance in terms of tool life, cutting forces and surface roughness.

The high speed machining (machining performed at very high rates of material removal. It is done such that there is a higher throughput of workpieces, or higher productivity, than is possible with conventional machining; in most cases, it is done with high speed machines) of Inconel 718 is another issue to be analyzed. Since Inconel 718 is considered to be a difficult-to-cut material, an innovative way such as laser-assisted machining should be used. Laser assisted machining has a vast scope in turning operations, and can be used to perform experiments to evaluate its effect on the machinability of Inconel 718.

References

- 1) Field, M., Machining Aerospace Alloys, Iron and Steel Institute, special report 94, 1968, pp. 151-160.
- 2) Warburton, P., "Problems of Machining Nickel-based Alloys, Iron and Steel Institute, special report 94, 1967, pp. 151-160.
- 3) Shaw, M., "Metal Cutting Principles", Oxford: Clarendon Press, New York, Oxford University Press, 1986.
- 4) Kalpakjian, S., "Manufacturing Processes for Engineering Materials", Third Edition, 1997.
- 5) Metals Handbook, vol. 1, 10th edition, ASM International, USA, pp. 950-980, 1990.
- 6) Sims, C.T., Hagel, W.C., "The Super Alloys", Wiley, New York, 1972.
- 7) Richards, N., Aspinwall, "Use of Ceramic Tools for Machining Nickel-based Alloys", International Journal for Machine Tools and Manufacture, vol. 29, no. 4, pp. 575-588, 1989.
- 8) White, C.H., "Nickel Based Alloys", Wiggin Alloy.
- 9) Ezugwu, E.O., Wang, Z.M., Machado, A.R., "The Machinability of Nickel-based alloys: A review", Journal of Materials Processing Technology", Vol. 86, pp. 1-16, 1999.
- 10) Jaspers, S., "Metal Cutting Mechanics and Material Behavior", Bibliotheek, Technische Universiteit Eindhoven.
- 11) "Chemical Composition of Inconel 718", Metaux Profusion Company.
- 12) Komanduri, R., Schroeder, T.A. "On Shear Instability in Machining a Nickel-Iron Base Superalloy", Journal of Engineering for Industry, vol. 108, pp. 93-100, May 1986.
- 13) Muzyka, D.R., "Physical Metallurgy and effects of process variables on the microstructure of wrought superalloys", ASTM Technical publication, vol. 672, pp. 526-546, 1979.

- 14) Paulonis, D.F., Oblak, J.M., and Duvall, D.S., "Precipitation in Nickel-based Alloy 718", Transactions of the ASM, vol. 62, pp. 611, 1969.
- 15) Nevitt, M.V., "Electronic Structure and alloy chemistry of Transition Elements", Beck, P.A., edition, Interscience Publishers, New York, pp. 169, 1963.
- 16) Oblak, J.M., Paulonis, D.F., Duvall, D.S. "Coherency strengthening in Nickel-base alloys hardened by DO22 γ'' precipitates", Metallurgical Transactions, vol. 5, pp. 143-153, 1974.
- 17) Muzyka, D.R., Maniar, G.N., "Microstructural approach to property optimization in wrought super alloys", ASTM STP, vol. 557, pp. 198-219, 1974.
- 18) Beardmore, P., Davies, R.G., and Johnston, T.L., "On the temperature dependence of the flow stress of Nickel-base Alloys", Transactions of the metallurgical society of AIME, vol. 245, pp. 1537-1545, 1969.
- 19) Recht, R.F., "Catastrophic thermoplastic shear", Transactions of ASME, vol. 31, pp. 186, 1964.
- 20) Rahman, M., Seah, W.K.H., Teo, T.T., "The machinability of Inconel 718", Journal of Materials Processing Technology, vol. 63, pp 199-204, 1997.
- 21) Yeo, B.S., "The Machinability of Inconel 718", 1993-1994.
- 22) Alauddin, M., Mazid, M.A., ElBaradi M. A., Hashmi, M.S.J., "Cutting Forces in the end milling of Inconel 718", Journal of Materials Processing Technology, vol. 77, pp 153-159, 1998.
- 23) Ezugwu, E.O., Wang, Z.M., Machado, A.R., "Wear of Coated Carbide Tools when Machining Nickel (Inconel 718) and Titanium base (Ti-6Al-4V) Alloys", Tribology Transactions, vol. 43, pp. 263-268, 2000.
- 24) Uhlmann, W., Ederer, G., "High Speed Turning of Inconel 718", Industrial Diamond Review, vol. 61, no.3, pp. 169-174, 2001.
- 25) Ezugwu, E.O., Bonney, J., Olajire, K. A., "Evaluation of the Machinability of Nickel-base Inconel 718 alloy wit Nano-Ceramic Cutting Tools", Tribology Transactions, vol. 45, pp. 506-511, 2002.
- 26) Schlauer, C., Peng, R.L., Oden, m., "Residual Stress in a Nickel-based Super Alloy introduced by turning", Material Science Forum, vol. 404-407, pp. 173-178, 2002.

- 27) Sadat A., Reddy, M., "Surface Integrity of Inconel 718 Nickel-based Super Alloy using controlled and natural contact length Tools-Part 1: Lubricated", *Experimental Mechanics*, vol. 32, no. 3, pp. 282-288, 1992.
- 28) Darwish, S.M., "The Impact of tool material and cutting parameters on the machinability of the Supermet 718 nickel-base Superalloy", *International Journal of Computer Applications in Technology*, vol. 17, no. 4, pp. 272-284, 2003.
- 29) Arunachalam, R.M., Mannan, M.A., Spowage, A.C., "Residual Stress and Surface Roughness when facing age hardened Inconel 718 with CBN and Ceramic Tools", *International Journal of Machine Tools & Manufacture*, vol. 44, pp. 879-887, 2004.
- 30) Liu, G., He, N., Man, Z.N., Li, L., "Cutting forces in the milling of Inconel 718", *Key Engineering Materials*, vol. 259-260, pp. 824-828, 2004.
- 31) Ezugwu, E.O., Bonney, J., Fadare, D.A., Sales, W.F., "Machining of nickel-base Inconel 718, alloy with ceramic tools under finishing conditions with various coolant supply pressures", *Journal of Materials Processing Technology*, vol. 162-163, pp. 909-914, 2005.
- 32) Ezugwu, E.O., Okeke, C.I., "Behavior of Coated Carbide Tools in High Speed Machining of a Nickel Base Alloy", *Tribology Transactions*, vol. 45, pp. 122-126, 2002.
- 33) Choudhury, I.A., and El-Baradie, M.A., "Machinability assessment of Inconel 718 by factorial design of experiment coupled with response surface methodology", *Journal of Materials Processing Technology*, vol. 95, pp. 30-39, 1999.
- 34) Arunachalam, R.M., Mannan, M.A., "Performance of CBN cutting tools in facing of Age Hardened Inconel 718", *Transactions of NAMRI/SME*, vol. 32, pp 525-532, 2004.
- 35) Itakura, K., Kuroda, M. Omokawa, H., Itani, H., Yamamoto, K., and Ariura, Y., "Wear Mechanism of Coated Cemented Carbide Tool in cutting of Inconel 718 Super-Heat-Resisting Alloy", *International Journal of Japanese Society for Precision Engineering*, Vol. 33, no.4, pp. 326-332, Dec.1999.

- 36) Jindal, P.C. Santhanam, A.T., Schleinkofer, U., Shuster, A.F., "Performance of PVD TiN, TiCN, and TiAlN coated cemented carbide tools in turning", *International Journal of Refractory Metals and Hard Materials*, vol. 17, pp. 163-170, 1999.
- 37) Coleman, J.R., *Tooling Production*, vol.50, pp. 46, 1984.
- 38) Jawaid, A., Koksai, S. Sharif, S., "Cutting performance and wear characteristics of PVD coated and uncoated carbide tools in face milling Inconel 718 aerospace alloy", *Journal of Materials Processing Technology*, vol. 116, pp. 2-9, 2001.
- 39) Ducros, C. Benevent, V. Sanchette, F., "Deposition, characterization and machining performance of multilayer PVD coatings on cemented carbide cutting tools", *Surface and Coatings Technology*, vol. 163-164, pp. 681-688, 2003.
- 40) Li, L., He, N., Wang, M., Wang, Z.G., "High speed cutting of Inconel 718 with coated carbide and ceramic inserts", *Journal of Materials Processing Technology*, vol. 129, pp. 127-130, 2002.
- 41) Prengel, H.G., Jindal, P.C., Wendt, K.H., Santhanam, A.T., Hegde, P.L., Penich, R.M., "A new class of high performance PVD coatings for carbide cutting tools", *Surface and Coatings Technology*, vol. 139, pp. 25-34, 2001.
- 42) Kitagawa, T., Kubo, A., Maekawa, K., "Temperature and wear of cutting tools in high-speed machining of Inconel 718 and Ti-6Al-6V-2Sn", *Wear*, vol. 202, pp. 142-148, 1997.
- 43) Liao, Y.S., Shiue, R.H., "Carbide tool wear mechanism in turning of Inconel 718 superalloy", *Wear*, vol. 193, pp. 16-24, 1996.
- 44) Ezugwu, E.O., Wang, Z.M., Okeke, C.I., "Tool Life and surface Integrity when machining Inconel 718 with PVD and CVD coated tools", *Tribology Transactions*, vol. 42, no. 2, pp. 353-360, 1999.
- 45) Hanasaki, j., Fujiwara, J., Touge, m., Hasegawa, Y., Uehara, K., "Tool wear of coated tools when machining a high nickel alloy", *CIRP Annals*, vol. 39, issue 1, pp. 77-80, 1990.
- 46) Narutaki, N., Yamane, Y., Hayashi, K., Kitagawa, T., "High Speed Machining of Inconel 718 with Ceramic Tools", *CIRP Annals*, vol. 42, issue 1, 1993.

- 47) Arunachalam, R.M., Mannan, M.A., "Surface Finish and Residual Stresses in Facing of Age Hardened Inconel 718", Material Science Forum. Vol. 437-438, pp. 503-506, 2003.
- 48) Ezugwu, E.O., Tang, S.H., "Surface abuse when machining cast iron (G-17) and nickel-base superalloy (Inconel 718) with ceramic tools", Journal of Materials Processing Technology, vol. 55, pp. 63-39, 1995.
- 49) Arunachalam, R.M., Mannan, M.A., Spowage, A.C., "Surface Integrity when machining age hardened Inconel 718 with coated carbide cutting tools", International Journal of Machine Tools & Manufacture, vol. 44, pp. 1481-1491, 2004.
- 50) Darwish, S.M., El-Tamimi, A.M., "Formulation of surface roughness models for machining Nickel Super Alloy with different tools", Materials and Manufacturing Processes, vol. 12, no. 3, pp. 395-408, 1997.
- 51) Society of Automotive Engineers Standard "AMS 5662", July 2004
- 52) International Standard ISO 3685 "Tool life testing in single-point turning tools", second edition 1993-11-15.
- 53) Pereira, J.M., Lerch, B.A. "Effect of heat treatment on the ballistic impact properties of Inconel 718 for jet engine fan containment applications" Glenn Research Center, Cleveland, Ohio, NASA report, July 2001.
- 54) Metals Handbook, Machining, ninth edition, vol.16.
- 55) "Personal Communication with Dr. Nejah Tounsi, Research Officer, Aerospace Manufacturing Technology Centre, National Research Council, Montreal, Canada, January, 2005.
- 56) Geng, H., "Manufacturing Engineering Handbook" McGraw-Hill Handbook, New York, Edition 2004.
- 57) Oxley, P.L.B., "The Mechanics of Machining: An Analytical Approach to Assessing Machinability", Chichester [England]: E. Horwood; New York: Halsted Press, 1989.
- 58) Attia, M.H., and Kops, L., A, "New Approach to Cutting Temperature Prediction Considering the Thermal Constriction Phenomenon in Multi-layer Coated Tools",

- CIRP Annals - College International de Recherches pour la Production - Bi-annual edition, vol. 53, no.1, pp. 47-52, 2004
- 59) Attia, M.H., and Kops, L., "Thermal consideration of the design of multilayer coated tools for high speed machining", ASME International Mechanical Engineering Congress and Exposition, November, 2004.
- 60) Lindstrom, B. "Relationship between contact length and machinability", Department of Production Engineering, Stockholm, Sweden, Presented at CIRP STC "C" Paris, January 30, 1992.
- 61) http://www.mame.mu.oz.au/manuf-sci3/436413/download/436-413notes_toolwear.pdf
- 62) Koning, W., Fritsch, R. and Kammermeier, D., "Physically vapor deposited coatings on tools: performance and wear phenomena", Surface and Coatings Technology, vol. 49, pp. 316-324, 1991.
- 63) Prengel, H.G., Santhanma, A.T., Penich, R.M., Jindal, P.C., and Wendth, K.H., "Advanced PVD-TiAlN coatings on carbide and cermet cutting tools", Surface and Coatings Technology, vol. 94, pp. 597-602, 1997.
- 64) Boothroyd, G. and Knight, W.A., "Fundamentals of Metal Cutting and Machine tools", 2nd edition, Marcel Dekker, Inc. New York, 1989